

Table of Contents:

Supporting Discussion: Molecular Robotics	Page 2-3
Material and Methods	Page 3-21
Supplementary Figures 1 to 23	Page 22-50
Supplementary Table 1	Page 51
Supplementary Figure 24	Page 52
Supplementary Table 2	Page 52
Supplementary Figures 25 to 28	Page 53-61
Supplementary Table 3	Page 62
Supplementary Figures 29 to 31	Page 63-80
Supplementary Table 4	Page 81
Supplementary Figure 32	Page 82-83
Supplementary References:	Page 84-86

SUPPORTING DISCUSSION: MOLECULAR ROBOTICS

Robots are often defined by their ability to sense their environment, perform computations, and take actions; as such, they have revolutionized our ability to automate factories, send autonomous vehicles to remote or dangerous locations, and improve our daily lives. The potential for autonomous sensing and acting at the molecular scale is illustrated by the sophisticated machinery within biological cells, where molecular motors and biochemical circuitry coordinate the cell's active responses to its environment. From a chemist's perspective, the potential for molecular robotics goes far beyond what is observed in biology, but the challenges of realizing that potential are daunting due to the need to synthesize behavior.

As with protein motors, an isolated molecular robot by itself serves no purpose; to be useful, it must interact with its environment of other molecules and molecular machines; it must behave. Despite vast differences in size, classical robotics¹⁻⁴ can provide a framework for designing interacting molecular machines with complex behaviors within their environments.

A simple example of a molecular robot would be a "walking" DNA molecule that can recognize and follow an arbitrary trail ("bread crumbs"). If such a simple molecular robot could be demonstrated, its capabilities then could be expanded by incorporating additional layers of control mechanisms from DNA nanotechnology and concepts from computer science. For example, integration of logic and memory into the robot's body would enhance the robot's ability to respond to its environment intelligently⁵; interactions between multiple molecular robots could lead to collective behavior⁶⁻⁸, and the ability to read and transform the landscape (e.g., pick up and deposit loads) would in theory provide the essential mechanism for Turing-universal algorithmic behavior⁹⁻¹².

Research in programmable DNA walkers¹³ started with non-autonomous remote-controlled systems^{14,15}, progressed to autonomous walkers that modify visited sites to achieve directed (but brief) motion on linear tracks¹⁶⁻¹⁹, or to achieve continuous processive (but undirected) motion in two or three dimensions²⁰, and shows promise for processive and directed walking on undisturbed tracks²¹. Theoretical work has envisioned how certain types of DNA walkers could be augmented with additional control mechanisms to act as finite state machines, universal Turing machines, and programmable molecular robots^{22,23}, but these schemes have not been experimentally demonstrated. Other work related to molecular robotics has demonstrated the controlled movement of dendrimers²⁴, nanowire motors²⁵, and nanocars²⁶. While synthesizing suitably well-defined tracks has been an important technical challenge for DNA-based walkers (no previous walker has been demonstrated to take more than three steps on a linear track), our interest herein is in how robotic behavior can be obtained from the interaction between a simple random walker and its environment.

In this work, we present an implementation of molecular robots that integrates aspects of DNA-based computing devices^{27-29,18}, complex structures³⁰⁻³⁶ and actuators^{37,20,13}. The DNA walkers chosen for this work, called “molecular spiders”, comprise an inert body and multiple catalytic “legs”. Specifically, here we use three-legged spiders with a streptavidin body. Spider legs are adapted from DNA enzyme 8-17 that binds and cleaves single-stranded oligodeoxynucleotide substrates with a single ribose moiety into two shorter products that have a lower affinity for the enzyme³⁸. In the context of substrates that are immobilized at sites on a surface, spider behavior can be modeled using local rules³⁹: a leg bound to substrate will cleave it at a low rate; a leg bound to product will detach at an intermediate rate; and a free leg will quickly bind (with little or no bias) a nearby substrate or product. For a multipedal spider positioned at the interface between regions of product and substrate, these rules predict that after a given leg cleaves and then lifts, it will by trial-and-error search out a nearby substrate to bind, thus moving the spider’s body toward the substrate region while enlarging the product region behind it. A Monte Carlo simulation using these rules is presented further below. On 2D surfaces or in a 3D matrix, such spider movement results in a random walk with memory of visited sites, while on a 1D linear track it results in directed motion as the substrate is consumed. Crucially, unlike related “burnt bridge” Brownian ratchet mechanisms used in DNA walkers^{14-17,19} and observed in nature⁴⁰, these local rules predict that multipedal spiders will not readily dissociate even from tracks consisting exclusively of product strands, and indeed will perform a rapid unbiased random walk there until they again encounter substrate.

Considering spider legs to be simultaneously sensors that detect nearby oligonucleotides and actuators that modify their environment to inhibit reverse motion, we exploit this sensor-actuator feedback to design prescriptive landscapes that direct the spiders’ motion along a predefined path (Figs 1c and d). A spider traversing this landscape of oligonucleotide substrates can sense the set of available cues within its reach and take action accordingly. Here, we show that in the context of a precisely-defined track laid out on two-dimensional (2D) DNA origami³³, the previously introduced processive but random walker²⁰ becomes a processive and directed walker capable of path-following behavior. The importance of these results lies not in the walkers reaching stable thermodynamic endpoints, but in reaching those points through autonomously guided dissipative processes that can be programmed. Such processes could, in the future, be used to couple the behavior of multiple walkers through their interactions with a common landscape.

MATERIALS AND METHODS

ABBREVIATIONS

iSp18 is a hexa-ethyleneglycol internal spacer; Bio is biotin; and BioTEG is biotin-tetra-ethyleneglycol.

PREPARATION OF SPIDERS

Materials and Instrumentation for the Preparation and Characterization of $\text{NICK}_{3.4A+1}$ and $\text{NICK}_{3.4A+1} \bullet (\text{Cy3})_3$. Synthesis and purification of the modified DNA strands used to construct $\text{NICK}_{3.4A+1}$ and $\text{NICK}_{3.4A+1} \bullet (\text{Cy3})_3$ were carried out by Integrated DNA Technologies (Coralville, IA) and used as received. Streptavidin was obtained from Pierce, product number 21125 (Rockford, IL). IE-HPLC purification was performed using a Shimadzu LC-6AD pump equipped with a Shimadzu SPD-M10A PDA detector, with separation carried out on an anion exchange TSKgel DEAE-NPR column, 4.6x50 mm (IDxL) (Tosoh Biosciences). Concentrations of oligonucleotides were determined on an Amersham Biosciences Ultrospec 3300 pro UV/visible spectrophotometer.

Assembly of $\text{NICK}_{3.4A+1}$. *Part A*; capture leg [5' - GCC GAG AAC CTG ACG CAA GT/iSp18//iSp18//3Bio/ - 3'] (**C**) (47 nmoles in 10 mL of 10 mM HEPES, 150 mM NaCl, pH 7.4) was added drop-wise to a stirred solution of streptavidin (STV) (5 mg, 94 nmoles in 1 mL of 10 mM K_3PO_4 , pH 6.5). The desired one-to-one conjugate product ("STV-(**C**)₁") was purified by ion exchange (IE) HPLC (see Supplementary Fig. 1 for details of purification conditions). *Part B*; deoxyribozyme leg [5' - /5BioTEG//iSp18//iSp18/TCT CTT CTC CGA GCC GGT CGA AAT AGT GAA AA - 3'] (**L**) (100 μM , in water) was titrated into the isolated 1:1 conjugate HPLC fraction from 'Part A' above, until all three remaining biotin binding sites of the 1:1 conjugate "STV-(**C**)₁" were occupied by **L** to give the final desired product "STV-(**C**)₁(**L**)₃" i.e. $\text{NICK}_{3.4A+1}$. The titration was monitored by IE-HPLC, and was deemed complete when a slight excess of **L** was observed with no intermediate species, i.e. no "STV-(**C**)₁(**L**)₁" or "STV-(**C**)₁(**L**)₂", present, see Supplementary Fig. 2. The assembly was purified by IE-HPLC (see Supplementary Fig. 2 for details of purification conditions) and the volume of the eluent reduced (by centrifugation) to give a final concentration of 2.3 μM , as determined by absorbance at 260 nm. Characterization of the assembly was carried out by IE-HPLC and PAGE (Supplementary Figs 1, 2, 3 and 4). The assembly was stable at -20 °C for at least six months.

Assembly of $\text{NICK}_{3.4A+1} \bullet (\text{Cy3})_{3^{}}$.** *Part A and part B* were carried out in identical fashion to the assembly of $\text{NICK}_{3.4A+1}$ above, except "(**C**)" was [5' - /5Cy3/GCC GAG AAC CTG ACG CAA GT/iSp18//iSp18//3Bio/ - 3'] and triethanolamine (20 mM) was used in place of HEPES and TRIS for the assembly and HPLC purification respectively. *Part C*; the volume of $\text{NICK}_{3.4A+1} \bullet (\text{Cy3})_1$, fraction isolated by HPLC, was concentrated to 1 mL (0.834 nmoles) and Cy3 Mono NHS ester (20 nmoles) (PA13101, Lot number 359269, GE Healthcare) dissolved in DMSO added to the solution containing the assembly (giving a total DMSO concentration of 10%). The resulting mixture was incubated at room temperature overnight, protected from light. Excess dye was separated from the $\text{NICK}_{3.4A+1} \bullet (\text{Cy3})_3$ product by gel filtration (PD-10 column, 17-0851-01, lot 367770, GE Healthcare). Ratio of dye to streptavidin-DNA assembly was obtained by

determining concentrations at 550 nm (ϵ_{\max} 150,000 M⁻¹cm⁻¹) and 260 nm (ϵ_{\max} 1,220,000 M⁻¹cm⁻¹) respectively.

** The number of Cy3 dyes per spider is an average. This particular protocol sometimes produced an average of four Cy3 dyes per spider molecule, hence such spiders will be notated in the text as **NICK_{3,4A+1}•(Cy3)₄**.

SURFACE PLASMON RESONANCE (SPR)

Materials and Instrumentation for SPR Experiments. Immunopure avidin was purchased from Pierce (Rockford, USA). We used a Biacore X system and commercially available Biacore SA sensor chips, and Biacore C1 sensor chips, from GE Healthcare (Piscataway, USA). 1× HBS buffer (10 mM HEPES, pH7.4 with 150 mM NaCl) was employed as running buffer.

Preparation of Substrates on pseudo-2D Hydrogel Matrix Surfaces for SPR.

A 20 μM solution of cleavable substrates (5'-BioTEG-TTTTTTTCCTACTATrAGGAAGAG, "r" precedes a ribonucleotide) was applied to both channels of the SA sensor chip (carboxymethylated dextran matrix pre-immobilized with streptavidin) for 16 min at 5 μL/min, followed by a 60 s wash with 4 M urea and 15 mM EDTA in both channels to remove any nonspecifically adsorbed materials. The quantity of substrates adsorbed was calculated by the change in measured mass as described²⁰.

Preparation of Substrates on 2D Monolayer Surfaces for SPR.

Avidin was covalently bound to the C1 sensor chip surface (a carboxymethylated monolayer) via amino groups using the following protocol. The carboxymethylated surface was first activated at a flow rate of 5 μL/min by using a 7 min injection pulse of an aqueous solution containing N-hydroxysuccinimide (NHS, 0.05 M) and N-ethyl-N'-(dimethylaminopropyl) carbodiimide (EDC, 0.2 M). Next, an 80 μL injection of 1 mg/mL avidin (in 1× HBS) was flowed over the activated surfaces of both channels for 40 min at 2 μL/min. The remaining activated sites on the chip surfaces were blocked with a 35 μL injection of an ethanolamine hydrochloride solution (1 M, pH 8.5). Then, a 20 μM solution of cleavable substrate was applied to both channels of C1 sensor chip for 20 min at 4 μL/min, followed by a 60 s wash with 4 M urea and 15 mM EDTA. Based on the average SPR responses for avidin (~2,010 RU, 0.03 pmole/mm²) and substrate (450 RU, 0.056 pmole/mm²), there are two substrates bound for each avidin molecule. The average intersubstrate distance is 5.5 nm.

SPR Monitoring of Dissociation of NICK_{3,4A+1} Spider on Non-cleavable Substrate and Product Surfaces.

The non-cleavable substrate analog (substrate in which rA was substituted with A) or product surfaces were prepared in a similar manner to the preparation of substrate on 2D monolayer surfaces. The spider was loaded to channel 2, with channel 1 serving as a negative control. We calculated the ratio of spider to non-cleavable substrate or product by measuring the change in SPR response units (RU) after the spider was flowed

onto the chip, then used the equation: ratio (spider/S or P) = M_w (S or P) \times RU(spider)/[M_w (spider) \times RU(S or P)] (Supplementary Fig. 5). Monitoring the dissociation of the spider was performed in 1 \times TA-Mg buffer (40 mM Tris, 20 mM acetic acid, 12.5 mM Magnesium acetate) with 1 mM ZnCl₂.

We could not directly measure the dissociation rate of spiders from cleavable substrate because 1) dissociation of the cleavage product from the surface accounts for the vast majority of the SPR response, and 2) the ratio of substrate to cleavage product changes with time, so the dissociation rate of spiders is not constant. Therefore, we instead monitored the SPR response to obtain the dissociation rate of spider on non-cleavable substrate, and product. We observed that over the course of 30 min >92% of spiders remained on a product covered surface and over the course of 60 min 86% remained bound (Supplementary Fig. 5). These percentages represent an upper-bound on spider dissociation from our tracks (which will be a mixture of substrates and products as the spider walks over it). So we estimate an upper-bound for the dissociation rate as less than 8-14 % over the time scale of our experiments on AFM and fluorescence microscopy.

SPR Monitoring of Cleavage of Substrates by NICK_{3.4A+1} Spider. Spiders (0.8–6.3 nM in 1 \times HBS buffer) were loaded only on channel 2 at 5 μ L/min, with channel 1 used as a negative control. The amount of spider applied was controlled by adjusting concentrations and the reaction times of spiders in the loading solution. Monitoring the cleavage of the substrate was initiated by switching to 1 \times TA-Mg buffer with 1 mM ZnCl₂ or 1 \times HBS buffer with 1 mM ZnCl₂ with the Biacore X system ‘Working Tools Wash’. Product formation in real time was measured through the decrease in mass, using the formula 1,000 RU = 1 ng \cdot mm⁻². Rates of cleavage were determined from the approximately linear region of the product release curves during the initial 10% of substrates cleaved. On the 2D monolayer surface, real-time processivity of spiders was measured to be ~79% (percentage of total substrate cleaved over the course of the experiment) at a 1:291 ratio of spider (17.8 RU) to substrate (448.4 RU) with a cleavage rate of 1.42 min⁻¹ per spider. On the pseudo-2D matrix surface, spiders showed a real-time processivity ~86% of total substrate cleaved at a 1:990 ratio of spider (26 RU) to substrate (2,222 RU) with a cleavage rate of 2.81 min⁻¹ per spider (Supplementary Fig. 6).

PREPARATION OF SPIDER-ORIGAMI ARRAYS

Assembly of Spider-Origami Arrays for Atomic Force Microscopy (AFM).

The spider arrays (Supplementary Figs 7-24) consist of M13mp18 viral DNA (New England Biolabs) and 202 ssDNA staples (Integrated DNA Technologies, see Supplementary Fig. 7 for DNA sequences). The arrays were annealed in 1 \times TA-Mg Buffer (40 mM Tris, 20 mM acetic acid, 12.5 mM Mg²⁺, pH 7.6) using a 1:3 ratio of M13 to staple strands and a final concentration of 10 nM (M13). The arrays were annealed in two hours from 94 °C to 25 °C using an Eppendorf PCR machine (Eppendorf). The **NICK_{3.4A+1}** or **NICK_{3.4A+1}•(Cy3)₃** were then added

to the arrays at a 1:1 ratio of START strand to spider and left at room temp overnight. Because origami folding is sensitive to stoichiometry, we expect that some fraction of origami are missing the START strand and are thus unable to position a spider before the TRACK is deposited. The substrate strand and CONTROL strand were then added at a 1:1 (for initial ABD, EABC and Before EABD samples) or 1:3 (for 15, 30 and 60 minute EABD samples) ratio of staple probes to substrate or CONTROL and allowed to bind overnight at room temperature (20 °C to 24 °C). We observed (by AFM) a larger percentage of apparently unbroken TRACKS when excess substrate was added. In the presence of excess substrate there is a low probability that a spider leg may bind to a free floating substrate or STOP strand that would deter or inhibit interactions with the TRACK. Note that the 8-17 deoxyribozyme has reduced but non-negligible activity in TA-Mg buffer (relative to maximal activity with Zn^{2+} ; see PAGE Activity Assays, below), suggesting that spiders bound at START may cleave immediately neighboring substrates during the overnight incubation. Since spiders undergo (unbiased) walks on product tracks with little dissociation, this possibility is not a concern. To minimize stacking interactions that can cause aggregation of origami, the staples on the left and right edges of the origami were removed. Schematics of the assembled origami landscapes are shown in Supplementary Figs 8, 11, 14, and 17.

Modification of Spider-Origami Arrays for Fluorescence Microscopy. To make the origami arrays compatible with fluorescence microscopy, we returned 4 of the removed staples to the corners of the origami. In order to affix the origami to slides for analysis, we divided the corresponding staples into two strands so that we could affix biotin labels onto the 5' end that is antiparallel to staple probes (as in Supplementary Figs 11b, 14b and 17b). We modified the CONTROL strand by adding a Cy5 fluorophore to its 3' end, which resulted in 6 Cy5 fluorophores labeling the STOP position. On all landscapes, CONTROL staples were replaced with staples lacking the non-cleave-able substrate probes. The EAC landscape used in both fluorescence microscopy and AFM experiments lacked a CONTROL site. In addition, the EAC arrays for fluorescence microscopy were annealed in 5× SSC buffer (75 mM sodium citrate, pH 7.0, 750 mM NaCl), and the EABC and EABD arrays in 1× TA-Mg buffer. Fluorescence microscopy was also performed for origami arrays containing a truncated substrate TRACK, or product TRACK. The product strand is 8 nucleotides shorter than the full length substrate and includes only the sequence 5' of the RNA base. The resulting 31 oligonucleotides have the same sequence as the corresponding portion of the full length cleavable substrate. All other assembly details for origami arrays for fluorescence microscopy including DNA concentrations, relative strand ratios, and binding conditions were unchanged.

ATOMIC FORCE MICROSCOPY

AFM Imaging. “Before” samples were deposited on mica without the addition of TRIGGER or $ZnCl_2$. “After” samples were prepared by releasing the spider from the START strand through the addition of a 27-base TRIGGER strand,

immediately followed by the addition of 10mM ZnCl_2 to a final concentration of 1 mM. Spiders were allowed to traverse the product or substrate TRACK array in solution for 15, 30, or 60 min (depending on the experiment) at room temperature before the origami were deposited on mica. Samples (2 μL) were deposited onto a freshly cleaved mica surface (Ted Pella, Inc.) and left to adsorb for 3 min. Buffer (1 \times TA-Mg, 400 μL) was added to the liquid cell and the sample was scanned in tapping mode on a Pico-Plus AFM (Molecular Imaging, Agilent Technologies) with NP-S tips (Veeco, Inc.). Each sample was scanned for 2-3 hrs before being discarded (therefore “30 minutes after” means that the sample spent 30 minutes in solution followed by up to 3 hours on mica). Note that the reduced but non-negligible deoxyribozyme cleavage rate in TA-Mg raises the possibility that spiders could move during the this imaging period; however, given the apparent difficulty of spider movement on mica-bound origami even in the presence of Zn^{2+} (see AFM Imaging for Movie) and the consistent trends in the time-lapse experiments (Fig. 2, main text), we conclude that very little movement takes place during the imaging period. All imaging by AFM was carried out at room temperature.

AFM Imaging for Movie. The sample (2 μL) was deposited onto a freshly cleaved mica surface and left to bind for 2 min. Then 1 μL of TRIGGER strand was added to the sample on the surface and after 2 min 270 μL of buffer and 30 μL of 10mM ZnCl_2 was added to the sample cell. The four images were taken over a 26-minute time frame with about 10 min between the saving of each scan. (It should be noted that many prior and subsequent attempts were made to capture another AFM movie using various optimizations of our buffer, and protocol, without success.) Although we were only able to capture one movie, reported in Fig. 3, we are convinced that it is not an artifact. The origami with the moving spider is substrate face-up while the three origami in the same image are substrate side down (see below for a discussion of how the face of the origami affects spider analysis). As a result spiders on the three adjacent origami are stationary over the time course of the movie. In addition the spider’s motion follows the TRACK in each frame (therefore it is not randomly diffusing, because it neither moves backwards nor off the TRACK). If the AFM tip were merely pushing the spider forward we would not expect the spider to turn in the transition from frame 3 to frame 4.

AFM Time Lapse Experiments. There is one seeming contradiction in our report that we would like to address here. If we were to suggest (as we do in Fig. 3) that the spider can walk on origami deposited on mica, then how could we expect to obtain viable statistics from time lapse experiments imaged for up to 3 hours? We assume that under these conditions, most spiders get stuck on the origami, while some small percentage of spiders are able to continue moving. We find that we can differentiate between samples deposited at 15 minutes from those deposited at 30 and 60 minutes (see Supplementary Table 1). These results help to explain why obtaining the AFM movie was so difficult.

Statistical Analysis of AFM images. We divided our flattened AFM images into 1 x 1 um images and numbered them. Within each of these images, we assigned a roman character to each origami (thus each origami we analyzed could be uniquely identified by a number and letter (i.e. “EABD Before 1e”, or “EABD 30 min 3a”; Supplementary Figs 9, 10, 12, 13, 15, 16, 18, 19). The origami arrays were classified by the following criteria: orientation (is the origami “face-up” or “face-down”?), number of spiders (0,1, multiple), location of spiders (START, TRACK, STOP, CONTROL), image quality (do imaging errors or sample impurities make the classification difficult?). This process was conducted independently by three people, for each data set excluding the EABD 15 minute and EABD 60 minute data sets, which were conducted by two people. The classifications were then compared: if two or more people agreed on the origami classification it was held, otherwise the origami was discarded from further analysis. By this method, we sought to ensure that our results are neither subjective nor irreproducible. While it is possible that some putative spiders were actually image artifacts or molecular contaminants, it is unlikely that this inaccuracy in our measurements could affect the main trends in our data or the qualitative conclusions we drew from them.

An origami that is “face up” is one that displays its substrates and spiders on the face opposite the mica; an origami that is “face down” displays its substrates on the face that rests on the mica (Supplementary Figs 20 and 21). Orientation was determined by landscape asymmetries in the positions of the TRACK and marker. By analyzing the statistics of origami classification, we concluded that the probability of an origami landing on one face or the other was approximately equal. However, we discovered that “face down” origami appeared to have a larger number of spiders at the STOP. We conducted a double-blind study in which 6 researchers were given an AFM image of origami and asked to classify these according to our criteria. We discovered that in the absence of spiders, all “face-up” origami were classified as vacant while a significant portion of “face-down” origami were classified as displaying a spider at the STOP site, when in fact there was none (Supplementary Fig. 22). Due to this “false positive” effect, we did not count “face-down” origami in our statistics. Approximately 50% of “face-up” origami were unoccupied by any spiders, and between 0 and 7% displayed more than one spider on the TRACK. Because the quantity of multiply occupied origami was small compared to the quantity of unoccupied and singly-occupied origami, we only considered singly-occupied origami to simplify our analysis (Fig. 2).

Experimental results for all four landscapes with substrate TRACKS showed that the fraction of spiders at the START diminishes with a concomitant increase in spiders observed on the STOP positions (Fig. 2c,g, main text, and Supplementary Fig. 23). Our shortest track (ABD, spanning 48 nm) efficiently delivers spiders to the STOP, with less than 20% of spiders on the TRACK after 30 min (Fig. 2c, main text). If the TRACK was omitted on the ABD landscape, spiders were equally distributed between the STOP and CONTROL sites after 30

min, implying that the track is needed for efficient delivery to the STOP site (Supplementary Fig. 24). On longer TRACKS (such as EABD, spanning ~ 90 nm) ~15% of spiders are delivered to the STOP within 15 min after release. Longer incubation times (30 and 60 min) increase the efficacy of delivering spiders to the STOP to up to 70%, (Fig. 2c,g, main text). Even at 60 min, however, we observed between 10-15% of spiders still on the TRACK. This outcome could be attributed to the distribution of spider velocities resulting from the stochastic nature of individual walks and possibly from backward steps onto product, initiating an unbiased random walk on product. We observed no significant difference in the efficacy of “turn right” and “turn left” actions (paths EABD and EABC, respectively) 30 min after release (Fig. 2c,g, main text).

PAGE ACTIVITY ASSAYS OF NICK_{3.4A+1}• (Cy3)₄.

The cleavage activity of spiders under various conditions in bulk solution was tested as follows. Reactions were initiated by combining NICK_{3.4A+1}• (Cy3)₄ (34 nM) with 4A substrate (5'-/5bio//iSp18//iSp18//iSp18//TTT TTT TTT TTC ACT AT(rA) GGA AGA G-Cy5, 34 nM) in the presence of either 1× SSC (15 mM sodium citrate (Mallinckrodt Inc.), pH 7.0, 150 mM NaCl) or 1× TA-Mg, and 0, 1, 2 or 10 mM ZnSO₄ (all reported concentrations are final). All reactions were supplemented with an oxygen scavenger system (1× OSS) consisting of 25 nM protocatechuate dioxygenase, 2.5 mM protocatechuate, and 1 mM Trolox as described⁴¹. Reactions (10 μL) were quenched after 0, 5, or 30 minutes with 2.5 μL of 0.25 M EDTA, and characterized by denaturing PAGE (Supplementary Fig. 25a). Fluorescence from Cy5 and Cy3 was detected on a Typhoon 9410 Variable Mode Imager (Amersham Biosciences) and the fraction of cleaved substrate quantified in ImageQuant 5.2 (Molecular Dynamics). Substrate was cleaved at least five-fold more slowly in 1× SSC + 1 mM Zn²⁺ than in 1× TA-Mg + 1 mM Zn²⁺, while cleavage in 1× SSC + 10 mM Zn²⁺ was only about two-fold slower than in 1× TA-Mg + 1 mM Zn²⁺ (Supplementary Fig. 25b). The maximal extent of cleavage is also about 9-fold lower in SSC + 1 mM Zn²⁺ than in TA-Mg + 1 mM Zn²⁺, consistent with a significant fraction of inactive deoxyribozyme-substrate complexes. This discrepancy among buffers is likely due to partial complexation of Zn²⁺ ions by citrate: from a direct Zn²⁺ concentration measurement in buffer using the low-affinity (30 μM) indicator dye Newport Green PDX (Molecular Probes) we estimate the free Zn²⁺ concentration in SSC buffer to be approximately 3-fold lower than in TA-Mg buffer at 1 mM total Zn²⁺. Nevertheless, these assays demonstrate that spiders are active under the buffer conditions used in Single Molecule Fluorescence Microscopy imaging (see below). A limiting factor for increasing the Zn²⁺ concentration above 1 mM is slow spontaneous Zn(OH)₂ precipitation at the near-neutral pH used in our studies. We therefore varied the buffer conditions in our Single Molecule Fluorescence Microscopy imaging experiments between 1× SSC with 0-10 mM ZnSO₄, 1× HBS buffer (10 mM HEPES, 150 mM NaCl, pH 7.4) with 0-5 mM

ZnSO₄, and 1× TA-Mg, carefully monitoring (and avoiding) any Zn(OH)₂ precipitation.

Further studies have examined the buffer-dependence of 8-17 spider leg cleavage activity in **NICK3.4A+1**; cleavage rates varied from 0.25-1.5 min⁻¹ in TA-Mg, TA-Mg with 1 mM Zn²⁺, and HEPES with 1 mM Zn²⁺ (Taylor, Pei, Stojanovic, unpublished results). In particular, the non-negligible cleavage rate in TA-Mg with no Zn²⁺ has implications for the AFM experiments prior to adding TRIGGER, as discussed above. Finally, these solution-based cleavage assays and the SPR assays (discussed above and in Supplementary Fig. 6), while useful for detection of cleavage activity under various conditions, may not be in quantitative agreement with the cleavage rate at the surface of an origami tile, where the locally high density of substrates and other surface effects may have a large impact on the rate-limiting step of this reaction.

SUPER-RESOLUTION PARTICLE TRACKING WITH FLUORESCENCE MICROSCOPY

Overview. For more facile real-time observation of the movement of individual spiders along tracks, we applied super-resolution imaging by total internal reflection fluorescence (TIRF) video microscopy⁴². Four biotin molecules were attached to the underside of the origami to facilitate its immobilization on the avidin-conjugated quartz slide. Experiments were performed using EAC, EABC, and EABD tracks. Spiders were covalently labeled with on average 2.3 Cy3 fluorophores (λ_{ex} 568 nm), and the STOP position was labeled with 6 Cy5 fluorophores (λ_{ex} 672 nm). This labeling scheme allowed us to colocalize spider position relative to its STOP using two-color single-molecule high-resolution colocalization (SHREC)⁴³ and monitor their relative movement by single-particle tracking⁴⁴. In a typical experiment, spider-loaded tracks were incubated with TRIGGER in the absence of Zn²⁺ ions and then immobilized on the slide (Supplementary Fig. 26). Within 20 min of commencing fluorescence imaging, we added Zn²⁺ to promote spider movement via substrate cleavage. As the 8-17 deoxyribozyme's activity depends sensitively on buffer conditions⁴⁵, we optimized our conditions for a combination of best catalytic activity and SMFM imaging quality, obtaining best results from SSC or HEPES with increased Zn²⁺ concentrations and no Mg²⁺ (see below and Supplementary Figs 6 and 25). The position of a spider on its origami path relative to the START was extracted over time by fitting the diffraction-limited point-spread functions (PSFs) to two-dimensional Gaussians in an up to 80-min sequence of wide-field images (time resolution 15-30 s) with a precision (standard deviation) of 10-30 nm. We controlled for focal drift and developed a consistent set of criteria to distinguish moving spiders from stationary ones as detailed below and in Supplementary Figs 27 and 28.

Preparation of Avidin-Coated Microscope Slides. Two 1-mm holes were drilled in each microscope slide (fused silica) to allow for buffer exchange. The slides were immersed in boiling "piranha" solution (5% (v/v) ammonium

hydroxide, 14% (v/v) hydrogen peroxide) for at least 20 min, then sonicated for 30 min in 1 M KOH, and flamed for several seconds with a propane torch. The slides were then aminosilanized by immersing them in a 5% (v/v) solution of 3-aminopropyltriethoxysilane (Sigma-Aldrich) in acetone for 1 h, rinsed with acetone, and dried for 1 h at 80 °C. A layer of the bifunctional crosslinking agent *para*-phenylene diisothiocyanate (PDITC) was covalently coupled to the aminosilanized surface by incubating the slides for 2 h in a solution of 0.2 % (w/v) PDITC, 10% (v/v) pyridine in *N,N*-dimethylformamide (spectroscopic grade). The slides were rinsed thoroughly with methanol and acetone, and 70 μ L of 0.5 mg/mL avidin (Sigma-Aldrich) was added to each slide, covered with a glass coverslip (VWR), and allowed to incubate for 2 h at room temperature in a closed container above a water bath to avoid drying out. The coverslips were removed, and the slides were washed thoroughly with deionized water, followed by 1 M NaCl plus 40 mM NaOH, and again washed with deionized water, then dried under nitrogen. A flow channel about 2-3 mm wide was made between the drilled holes with two strips of double-sided tape, a coverslip was placed on the tape, and the edges were sealed with Epoxy glue (Hardman Adhesives). A schematic of the resulting surface structure is shown in Supplementary Fig. 26. Slides were stored in an evacuated desiccator at 4 °C for up to four weeks.

Fluorescence Microscopy. For the EAC, EABC, and EABD tracks, spider-origami complexes at 10 nM in the annealing buffer were combined with an equal volume of 1 μ M to 10 μ M TRIGGER strand in water and incubated for 30-60 min on ice in the absence of Zn²⁺ ions. The mixture was then diluted to 10 pM in the imaging buffer: for the EAC track, 1 \times SSC or HBS; for EABC and EABD tracks, 1 \times TA-Mg. (Note that for the EABC and EABD tracks, the reduced but non-negligible deoxyribozyme cleavage rate in TA-Mg raises the concern that pre-incubation with TRIGGER may allow some spider movement prior to imaging; however, the reduced temperature would be expected to inhibit such movement.) All buffers used for fluorescence imaging were supplemented with 1 \times -5 \times OSS to reduce the rate of signal loss through fluorophore photobleaching. The spider-origami complexes were immobilized on avidin-coated microscope slides for imaging.

Samples were imaged at room temperature by a prism-based total internal reflection fluorescence microscope with a 1.2 NA 60 \times water objective (IX71, Olympus). Cy3 excitation was provided by a 532-nm green laser (ultra-compact diode-pumped Nd:YAG laser GCL-025-S, CrystaLaser) and Cy5 excitation by a 638-nm red diode laser (Coherent CUBE 635-25C, Coherent Inc.). The Cy3 and Cy5 emission signals were separated by a dichroic mirror with a cutoff of 610 nm (Chroma) and projected side by side onto an ICCD camera chip (iPentamax HQ Gen III, Roper Scientific, Inc.). Relay lenses matched the microscope image with the camera focal plane and the IX71 internal 1.6 \times magnifier (final effective pixel length 133 nm) was used during collection of all traces except EAC 1 and 2 (Supplementary Fig. 29) in which no magnifier was used (effective pixel length 196 nm). The donor channel image was passed through a band pass filter

(HQ580/60m, Chroma) and the acceptor channel was passed through a long pass filter (HQ655LP, Chroma). A cleanup filter (z640/20, Chroma) was placed at the output of the red laser to reject any extraneous or infrared light. A Newport ST-UT2 vibration isolation table was used in all experiments. After introducing imaging buffer without oxygen scavenger to the slide flow channel, a small fluorescent background was observed; this was bleached briefly by exposing the slide to excitation light from both lasers until the background stabilized. The origami sample with oxygen scavenger was then introduced into the sample channel in the dark, allowed to incubate for 2-10 minutes, and the excess flushed out with fresh imaging buffer. The sample was imaged at room temperature with excitation from both lasers using a 1- to 2.5-s signal integration time and a 12.5- to 27.5-s delay (i.e., 2-4 frames per min). After 0-20 min of imaging, depending on the experiment, the same imaging buffer containing or lacking ZnSO_4 was introduced into the flow channel, and the sample was imaged for an additional 60-70 min. For substrate-covered EAC tracks in SSC, the concentration of ZnSO_4 introduced was either 0 or between 1 and 10 mM. For substrate-covered EABD and EABC tracks, the ZnSO_4 concentration was 0 or 1 mM ZnSO_4 . For substrate-covered EAC tracks in $1\times$ HBS, the ZnSO_4 concentration was 0 or 5 mM.

EAC track origami with product-covered tracks were prepared and imaged as described above for the substrate-covered EAC track origami in SSC buffer. Due to concerns about releasing spiders from the START prematurely on product tracks where the walk is independent of cleavage activity, experiments were also conducted in which the spider-origami assemblies were not incubated with TRIGGER 30-60 min prior to imaging, as described above, but instead SSC imaging buffer containing 1 mM ZnSO_4 and 10 μM TRIGGER was added to the sample channel 10-15 min before imaging. In both types of experiments, ZnSO_4 was not introduced until immediately prior to imaging by fluorescence microscopy.

Fitting and Filtering of Particle Tracking Data. Point spread functions (PSFs) of fluorescence emission from individual spiders and origami were imaged by fluorescence microscopy, and their relative positions tracked through time by fitting 2-D Gaussian functions to the PSFs. First, PSFs from Cy3 (spider) and Cy5 (origami) were imaged on spectrally separated halves of the ICCD camera using WinView32 software (Roper Scientific, Inc.). PSFs were identified in the ICCD output and paired with their corresponding partner using methods described previously⁴⁶, resulting in intensity traces such as those shown in Supplementary Figs 29 and 30 that reflect the total photon count per movie frame for each PSF over time. The Cy3 and Cy5 channels were registered with a locally weighted mean mapping⁴³ using fluorescent beads that appear in both channels (Fluospheres, red fluorescent (580/605), 0.2 μm , Molecular Probes FluoSpheres F8801), to establish with ~ 50 -nm accuracy that the Cy3 PSF in each pair was located within 200 nm of its Cy5 partner. To ensure adequate

signal intensity and duration for tracking, candidate PSF pairs were only included in the analysis if they met both of the following criteria:

1. Cy3 and Cy5 signal of more than 1,000 photon counts per frame for at least 25 min (1-33% of all pairs fulfilled this criterion per experiment)
2. No erratic signal intensities such as from excessive blinking or nearby unresolved PSFs (23-95% of all remaining pairs fulfilled this criterion per experiment)

Traces that were discarded based on low or absent signal intensity from either Cy3 or Cy5 likely resulted from incompletely labeled spider-origami complexes, fragmented or disassembled complexes, or other fluorescent contaminants. Each PSF in the remaining pairs (0.4-22% of all candidate pairs) was fit, frame-by-frame, with a two-dimensional Gaussian function (Supplementary Fig. 27d) of the form:

$$f(x, y) = z_0 + A \exp \left\{ \frac{1}{2} \left[\left(\frac{x - \mu_x}{\sigma_x} \right)^2 + \left(\frac{y - \mu_y}{\sigma_y} \right)^2 \right] \right\} \quad (1)$$

The position values μ_x and μ_y from Gaussian fitting of each Cy5 PSF (Supplementary Fig. 27 e, g) were subtracted, frame-by-frame, from those of its corresponding Cy3 partner. The resulting difference trajectory was then plotted against time for each Cy3-Cy5 pair to show the motion of each spider relative to its Cy5-labeled STOP position (Supplementary Fig. 27 f, h). This subtraction served as a necessary internal drift control since, as shown in Supplementary Fig 27, there was often significant drift through the x-y plane in the course of a typical 30-80 min movie. Brief aberrant position measurements, such as those caused by transient binding of nearby fluorescent contaminants, were identified by a large distance from the median position (> 3 standard deviations in the x or y direction) or sudden displacements of >100 nm within a single frame, and removed. Focal drift throughout an experiment, if severe, sometimes resulted in an apparent motion of Cy3 relative to Cy5 (data not shown). This focal drift was evident visually from the original video image as well as from very asymmetric PSF shapes during Gaussian fitting. Such traces were also discarded.

Probable moving spiders were selected using the following criteria:

1. Relative motion of Cy3 and Cy5 > 45 nm, corresponding to 2-3 times the standard deviation in individual position measurements (33-44% of all fitted pairs fulfilled this criterion per experiment)
2. No discontinuities in position, i.e., sudden jumps in position of 45 nm or greater (89-100% of all fitted pairs fulfilled this criterion per experiment)
3. Apparent movement < 45 nm prior to zinc addition (88-100% of all fitted pairs fulfilled this criterion per experiment)

This process is illustrated in Supplementary Fig. 28 for representative experiments from the EAC, EABC, and EABD constructs. The resulting spiders (22-39% of all fitted traces) are included in Supplementary Fig. 29. Examples of spider trajectories that did not satisfy all three of these criteria are also shown in Supplementary Figs 29 (EAC Tier 2) and 30 (all stationary spiders observed on the EAC track in HBS). A statistical summary of this filtering process for the EAC, EABD, and EABC tracks is presented in Supplementary Table 3.

Representation of Spider Trajectories. To smooth the trajectories for presentation, a 16-frame rolling average was applied separately to the trajectories of Cy3 and Cy5 before subtracting them for drift correction (black line in Supplementary Figs 29b and 30b). The error bars shown in Supplementary Figs 29b and 30b are the standard deviations of the raw trajectory from the temporally corresponding points in the smoothed trajectory. For ease of viewing in Fig. 4a (main text) and Supplementary Fig. 31, the trajectories were instead smoothed with an 8-frame rolling average followed by a 4-frame sequential average before drift correction.

Measurement of Displacement. Net displacement was determined as follows for motion of each spider on the EAC track. An initial position (x_0, y_0) was defined as the arithmetic mean of the first 16 position measurements after the time t_{zinc} at which $ZnSO_4$ or control buffer lacking zinc ions was added ($t = 0$ min in Supplementary Figs 29 and 30). For traces containing data prior to t_{zinc} , the initial position was instead calculated as the mean of the 16 position measurements centered on t_{zinc} (i.e., the interval from frame -7 to frame 8, where t_{zinc} occurs at frame 0). The center time coordinate of this averaged initial position (x_{start}, y_{start}) was designated t_{start} (i.e., the interval from frame -7 to frame 8, where t_{zinc} occurs at frame 0). The distance of (x_{start}, y_{start}) from each subsequent position measurement (x_i, y_i) was then calculated to obtain the spider's net displacement over time (green line, Supplementary Figs 29c and 30c). As has been noted in similar distance determinations⁴³, these displacement measurements are artificially increased when equal to or less than the noise level (hence why displacement typically does not equal 0 nm near $t = 0$ min). Therefore, an analogous displacement vs. time curve was calculated from the smoothed trajectory (black line in Supplementary Figs 29b and 30b) and was plotted as a black line in Supplementary Figs 29c and 30c. This smoothed displacement has a value of zero at t_{start} , resulting in a systematic deviation from the noise-inflated raw curve at low displacements. The time of stopping t_{stop} was defined as the time coordinate of the first local maximum in the smoothed displacement curve that approaches within 20 nm of the global maximum in the smoothed displacement curve (considering only the interval from t_{zinc} to the end of the trace). The value of 20 nm is a typical standard deviation in our position measurements. The total net displacement d (inset box, Supplementary Figs 29b and 30b) was then defined as the smoothed displacement value at t_{stop} . The time of travel Δt was defined as the difference $t_{stop} - t_{start}$, and the mean magnitude of velocity was calculated for each EAC spider as $v = d/\Delta t$ (box,

Supplementary Figs 29b and 30b). The resulting displacement vs. time plots are shown in Supplementary Figs 29c and 30c. The mean position and standard error of the mean (SEM) values from the smoothed x- and y- measurements (black line in Supplementary Figs 29b and 30b) were used to calculate the SEM for each displacement determination by propagation of errors. The values of the SEM were averaged across all displacement determinations in a given trajectory to obtain the overall error in the displacement measurements for that spider (σ , Fig. 4b and Supplementary Figs 29c and 30c).

Interpretation. In some traces we observed movement before addition of Zn^{2+} ; we could not determine whether these represented spiders walking in the absence of Zn^{2+} or were due to other causes. We also observed several moving traces that exhibit net displacements significantly smaller than others, which similarly is consistent with spiders having finished (part of) their tracks early, taking the wrong direction after walking in the absence of Zn^{2+} , prematurely stopping or stalling on the track, and/or taking backward steps onto product. These issues are discussed in more detail below. In the following, we enumerate all independent lines of evidence that these time traces represent genuine walking spiders:

1. The highest density of PSFs we observed in each channel with $\geq 1,000$ photon counts over at least 25 minutes was $0.03 \mu\text{m}^{-2}$. Given this density, the probability that a Cy3 and Cy5 PSF will colocalize to within 200 nm of one another by coincidence is 0.9%⁴⁷. However, in each experiment we observe that, on average, 31% of PSFs in one channel are colocalized with a PSF in the other channel. This strongly suggests that the majority of signals originate from spiders bound to origami.
2. We find most of the trajectories longer than 45 nm to be consistent in length and shape with a progressive walk on the respective track design (Supplementary Figs 28 and 29b). In particular the trajectories observed on the EAC track in SSC buffer, which are nearly linear and often stop nearly 100 nm from the starting position (EAC 1, 2, 4, 5, 9, 12, 13, and 15), are in good agreement with expectations based on the track design.
3. Comparison of experiments to negative controls (such as in Supplementary Figs 28d and 30), rules out instrument drift as the sole source of the observed spider motion.
4. Moving and non-moving spiders are seen alongside each other in experiments conducted in the presence of both Zn^{2+} ion and release strand (Supplementary Fig. 28a-c), providing further fiduciary markers and a strong argument against instrument drift as the cause for movement.
5. Ensemble MSD (Supplementary Fig. 32a) and RMSD plots (Fig. 4c, main text) of the 15 Tier 1 EAC spiders (Supplementary Fig. 29) are consistent with an approximately 100-nm walk across the prescribed linear substrate track.

Especially when considered in combination with the results from our AFM studies, the fluorescence microscopy data are most consistent with processive

walking of individual spiders on DNA origami. While the stopping distances are not strong evidence (filtering precluded walks shorter than 45nm, and photobleaching may have precluded having many walks longer than 100nm), this interpretation is confirmed by control experiments lacking zinc in the buffer and on product tracks, as discussed below.

The large percent of spiders moving less than 45 nm (22-67 % of all PSF pairs fit to Gaussians in a given experiment) likely results from some combination of the following: 1) immobile contaminants that fluoresce in both channels, thus having the appearance of a colocalized Cy3-Cy5 pair; 2) a substantial fraction of inactive or slowly cleaving spider legs, especially in SSC + 1 mM Zn²⁺, 3) failed or delayed release of a spider from the START position, 4) spiders binding initially at the STOP instead of the START position (though precautions against this were taken in the assembly of origami-spider complexes), or 5) undirected, random diffusion of a spider on previously cleaved or damaged substrate. As we cannot distinguish between these possibilities, the estimated percent of non-moving spiders must be taken as an upper bound.

Most of the trajectories from the EAC track show clearly biased, generally linear motion with few or no discontinuities in displacement (Supplementary Fig. 28). However, some spiders exhibit non-monotonically increasing displacements with time (e.g. EAC 5) that could have resulted, for example, from spiders taking steps backwards onto cleavage product. Furthermore, some trajectories exhibit unexplained irregularities in the 2-D motion trajectory, displacement or velocity measurements (Supplementary Fig. 29, EAC 16-19). These issues are described in the captions above the respective traces in Supplementary Fig. 29. For instance, the net displacement values of EAC 16 and 18 at $t > 0$ are less than 45 nm and therefore less reliable. Some putative spiders (EAC 17, 18, and 19) also show significant displacement before addition of Zn²⁺ at $t = 0$. Slight focal drift or an instrumental perturbation might have resulted in an apparent displacement between the PSFs⁴⁸ in these traces, particularly during the addition of Zn²⁺-containing buffer. Although this addition was performed slowly and carefully (generally at a rate of 1 mL/min or less), it occasionally brought the image out of focus. Such slight focal drift could also affect the measurement of net displacement values. For example, similar influences could have given rise to the few trajectories that showed an apparent net displacement larger than the track length of 110 nm (e.g., EAC 10). Alternatively, although the 8-17 deoxyribozyme legs are inactive in 1× SSC lacking ZnSO₄ (see Supplementary Fig. 25), the spider might still exhibit slow diffusion on a surface of substrate. It is also possible that some origami assemblies exhibit rotational dynamics relative to the slide that contribute to the observed motion of PSFs. Finally, the calculation of net displacement for some spiders is likely biased by early photobleaching which may prevent observation of the entire trajectory of the spider (see, for example, EAC 3).

Calculation of Ensemble Mean Square Displacement and Root Mean Square Displacement. To characterize the ensemble behavior of spiders, ensemble mean square displacement (MSD, Supplementary Fig. 32) and root mean square displacement (RMSD, Fig. 4c-d, main text) versus time plots were generated. To calculate the individual displacements plotted in figure 4c-d, and used to calculate the MSD and RMSD, an initial position (x_{start}, y_{start}) was first calculated as the arithmetic mean of the 16 points of the raw trajectory closest to the time at which $ZnSO_4$ or control buffer lacking zinc ions was added, t_{zinc} (i.e., the interval from frame -7 to frame 8 if data were taken before t_{zinc} , or the interval from frame 1 to frame 16, if data acquisition began at t_{zinc}). Trajectory data were averaged separately for Cy3 and Cy5 in (sequential) one-minute intervals, and the averaged trajectory of Cy5 was subtracted from that of Cy3 to correct for microscope stage drift. Each displacement value was then calculated as the distance of each averaged position (x_i, y_i) from the initial position (x_{start}, y_{start}) . This same procedure was applied to data acquired at the rate of two, three, and four frames per minute. The displacement of each spider for each 1-minute time interval was squared and then averaged across all spiders within a given dataset to yield the ensemble MSD as a function of time. The square root of the ensemble MSD was calculated for each time interval to yield the ensemble RMSD as a function of time. Note that outliers were removed from the raw data as described above (Filtering and Fitting of Particle Tracking Data).

For comparison with Tier 1 EAC spiders, MSD and RMSD versus time plots were also generated from the 7 EAC spiders in a no-zinc control experiment on the EAC substrate track in $1\times$ SSC. These spiders were subjected to the same selection criteria as the Tier 1 EAC spiders except that they were not required to move ≥ 45 nm for inclusion in the MSD plot (by this criterion, no moving spiders were observed in this control). Both of these MSD plots are shown in Supplementary Fig. 32a, and the RMSD plots shown in Fig. 4c.

In an attempt to determine the relative impact of substrate cleavage on the motion of EAC spiders (compared to that of the presence of START and STOP sites), control experiments were conducted on EAC tracks covered with cleavage product instead of substrate in $1\times$ SSC and 1 mM $ZnSO_4$. For consistency, identical experimental procedures were applied, including addition of Zn^{2+} immediately prior to imaging (although product walks are not expected to be zinc-dependent). To reduce the risk of bias in comparing these two types of experiments, we employed a less stringent set of selection criteria than those described above. Specifically, all spider trajectories with Cy3 and Cy5 signal intensity above an arbitrary cutoff were retained. Individual data points in a trajectory were discarded if the ellipticity E exceeded 0.3 ($E = 1 - w_{minor}/w_{major}$, where w_{minor} and w_{major} are the full widths at half maximum along the major and minor axes of the fitted 2-D Gaussian function, respectively). Position measurements greater than three standard deviations from the median of all position measurements within a trace in either the x- or y-direction (or 500 nm from the position of the spider when zinc was added, whichever is smaller) were

regarded as outliers and discarded. An application of these more inclusive criteria first to our substrate-covered track data resulted in 85 traces that were converted to the ensemble MSD and RMSD versus time plots described above; the results are shown in Supplementary Fig. 32b and Fig. 4d of the main text (see Supplementary Table 4 for full statistics of selection based on these criteria). The roughly twofold difference in steepness from and less pronounced curvature than the substrate MSD plot in Supplementary Fig. 32a are likely due to the inclusion of a larger number of slow-moving or stationary spiders in Supplementary Fig. 32b.

We found that the ensemble MSD versus time plot for the product-covered linear EAC track in $1\times$ SSC and 1 mM ZnSO_4 , generated using the more inclusive selection criteria above, dramatically depends on whether the TRIGGER was added 10-15 min (short incubation) or 30-60 min before the experiment (long incubation, similar to our protocol for the linear substrate track). In the former case, the MSD plot of 18 spiders increases non-linearly with a concave up slope curvature greater than that seen for the substrate track, while in the latter case, linear behavior with a much shallower slope is observed in an MSD plot of 29 spiders (Supplementary Fig. 32b). Since Zn^{2+} is not predicted to be required for diffusive walking on a product surface, a long pre-incubation with TRIGGER is expected to allow many spiders to prematurely walk and possibly be captured by the STOP site prior to the onset of imaging, resulting in a much lower net displacement over the time window of observation. However, when the TRIGGER is added 10-15 min before the experiment, the spider release from the START position may become rate-limiting to effect an initial delay followed by Brownian diffusion of the released spiders along the track. This possibility prevents a direct comparison of the MSD plot of the latter experiment with that of the linear substrate track in Supplementary Fig. 32b (see also discussion of Monte Carlo simulations below). We therefore conclude that we cannot distinguish the behavior of spiders on substrate- and product-covered tracks with confidence from these experiments except insofar as they respond differently to pre-incubation with the TRIGGER.

As an additional control, MSD versus time plots (Supplementary Fig. 32c) were created for the EAC spiders in HBS buffer shown in Supplementary Fig. 30. The MSD plot begins with the addition of HBS buffer containing 0 mM (EAC 1-21H) or 5 mM (EAC 1-16HZ) ZnSO_4 . As for the MSD of the Tier 1 EAC substrate track spiders observed in $1\times$ SSC, the presence of zinc increases the slope of the MSD versus time plot for spiders in $1\times$ HBS, suggesting that the movement of spiders on the EAC substrate track is zinc-dependent in these buffers.

Monte Carlo simulations of spiders on EAC track. To aid in the interpretation of our experimental results, Monte Carlo simulations of simplified models of spiders walking on EAC tracks were conducted as follows. The spider consists of three legs, each of which can exist in an unbound state or bind a specific substrate or product within a 2-dimensional array based on the EAC track

dimensions. The three legs are constrained to bind substrates within 10 nm (an estimated effective leg span) of all other bound legs, and can bind any such substrate with equal probability as long as that substrate is not already bound by another leg. The spider's body position is taken as the arithmetic mean of the positions of all legs bound to the substrate array.

At each time step of the simulation, each leg acts independently to perform one or more of the following actions:

- If bound to a substrate, it can cleave it or not.
- If it is bound to a substrate or product, it can dissociate or remain bound.
- If it is unbound, it binds a substrate or product within 10 nm of other bound legs within the same timestep of the simulation.

Each of the first two of these actions has an associated probability P_i that can be related to an effective first-order rate constant k_i according to $P_i = (1 - \exp(-k_i \cdot t))$, where t is the length of a timestep, chosen here as 1 second. There are thus three adjustable probability parameters: the probability of cleaving a bound substrate (P_{cleave}), of dissociating from a bound substrate ($P_{off,substrate}$), and of dissociating from a bound product ($P_{off,product}$). The legspan is a fourth adjustable parameter. Note that, for simplicity, it is assumed that hybridization to a new site is instantaneous compared to a timestep, and independent of whether that substrate has been cleaved.

At the beginning of each simulation, the spider is positioned with all three legs bound to substrates (or products) within 10 nm of one end of the track corresponding to the START position. At the opposite end of the track are six non-cleavable substrates which constitute the STOP site. The spider's legs are then allowed to freely cleave, dissociate, and bind substrates and products. The legs must remain within 10 nm of the START end until the spider is released by a TRIGGER event which occurs with a probability $P_{release}$. Each simulation ran for 35 min (2100 time steps).

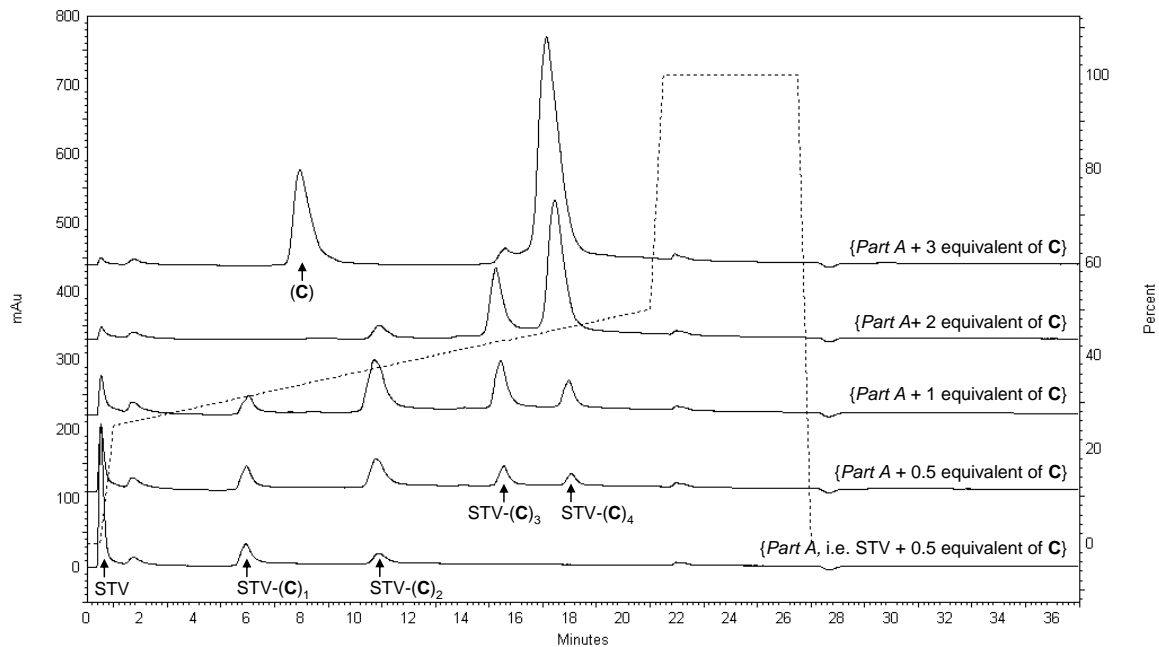
Probabilities for cleavage of and dissociation from substrates were determined from effective first-order rate constants: $k_{cleave} = 1 \text{ min}^{-1}$, $k_{off,substrate} = 0.002 \text{ s}^{-1}$, $k_{off,product} = 0.2 \text{ s}^{-1}$. These rate constants are within one order of magnitude of those determined by bulk fluorescence experiments in 10 mM HEPES, 150 mM NaCl and 1 mM ZnCl₂, pH 7.4 (data not shown), preserve the experimentally observed ratio $k_{off,substrate}/k_{off,product}$, and are compatible with sound principles of nucleic acid thermodynamics and kinetics⁴⁹.

Ensemble MSD versus time curves (Supplementary Fig. 32d) were calculated based on the current spider's body position relative to its first observed position, and are an average over either 20, 80 (thin lines), or 1,000 (thick lines) simulated spider trajectories. When allowed to walk on a linear EAC track containing cleavable substrates, simulated spiders yielded an MSD plot with positive (concave up) curvature, similar to the slightly positive curvature seen in the experimental plots (Supplementary Figs 32a-c). In contrast, when walking on an

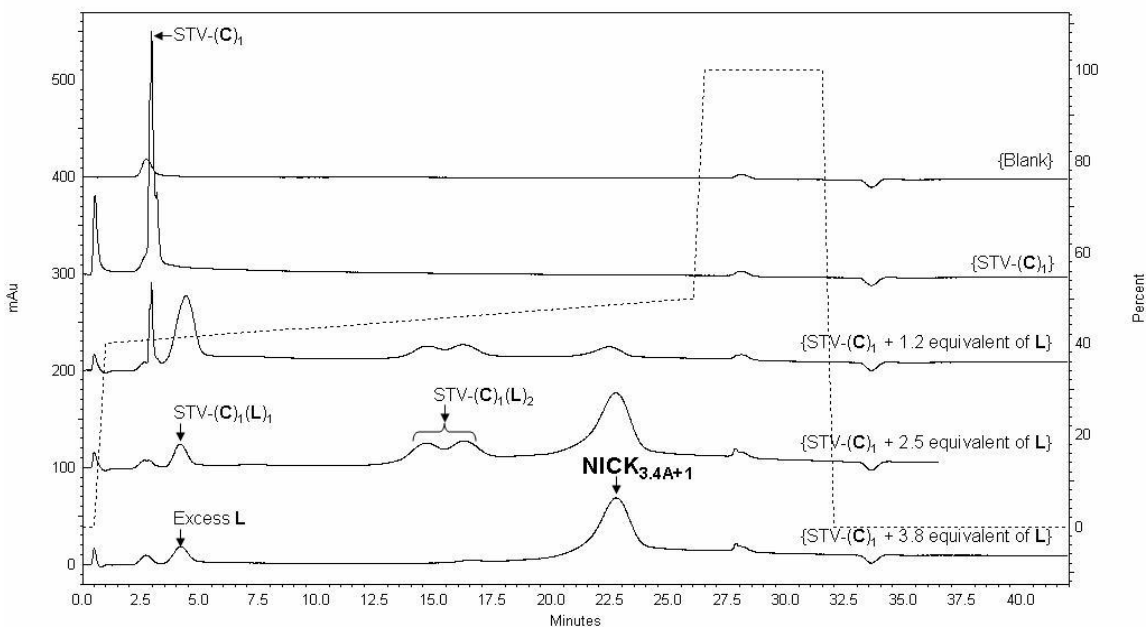
EAC track with cleavage product, the spiders yield an MSD curve that first increases linearly, then asymptotically approaches a maximum value corresponding to the STOP position (spiders undergoing an undirected walk are still able to bind and become trapped at the non-cleavable STOP). However, positive MSD curvature is also obtained from a product track simulation if the spider is released from the START with a half-life of 10 min (rather than immediately), so we cannot rule out a lag phase as contributing to the positive curvature of the experimentally observed ensemble MSD versus time plots. Furthermore, simulations of only 20-80 spiders yielded a fairly broad range of MSD behaviors, often obscuring the idealized curvature and slope; this suggests that our experimental MSD plots, constructed from 85 or fewer spiders, may not represent the fully converged behavior of the system.

The qualitative features of MSD versus time plots generated from these simulations, such as curvature (linear or concave-up) and maximal extent of increase, are robust to variations in k_{off} , and k_{cleave} at least one order of magnitude about their experimentally observed values. However, the precise values of the parameters can affect the slope of the MSD versus time plots. The relative slopes of product and substrate walks are quite sensitive to the effective legspan parameter. Furthermore, the introduction of unequal association probabilities for substrate and product can affect the slope and curvature of these plots. Still, these simulations show that the observed ensemble MSD versus time behavior for the linear EAC substrate track is consistent with the proposed mechanism of spider locomotion based on reasonable kinetic parameters, even if other mechanisms cannot be conclusively ruled out.

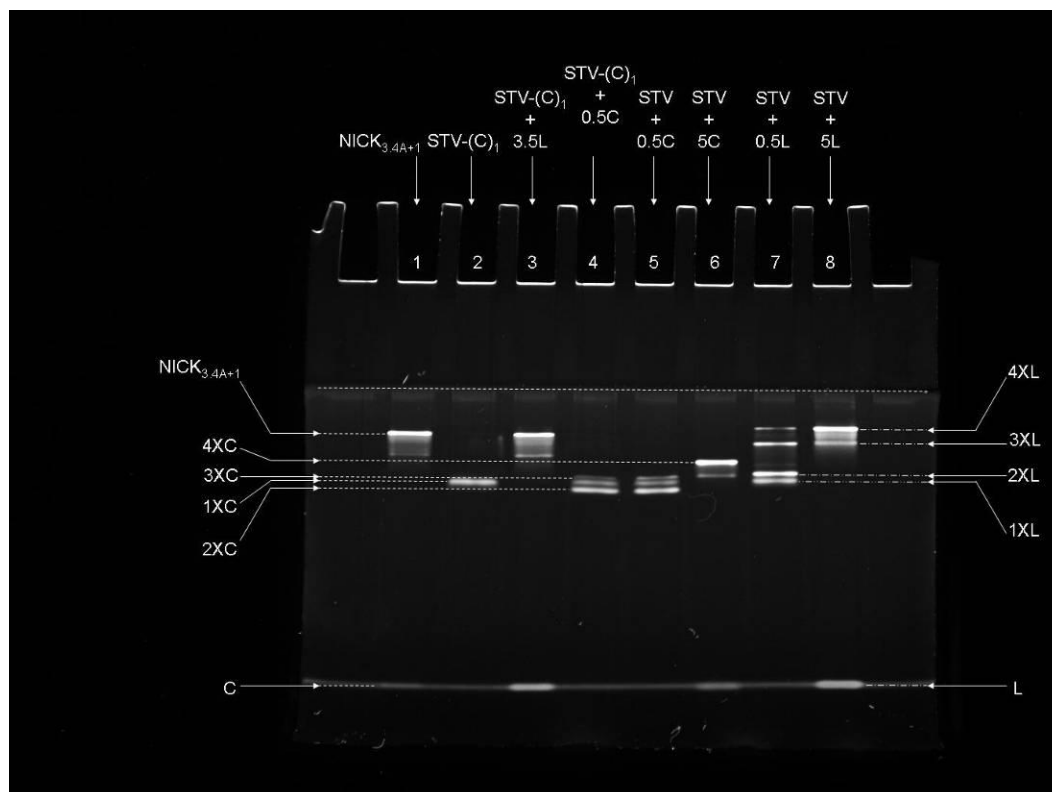
Supplementary Figure 1 | IE HPLC trace showing: ‘Part A’ mixture for NICK_{3.4A+1} from which “STV-(C)₁” was isolated (lowest trace); Other traces show the ‘Part A’ mixture with increasing amounts of C added (Note: “equivalent” amounts were based on the reported lyophilized amount of product supplied and not determined by absorption at 260 nm, which likely accounts for the introduction of a systematic error in the actual number of equivalents as observed by excess oligonucleotide present in the top trace). The 260nm/280nm ratios for the peaks of the middle trace are (left-to-right) 1.06, 1.28, 1.39, and 1.44, consistent with each consecutive peak containing a higher ratio of DNA-to-streptavidin than the peak preceding it. The 260nm/280nm ratio for peak “(C)” is 1.94, consistent with the absorption characteristics of pure DNA. See right y-axis for buffer B gradient (dotted line) as a percentage of buffers A plus B. Buffer A was composed of 20 mM TRIS, and buffer B, 20 mM TRIS/1 M NaCl, both adjusted to pH 7.4. The total flow rate of buffer A and B was 1 min⁻¹.



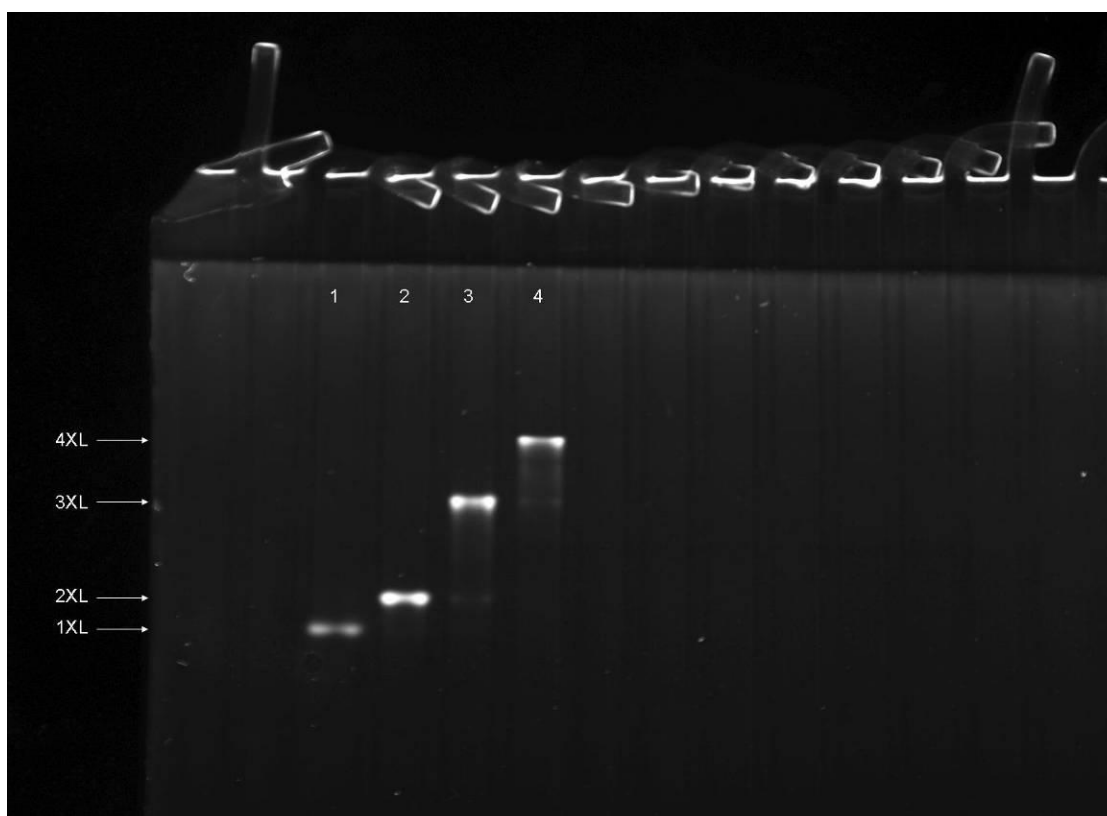
Supplementary Figure 2| IE HPLC trace showing titration of STV-(C)₁ with increasing equivalents of L. 260nm/280nm ratios are STV-(C)₁ 1.09; STV-(C)₁(L)₁ 1.38; STV-(C)₁(L)₂ 1.53 and 1.49 (taken at the two apparent maxima respectively for STV-(C)₁(L)₂); **NICK**_{3,4A+1} 1.59; and **L** 2.05 (see caption for Supplementary Fig. 1 for explanation of absorption wavelength ratio 260/280). See right y-axis for buffer B gradient (dotted line) as a percentage of buffers A plus B. Buffer A was composed of 20 mM TRIS, and buffer B, 20 mM TRIS/1 M NaCl, both adjusted to pH 7.4. The total flow rate of buffer A and B was 1 min⁻¹.



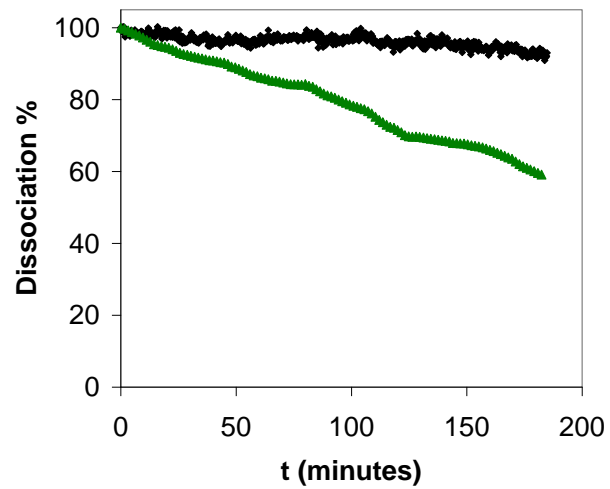
Supplementary Figure 3 | Gel characterization of spider assembly. PAGE characterization of **NICK_{3,4A+1}** showing that isolated **NICK_{3,4A+1}** (lane 1) contains the strand C, i.e. the capture strand 5' - GCC GAG AAC CTG ACG CAA GT/iSp18//iSp18//3Bio/ - 3', and strand L, i.e. the deoxyribozyme or "leg" strand 5' - /5BioTEG//iSp18//iSp18/TCT CTT CTC CGA GCC GGT CGA AAT AGT GAA AA - 3' in a ratio of 1:3. Native stacking gel with a 12% acrylamide separation layer and a 4% acrylamide stacking layer; running buffer is TRIS-glycine. Bands were stained with SYBR Gold (Invitrogen). STV is streptavidin. 1XC is an assembly consisting of one streptavidin conjugated to one capture strand C, 2XC is an assembly consisting of one streptavidin conjugated to two capture strands, etc (assignments of bands 1XC, 2XC, 3XC, and 4XC are made based on results shown in Supplementary Fig. 1). Lane 1 is the isolated **NICK_{3,4A+1}** assembly; Lane 2 is the isolated streptavidin-(mono)capture strand conjugate (STV-(C)₁) used to form **NICK_{3,4A+1}** by adding the "leg" strand L to the three remaining biotin binding sites; Lane 3 is the unpurified result on adding 3.5 equivalents of "leg" strand, L, to STV-(C)₁; Lane 4 is the titration of a half equivalent of C with STV-(C)₁ showing migration distances of STV-(C)_n (where n = 1-3); Lane 5 is the titration of a half equivalent of C with STV; Lane 6 the titration of a excess C with STV; Lane 7 is the titration of a half equivalent of L with STV, where 1XL is an assembly consisting of one streptavidin conjugated to one "leg" strand L, 2XL is an assembly consisting of one streptavidin conjugated to two "leg" strands L etc. (assignments of bands 1XL, 2XL, 3XL, and 4XL are made based on results shown in Supplementary Fig. 4 and in reference 20); Lane 8 is the titration of excess L with STV.



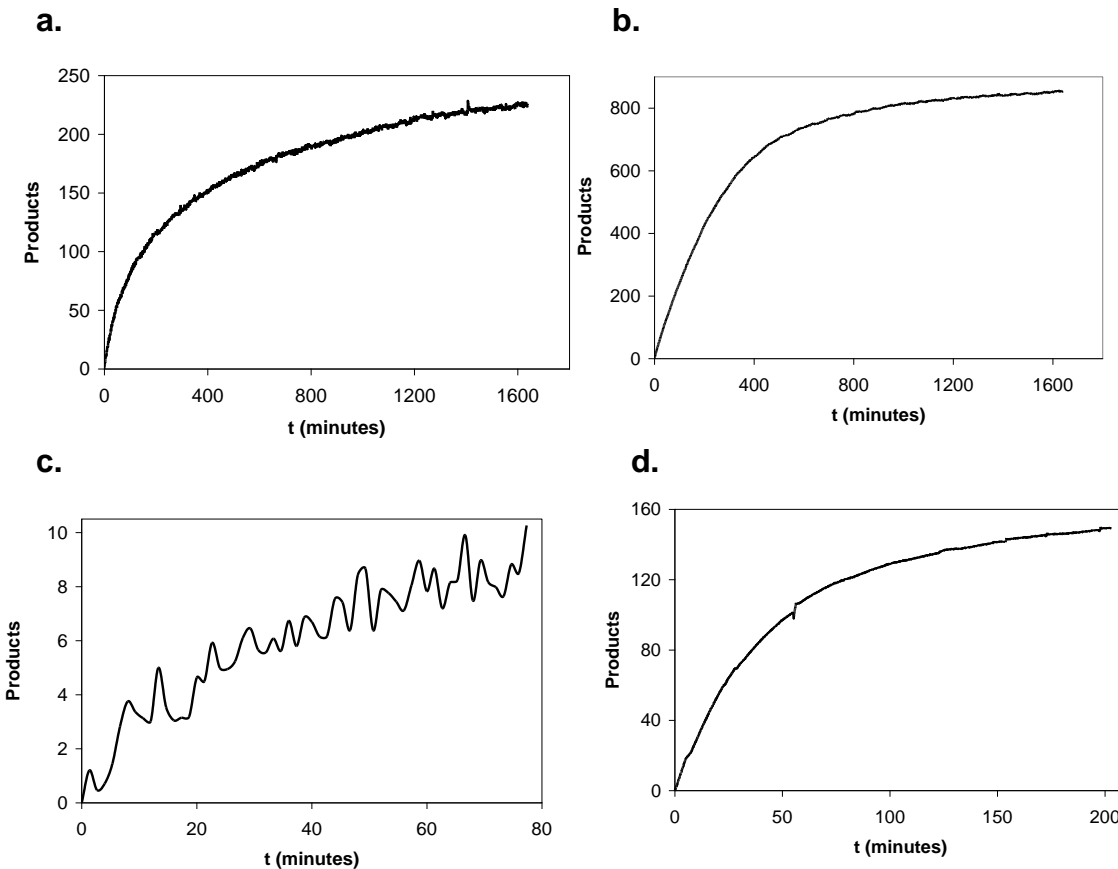
Supplementary Figure 4 | Gel characterization of assembled spiders. PAGE characterization of $\text{NICK}_{n,4A}$ (where $n = 1\text{-to-}4$) supporting assignments of lane 8 in Supplementary Fig. 3. Native stacking gel with a 10% acrylamide separation layer and a 4% acrylamide stacking layer; running buffer is TRIS-glycine. Bands were stained with SYBR Gold (Invitrogen). STV-(L) $_n$ conjugates used in this gel were isolated and characterized as previously described above (Supplementary Fig. 1). 1XL is an assembly consisting of one streptavidin conjugated to one “leg” (i.e. deoxyribozyme strand L), 2XL is an assembly consisting of one streptavidin conjugated to two “legs,” etc.



Supplementary Figure 5 | Spider dissociation. Dissociation curves for **NICK_{3.4A+1}** spider from non-cleavable substrate (black trace, 1:89 ratio of spider to substrate) and product (green trace, 1:97 ratio of spider to product) on the 2D monolayer surfaces.



Supplementary Figure 6 | Spider cleavage sensorgrams. **a.** Sensorgram (y-axis is products released per spider, the number of products released was obtained by conversion of SPR response unit (RU) to mass using the standard formula $1,000 \text{ RU} = 1 \text{ ng} \cdot \text{mm}^{-2}$) of **NICK_{3.4A+1}** spider on the 2D monolayer surface showing the real-time substrate cleavage at a 1:291 ratio of spider to substrate with a cleavage rate of 1.42 min^{-1} per spider in $1 \times$ TA-Mg buffer with 1 mM ZnCl_2 . **b.** Sensorgram of **NICK_{3.4A+1}** spider on the pseudo-2D matrix surface showing the real-time substrate cleavage at a 1:990 ratio of spider to substrate with a cleavage rate of 2.81 min^{-1} per spider in $1 \times$ TA-Mg buffer with 1 mM ZnCl_2 . **c.** Sensorgram of **NICK_{3.4A+1}·(Cy3)₄** spider on the pseudo-2D matrix surface showing the real-time substrate cleavage at a 1:50 ratio of spider to substrate with a cleavage rate of 0.18 min^{-1} per spider in $1 \times$ SSC with 2 mM ZnSO_4 . **d.** Sensorgram of **NICK_{3.4A+1}·(Cy3)₄** spider on the pseudo-2D matrix surface showing the real-time substrate cleavage at a 1:180 ratio of spider to substrate with a cleavage rate of 2.72 min^{-1} per spider in HBS buffer with 1 mM ZnSO_4 . All cleavage reactions were monitored with a flow rate of $20 \mu\text{L}/\text{min}$.

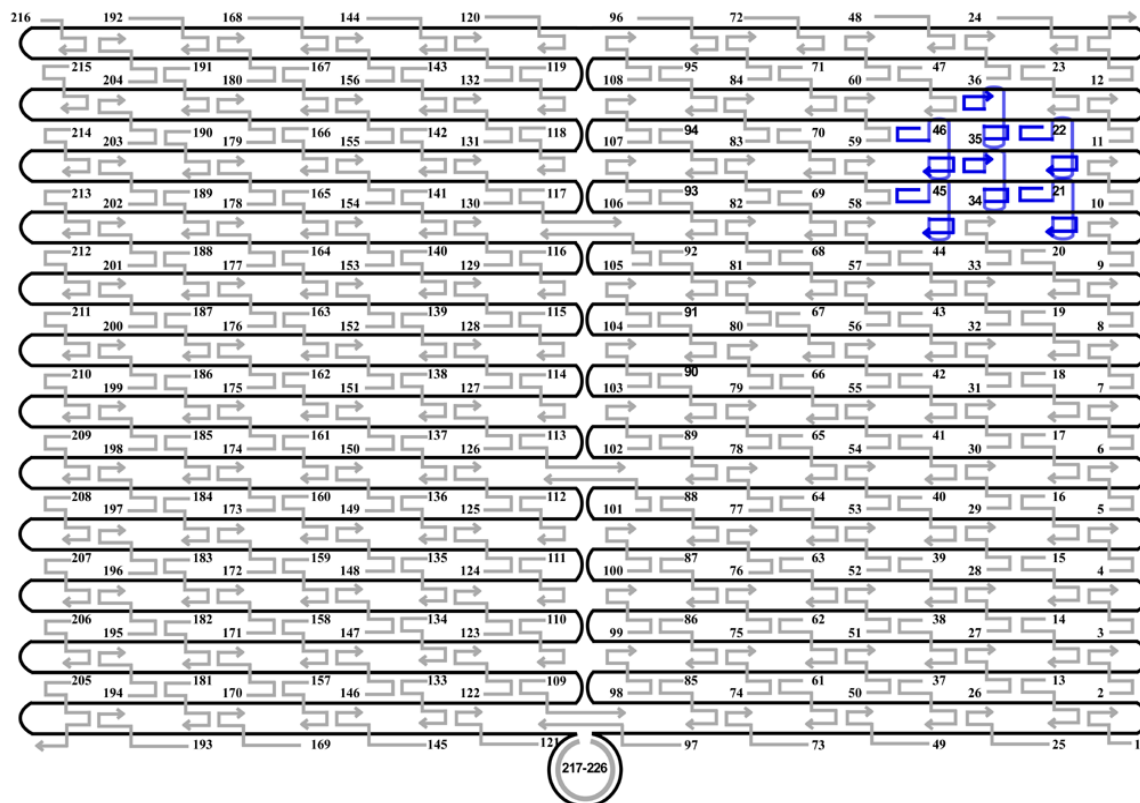


DNA Sequences

M13mp18 sequence can be found at the following web-address http://www.neb.com/nebecomm/tech_reference/restriction_enzymes/sequences/m13mp18.txt.

Supplementary Figure 7 | Schematic of the rectangular shaped DNA origami structure with the staple strand location and numbering marked.

This is a representation of a plain origami structure with the marker included. In this drawing, the continuous black colored strand represents circular M13 viral genome and all the staple strands are shown in grey with arrows pointing the 3'-ends of the sequences. Numbers denote the sequence of the strands below. The blue strands denote the dumbbell hairpins used as a marker to aid in identification of origami by AFM.



Name Sequence

- 1 TTTTCGATGGCCCACTACGTAAACCGTC
- 2 TATCAGGGTTTTTCGGTTTGCGTATTGGGAACGCGCG
- 3 GGGAGAGGTTTTTGTAAAACGACGGCCATTCCCAGT
- 3A GGGAGAGGTTTTTGTAAAAC
- 3B Biotin GACGGCCATTCCCAGT
- 4 CACGACGTTTTTGTAAATGGGATAGGTCAAACGGCG
- 5 GATTGACCTTTTGATGAACGGTAATCGTAGCAAACA
- 6 AGAGAATCTTTTGGTTGTACCAAAAACAAGCATAAA

7 GCTAAATCTTTTCTGTAGCTCAACATGTATTGCTGA
8 ATATAATGTTTTATTGAATCCCCCTCAAATCGTCA
9 TAAATATTTTTTGGGAAGAAAATCTACGACCAGTCA
10 GGACGTTGTTTTTCATAAGGGAACCGAAAGGCGCAG
11 ACGGTCAATTTTGACAGCATCGGAACGAACCCTCAG
11A ACGGTCAATTTTGACAGCAT
11B Biotin CGGAACGAACCCTCAG
12 CAGCGAAAATTTTACTTTCAACAGTTTCTGGGATTTTGCTAAACTTTT
13 TGGTTTTTAACGTCAAAGGGCGAAGAACCATC
14 CTTGCATGCATTAATGAATCGGCCCGCCAGGG
15 TAGATGGGGGGTAACGCCAGGGTTGTGCCAAG
16 CATGTCAAGATTCTCCGTGGGAACCGTTGGTG
17 CTGTAATATTGCCTGAGAGTCTGGAAAAGTAG
18 TGCAACTAAGCAATAAAGCCTCAGTTATGACC
19 AACAGTTGATGGCTTAGAGCTTATTTAAATA
20 ACGAACTAGCGTCCAATACTGCGGAATGCTTT
21 CTTTGAAAAGAACTGGTCCTCTTTTGAGGAACAAGTTTTCTTGT
CTCATTATTTAATAAA
22 ACGGCTACTTACTTAGTCCTCTTTTGAGGAACAAGTTTTCTTGT
CCGGAACGCTGACCAA
23 GAGAATAGCTTTTGCGGGATCGTCGGGTAGCA
24 ACGTTAGTAAATGAATTTTCTGTAAGCGGAGT
25 ACCCAAATCAAGTTTTTTGGGGTCAAAGAACG
26 TGGACTCCCTTTTACCAGTGAGACCTGTCGT
27 GCCAGCTGCCTGCAGGTCGACTCTGCAAGGCG
28 ATTAAGTTCGCATCGTAACCGTGCGAGTAACA
29 ACCCGTCGTCATATGTACCCCGGTAAAGGCTA
30 TCAGGTCACTTTTGCGGGAGAAGCAGAATTAG
31 CAAAATTAAGTACGGTGTCTGGAAGAGGTCA
32 TTTTTGCGCAGAAAACGAGAATGAATGTTTAG
33 ACTGGATAACGGAACAACATTATTACCTTATG
34 CGATTTTAGAGGACAGTCCTCTTTTGAGGAACAAGTTTTCTTGT
ATGAACGGCGCGACCT
35 GCTCCATGAGAGGCTTTTCTCTTTTGAGGAACAAGTTTTCTTGT
TGAGGACTAGGGAGTT
36 AAAGGCCGAAAGGAACAACACTAAAGCTTTCCAG
37 AGCTGATTACAAGAGTCCACTATTGAGGTGCC
38 CCCGGGTACTTTCCAGTCGGGAAACGGGCAAC
39 GTTTGAGGGAAAGGGGGATGTGCTAGAGGATC
40 AGAAAAGCAACATTAATGTGAGCATCTGCCA
41 CAACGCAATTTTTGAGAGATCTACTGATAATC
42 TCCATATACATACAGGCAAGGCAACTTTATTT
43 CAAAATCATTGCTCCTTTTGATAAGTTTCAT
44 AAAGATTCAGGGGGTAATAGTAAACCATAAAT
45 CCAGGCGCTTAATCATTCTCTTTTGAGGAACAAGTTTTCTTGT
TGTGAATTACAGGTAG

46 TTTTCATGAAAATTGTGTCCTCTTTTGAGGAACAAGTTTTCTTGT
TCGAAATCTGTACAGA
47 AATAATAAGGTGCGCTGAGGCTTGCAAAGACTT
48 CGTAACGATCTAAAGTTTTGTCGTGAATTGCG
49 GTAAAGCACTAAATCGGAACCCCTAGTTGTTCC
50 AGTTTGGAGCCCTTCACCGCCTGGTTGCGCTC
51 ACTGCCCCGCCGAGCTCGAATTCGTTATTACGC
52 CAGCTGGCGGACGACGACAGTATCGTAGCCAG
53 CTTTCATCCCCAAAAACAGGAAGACCGGAGAG
53A CTTTCATCCCCAAAA
53B Biotin CAGGAAGACCGGAGAG
54 GGTAGCTAGGATAAAAATTTTTAGTTAACATC
55 CAATAAATACAGTTGATTCCCAATTTAGAGAG
56 TACCTTTAAGGTCTTTACCCTGACAAAGAAGT
57 TTTGCCAGATCAGTTGAGATTTAGTGGTTTAA
57A TTTGCCAGATCAGTTG
57B Biotin AGATTTAGTGGTTTAA
58 TTTCAACTATAGGCTGGCTGACCTTGTATCAT
59 CGCCTGATGGAAGTTTCCATTAAACATAACCG
60 ATATATTCTTTTTTTCACGTTGAAAATAGTTAG
61 GAGTTGCACGAGATAGGGTTGAGTAAGGGAGC
62 TCATAGCTACTCACATTAATTGCGCCCTGAGA
63 GAAGATCGGTGCGGGCCTCTTCGCAATCATGG
64 GCAAATATCGCGTCTGGCCTTCCTGGCCTCAG
65 TATATTTTAGCTGATAAATTAATGTTGTATAA
66 CGAGTAGAACTAATAGTAGTAGCAAACCCCTCA
67 TCAGAAGCCTCCAACAGGTCAGGATCTGCGAA
68 CATTCAACGCGAGAGGCTTTTGCATATTATAG
69 AGTAATCTTAAATTGGGCTTGAGAGAATACCA
70 ATACGTAAAAGTACAACGGAGATTTTCATCAAG
71 AAAAAAGGACAACCATCGCCCACGCGGGTAAA
72 TGTAGCATTCCACAGACAGCCCTCATCTCCAA
73 CCCCATTAGAGCTTGACGGGGAATCAAAA
74 GAATAGCCGCAAGCGGTCCACGCTCCTAATGA
75 GTGAGCTAGTTTCTGTGTGAAATTTGGGAAG
76 GGCGATCGCACTCCAGCCAGCTTTGCCATCAA
77 AAATAATTTTAAATTGTAAACGTTGATATTCA
78 ACCGTTCTAAATGCAATGCCTGAGAGGTGGCA
79 TCAATTCTTTTAGTTTGACCATTACCAGACCG
80 GAAGCAAAAAAGCGGATTGCATCAGATAAAAA
81 CCAAATATAATGCAGATACATAAACACCAGA
82 ACGAGTAGTGACAAGAACCGGATATACCAAGC
83 GCGAAACATGCCACTACGAAGGCATGCGCCGA
84 CAATGACACTCCAAAAGGAGCCTTACAACGCC
85 CCAGCAGGGGCAAAATCCCTTATAAAGCCGGC
86 GCTACAATGTAAAGCCTGGGGTGGGTTTGCC

87 GCTTCTGGTCAGGCTGCGCAACTGTGTTATCC
88 GTTAAAATTTTAACCAATAGGAACCCGGCACC
89 AGGTAAAGAAATCACCATCAATATAATATTTT
90 TCGCAAATGGGGCGCGAGCTGAAATAATGTGT
91 AAGAGGAACGAGCTTCAAAGCGAAGATACATT
92 GGAATTACTCGTTTACCAGACGACAAAAGATT
93 CCAAATCACTTGCCCTGACGAGAACGCCAAAA
94 AAACGAAATGACCCCCAGCGATTATTCATTAC
95 TCGGTTTAGCTTGATACCGATAGTCCAACCTA
96 TGAGTTTCGTCAACCAGTACAACTTAATTGTA
97 GAACGTGGCGAGAAAGGAAGGGAACAACTAT
98 CCGAAATCCGAAAATCCTGTTTGAAGCCGGAA
99 GCATAAAGTTCCACACAACATACGAAGCGCCA
100 TTCGCCATTGCCGGAAACCAGGCATTAATCA
101 GCTCATTTTTCGCATTAAATTTTTGAGCTTAGA
102 AGACAGTCATTCAAAGGGTGAGAAGCTATAT
103 TTTCATTTGGTCAATAACCTGTTTATATCGCG
103A TTTCATTTGGTCAATA
103B Biotin ACCTGTTTATATCGCG
104 TTTTAATTGCCCGAAAGACTTCAAACACTAT
105 CATAACCCGAGGCATAGTAAGAGCTTTTTAAG
106 GAATAAGGACGTAACAAAGCTGCTCTAAAACA
107 CTCATCTTGAGGCAAAGAATACAGTGAATTT
108 CTAAACATCAGCTTGCTTTCGAGCGTAACAC
109 ACGAACCAAAACATCGCCATTAATGGTGGTT
110 CGACAACCTAAGTATTAGACTTTACAATACCGA
111 CTTTTACACAGATGAATATACAGTAAACAATT
112 TTAAGACGTTGAAAACATAGCGATAACAGTAC
113 GCGTTATAGAAAAGCCTGTTTAGAAGGCCGG
114 ATCGGCTGCGAGCATGTAGAAACCTATCATAT
115 CCTAATTTACGCTAACGAGCGTCTAATCAATA
116 AAAAGTAATATCTTACCGAAGCCCTTCCAGAG
117 TTATTCATAGGGAAGGTAAATATTCATTCAGT
118 GAGCCGCCCCACCACCGGAACCGCGACGGAAA
119 AATGCCCCGTAACAGTGCCCGTATCTCCCTCA
120 CAAGCCCAATAGGAACCCATGTACAAACAGTT
121 CGGCCTTGCTGGTAATATCCAGAACGAACTGA
122 TAGCCCTACCAGCAGAAGATAAAAACATTTGA
123 GGATTTAGCGTATTAAATCCTTTGTTTTCAGG
124 TTTAACGTTTCGGGAGAAACAATAATTTTCCCT
125 TAGAATCCCTGAGAAGAGTCAATAGGAATCAT
126 AATTACTACAAATTCTTACCAGTAATCCCATC
127 CTAATTTATCTTTCCTTATCATTATCCTGAA
128 TCTTACCAGCCAGTTACAAAATAAATGAAATA
129 GCAATAGCGCAGATAGCCGAACAATTCAACCG
130 ATTGAGGGTAAAGGTGAATTATCAATCACCGG

128 AACCAGAGACCCTCAGAACCGCCAGGGGTCAG
132 TGCCTTGACTGCCTATTTTCGGAACAGGGATAG
133 AGGCGGTCATTAGTCTTTAATGCGCAATATTA
134 TTATTAATGCCGTCAATAGATAATCAGAGGTG
135 CCTGATTGAAAGAAATTGCGTAGACCCGAACG
136 ATCAAAATCGTCGCTATTAATTAACGGATTCTG
137 ACGCTCAAAATAAGAATAAACACCGTGAATTT
138 GGTATTAAGAACAAGAAAAATAATTAAGCCA
139 ATTATTTAACCCAGCTACAATTTTCAAGAACG
140 GAAGGAAAATAAGAGCAAGAAACAACAGCCAT
141 GACTTGAGAGACAAAAGGGCGACAAGTTACCA
142 GCCACCACTCTTTTCATAATCAAACCGTCACC
143 CTGAAACAGGTAATAAGTTTTAACCCCTCAGA
144 CTCAGAGCCACCACCCTCATTTTCCTATTATT
145 CCGCCAGCCATTGCAACAGGAAAAATATTTTT
146 GAATGGCTAGTATTAACACCGCCTCAACTAAT
147 AGATTAGATTTAAAAGTTTGAGTACACGTAAA
148 ACAGAAATCTTTGAATACCAAGTTCCTTGCTT
149 CTGTAAATCATAGGTCTGAGAGACGATAAATA
150 AGGCGTTACAGTAGGGCTTAATTGACAATAGA
151 TAAGTCCTACCAAGTACCGCACTCTTAGTTGC
152 TATTTTGCTCCCAATCCAAATAAGTGAGTTAA
153 GCCCAATACCGAGGAAACGCAATAGGTTTACC
154 AGCGCCAACCATTTGGGAATTAGATTATTAGC
155 GTTTGCCACCTCAGAGCCGCCACCGATACAGG
156 AGTGTACTTGAAAGTATTAAGAGGCCGCCACC
157 GCCACGCTATACGTGGCACAGACAACGCTCAT
158 ATTTTGCGTCTTTAGGAGCACTAAGCAACAGT
159 GCGCAGAGATATCAAATTATTTGACATTATC
160 TAACCTCCATATGTGAGTGAATAAACAAAATC
160A TAACCTCCATATGTGA
160B Biotin GTGAATAAACAAAATC
161 CATATTTAGAAATACCGACCGTGTTACCTTTT
162 CAAGCAAGACGCGCCTGTTTATCAAGAATCGC
163 TTTTGTTTAAGCCTTAAATCAAGAATCGAGAA
164 ATACCCAAGATAACCCACAAGAATAAACGATT
164A ATACCCAAGATAACCC
164B Biotin ACAAGAATAAACGATT
165 AATCACCAAATAGAAAATTCATATATAACGGA
166 CACCAGAGTTTCGGTCATAGCCCCCGCCAGCAA
167 CCTCAAGAATACATGGCTTTTGATAGAACCAC
168 CCCTCAGAACCGCCACCCTCAGAACTGAGACT
169 GGAAATACCTACATTTTGACGCTCACCTGAAA
170 GCGTAAGAGAGAGCCAGCAGCAAAAAGGTTAT
171 CTAATAAGAAACAAGAAACCACCAGGGTTAG
172 AACCTACCGCGAATTATTCATTTCCAGTACAT

173 AAATCAATGGCTTAGGTTGGGTTACTAAATTT
174 AATGGTTTACAACGCCAACATGTAGTTCAGCT
175 AATGCAGACCGTTTTTATTTTCATCTTGCGGG
176 AGGTTTTGAACGTCAAAAATGAAAGCGCTAAT
177 ATCAGAGAAAGAACTGGCATGATTTTATTTTG
178 TCACAATCGTAGCACCATACCATCGTTTTCA
179 TCGGCATTCCGCCGCCAGCATTGACGTTCCAG
180 TAAGCGTCTGAAGGATTAGGATTAGTACCGCCA
181 CTAAAGCAAGATAGAACCCTTCTGAATCGTCT
182 CGGAATTATTGAAAGGAATTGAGGTGAAAAAT
183 GAGCAAAAACCTTCTGAATAATGGAAGAAGGAG
184 TATGTAACCTTTTTTAATGGAAAAATTACCT
185 AGAGGCATAATTTTCATCTTCTGACTATAACTA
186 TCATTACCCGACAATAAACACATATTTAGGC
187 CTTTACAGTTAGCGAACCTCCCGACGTAGGAA
188 TTATTACGGTCAGAGGGTAATTGAATAGCAGC
189 CCGGAAACACACCACGGAATAAGTAAGACTCC
190 TGAGGCAGGCGTCAGACTGTAGCGTAGCAAGG
191 TGCTCAGTCAGTCTCTGAATTTACCAGGAGGT
192 TATCACCGTACTCAGGAGGTTTAGCGGGGTTT
193 GAAATGGATTATTTACATTGGCAGACATTCTG
194 GCCAACAGTCACCTTGCTGAACCTGTTGGCAA
195 ATCAACAGTCATCATATTCCTGATTGATTGTT
196 TGGATTATGAAGATGATGAAACAAAATTTTCAT
197 TTGAATTATGCTGATGCAAATCCACAAATATA
198 TTTTAGTTTTTCGAGCCAGTAATAAATTCTGT
199 CCAGACGAGCGCCCAATAGCAAGCAAGAACGC
200 GAGGCGTTAGAGAATAACATAAAAAGAACCCC
201 TGAACAAACAGTATGTTAGCAAACCTAAAAGAA
202 ACGCAAAGGTCACCAATGAAACCAATCAAGTT
203 TGCCTTTAGTCAGACGATTGGCCTGCCAGAAT
204 GGAAAGCGACCAGGCGGATAAGTGAATAGGTG
205 AAACCCTCTTTTACCAGTAATAAAAGGGATTACCAGTCACACGTTTT
206 GATGGCAATTTTAATCAATATCTGGTCACAAATATC
206A GATGGCAATTTTAATCAATA
206B Biotin TCTGGTCACAAATATC
207 AAAACAAATTTTTTTCATCAATATAATCCTATCAGAT
208 ACAAGAATTTTATTAATTACATTTAACACATCAAG
209 TAAAGTACTTTTTCGCGAGAAAACTTTTATCGCAAG
210 TATAGAAGTTTTTCGACAAAAGGTAAAGTAGAGAATA
211 GCGCATTATTTTGCTTATCCGGTATTCTAAATCAGA
212 TACATACATTTTGACGGGAGAATTAACACTACAGGGAA
213 AGCACCGTTTTTTAAAGGTGGCAACATAGTAGAAAA
214 ACAACAATTTTAATCAGTAGCGACAGATCGATAGC
214A ACAACAATTTTAATCAGTA
214B Biotin GCGACAGATCGATAGC

215 AGGGTTGATTTTATAAATCCTCATTAAATGATATTC
 216 TTTTATAAGTATAGCCCGGCCGTCGAG
 217 AACATCACTTGCCTGAGTAGAAGAACT
 218 TGTAGCAATACTTCTTTGATTAGTAAT
 219 AGTCTGTCCATCACGCAAATTAACCGT
 220 ATAATCAGTGAGGCCACCGAGTAAAAG
 221 ACGCCAGAATCCTGAGAAGTGTTTTT
 222 TTAAAGGGATTTTAGACAGGAACGGT
 223 AGAGCGGGAGCTAAACAGGAGGCCGA
 224 TATAACGTGCTTTCCTCGTTAGAATC
 225 GTECTATGGTTGCTTTGACGAGCACG
 226 GCGCTTAATGCGCCGCTACAGGGCGC

The following three sequences are attached to the 5' end of the staple sequences, as a probe, for the START position, binding of the cleavable substrate, and binding of the non-cleavable substrate. For fluorescence microscopy, strands 3A, 3B, 11A, 11B, 206A, 206B, 214A, 214B were incorporated into the origami and CONTROL staples were replaced with staples lacking the non-cleave-able substrate probes.

Spider START (green)

5'- GATGTCTACTTGCGTCAGGTTCTCGGC[staple]

Spider Cleavable Substrate Probes (brown)

5'- CCTCTCACCCACCATTCATC[staple]

Spider Non-Cleavable Substrate Probes (for STOP and CONTROL; red)

5'- GGTTTCAGTTCGTTGAGCCAG[staple]

Spider Cleavable Substrate

5'- GATGAATGGTGGGTGAGAGGTTTTTCACTATrAGGAAGAG

Spider Non-Cleavable Substrate (STOP and CONTROL)

5'- CTGGCTCAACGAACTGAACC TTTTTCCTACTATAGGAAGAG

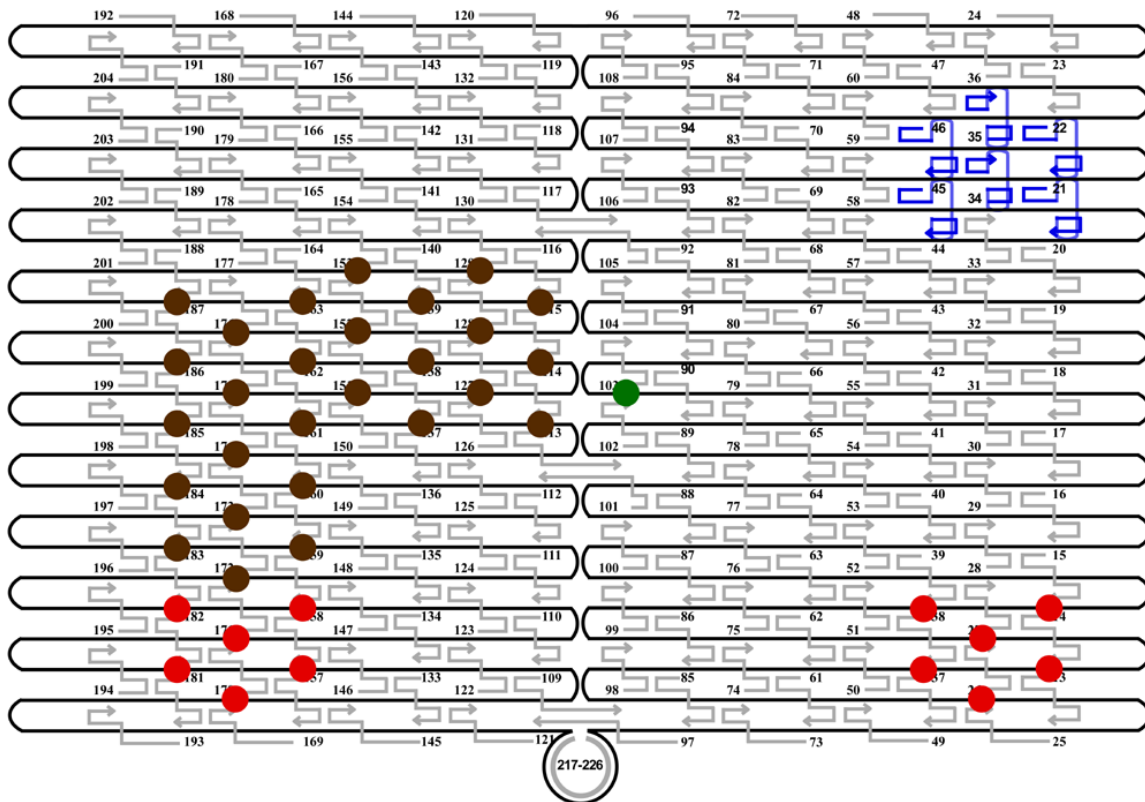
Spider Non-Cleavable Substrate (STOP) for fluorescence microscopy

5'- CTGGCTCAACGAACTGAACC TTTTTCCTACTATAGGAAGAG-Cy5

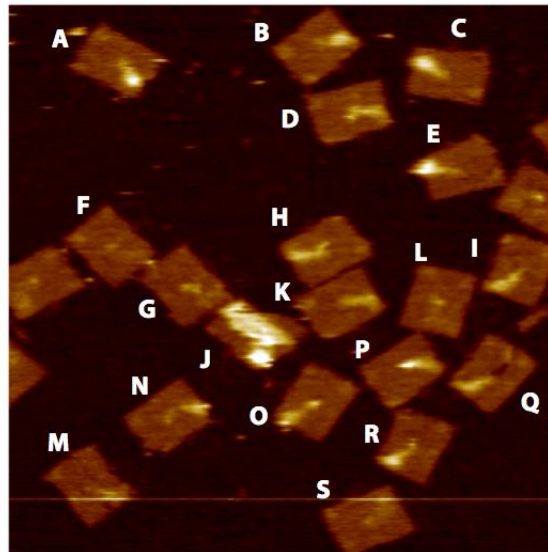
Spider TRIGGER Strand

5'- GCCGAGAACCTGACGCAAGTAGACATC

Supplementary Figure 8 | Schematic of the ABD origami design. Green represents the START position, brown the probes for the substrate, and red the probes for the STOP and CONTROL.

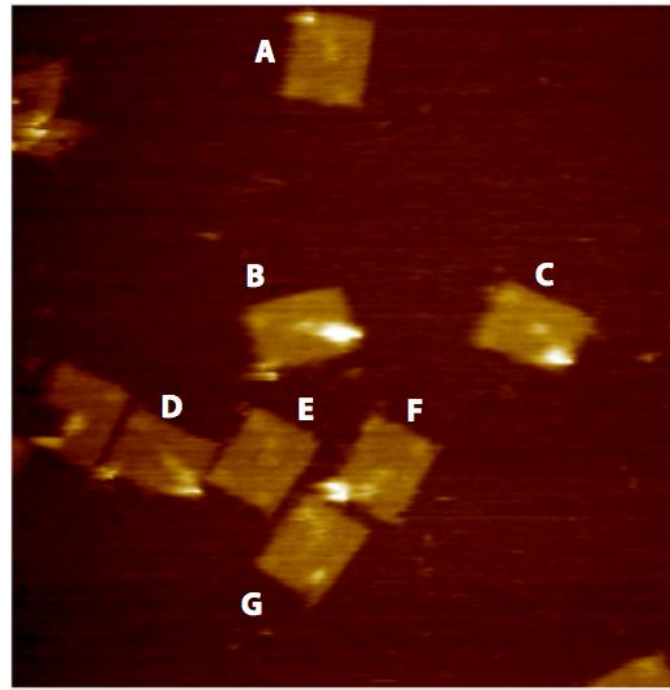


Supplementary Figure 9 | Wide Field AFM images and classifications used for statistical analysis of ABD design. AFM images of the spider before release.



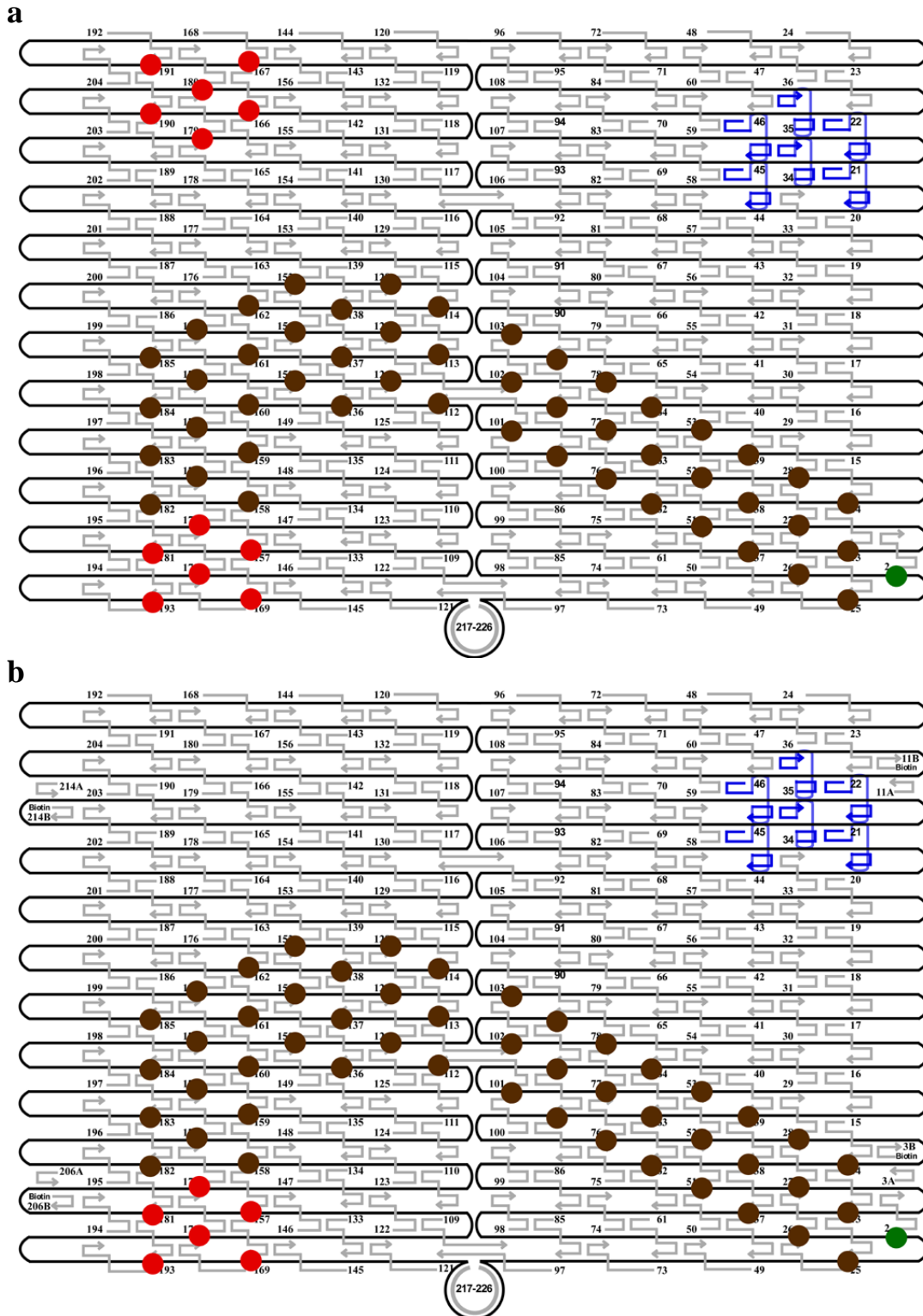
	up	Down	#Spiders	START	TRACK	STOP	CONTROL	inscrutable
a	0	1	1	0	0	1	0	0
b								1
c								1
d	0	1	0	0	0	0	0	0
e	0	1	1	0	0	1	0	0
f								1
g	1	0	1	1	0	0	0	0
h								1
i	0	1	0	0	0	0	0	0
j								1
k	0	1	0	0	0	0	0	0
l	1	0	1	1	0	0	0	0
m								1
n	0	1	1	0	0	1	0	0
o	0	1	1	0	0	1	0	0
p	0	1	1	1	0	0	0	0
q								1
r	0	1	1	0	0	1	0	0
s	1	0	0	0	0	0	0	0

Supplementary Figure 10 | Wide Field AFM images and classifications used for statistical analysis of ABD design. AFM images of the spider after release.

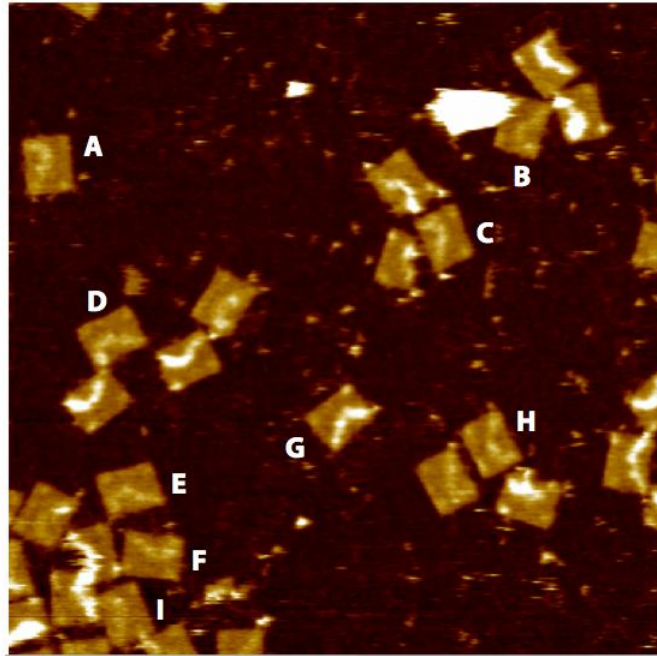


	up	down	#Spiders	START	TRACK	STOP	CONTROL	inscrutable
a	1	0	1	0	0	1	0	0
b	0	1	1	0	0	1	0	0
c	0	1	1	0	0	1	0	0
d	0	1	0	0	0	0	0	0
e								1
f	0	1	1	0	0	1	0	0
g	1	0	0	0	0	0	0	0

Supplementary Figure 11 | Schematic of the EABD origami design. Green represents the START position, brown the probes for the substrate, and red the probes for the STOP and CONTROL. **a**, AFM design and **b**, fluorescence microscopy design.

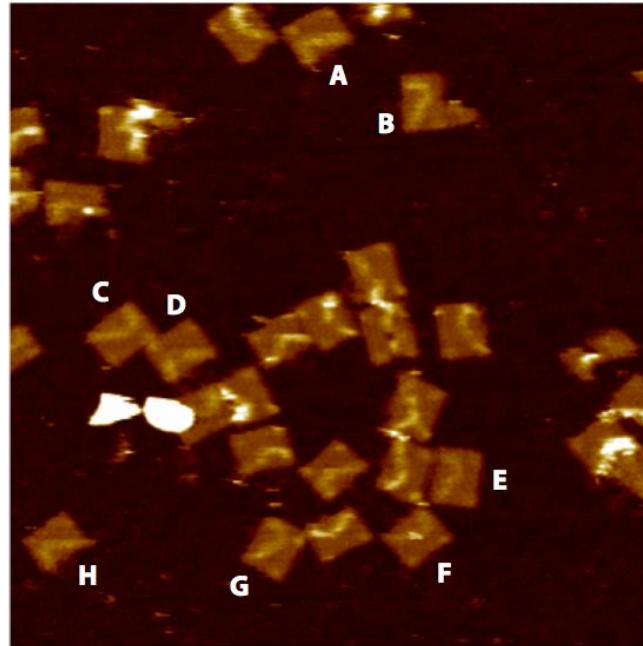


Supplementary Figure 12 | Wide Field AFM images and classifications used for statistical analysis of EABD design. AFM images of the spider before release.



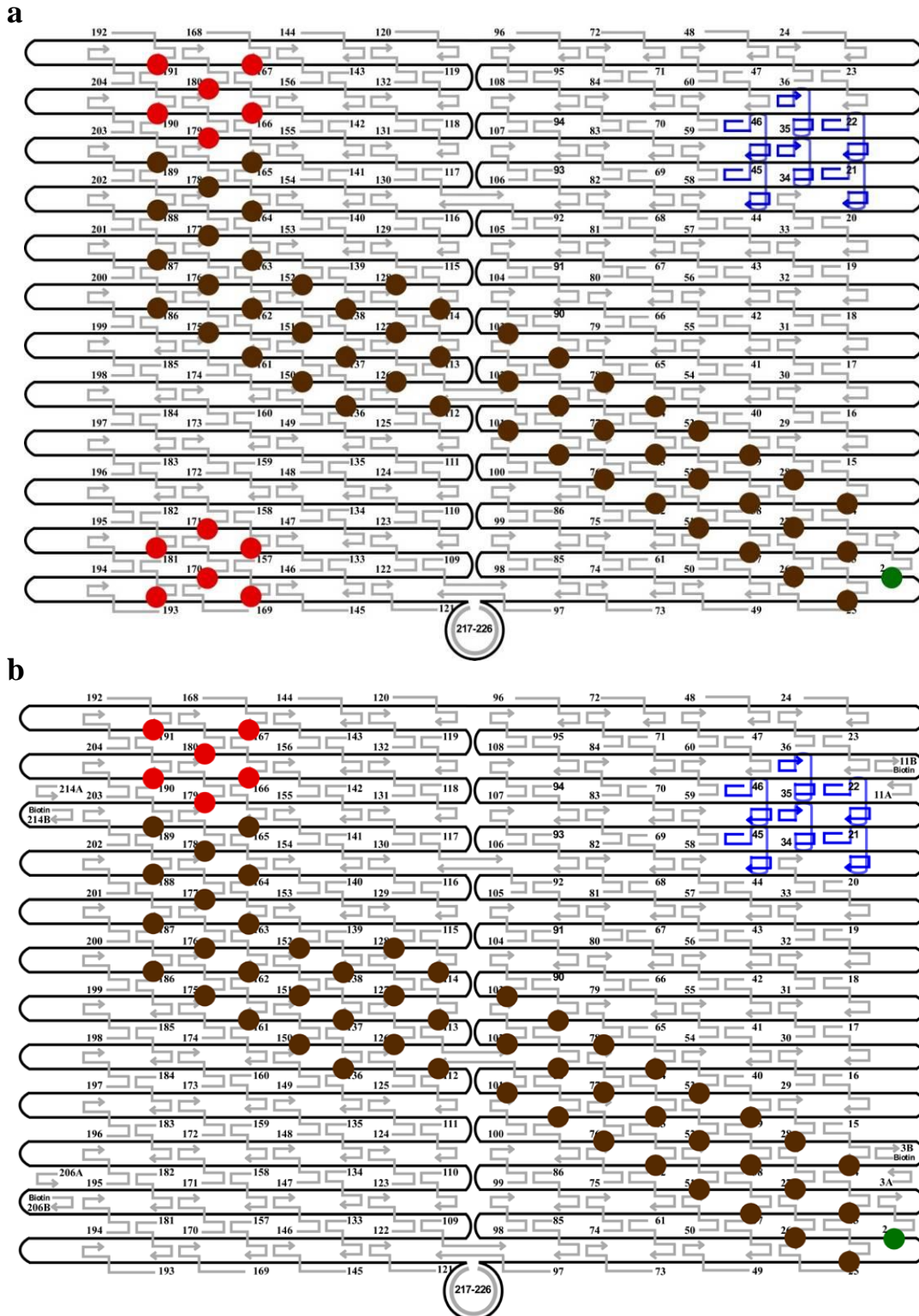
	up	Down	#Spiders	START	TRACK	STOP	CONTROL	inscrutable
a	1	0	0	0	0	0	0	0
b								1
c	1	0	1	1	0	0	0	0
d	1	0	1	0	0	1	0	0
e	1	0	0	0	0	0	0	0
f	1	0	0	0	0	0	0	0
g	1	0	1	1	0	0	0	0
h	1	0	1	1	0	0	0	0
i								1

Supplementary Figure 13 | Wide Field AFM images and classifications used for statistical analysis of EABD design. AFM images of the spider after release.

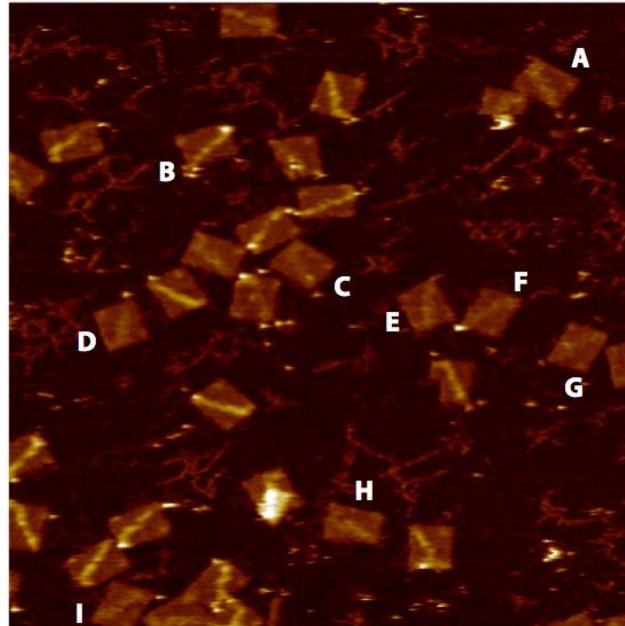


	up	down	#Spiders	START	TRACK	STOP	CONTROL	inscrutable
a	1	0	0	0	0	0	0	0
b								1
c	1	0	0	0	0	0	0	0
d	1	0	0	0	0	0	0	0
e	1	0	0	0	0	0	0	0
f	1	0	1	0	1	0	0	0
g	1	0	0	0	0	0	0	0
h	1	0	0	0	0	0	0	0

Supplementary Figure 14 | Schematic of the EABC origami design. Green represents the START position, brown the probes for the substrate, and red the probes for the STOP and CONTROL. **a**, AFM design and **b**, fluorescence microscopy design.

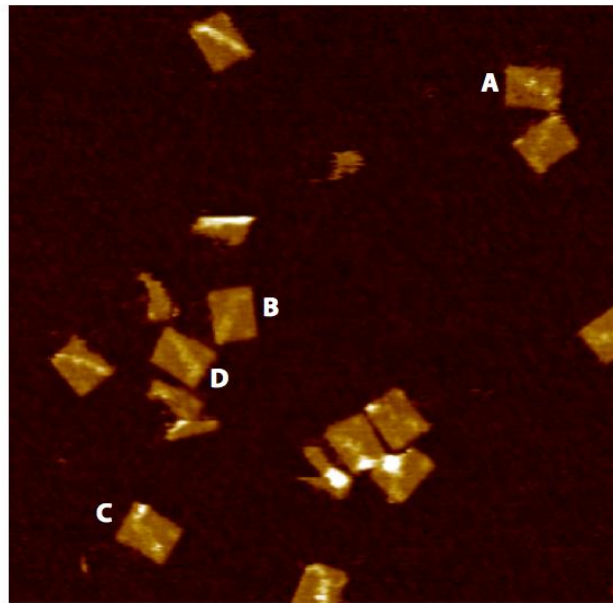


Supplementary Figure 15 | Wide Field AFM images and classifications used for statistical analysis of EABC design. AFM images of the spider before release.



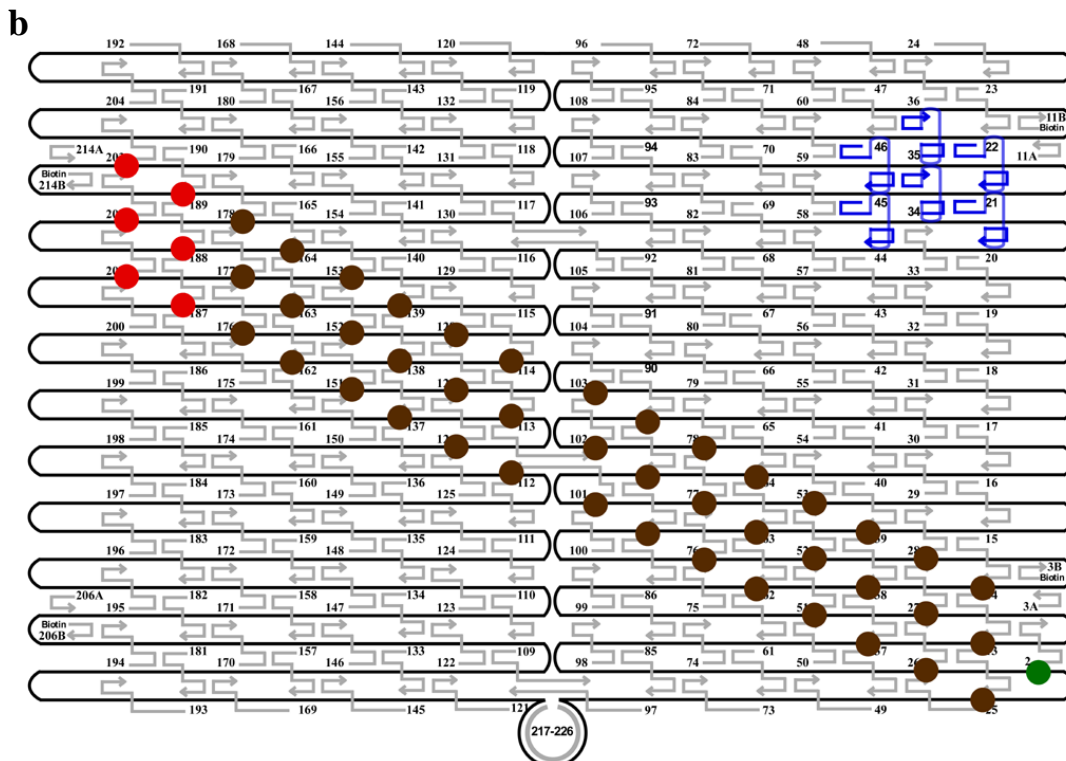
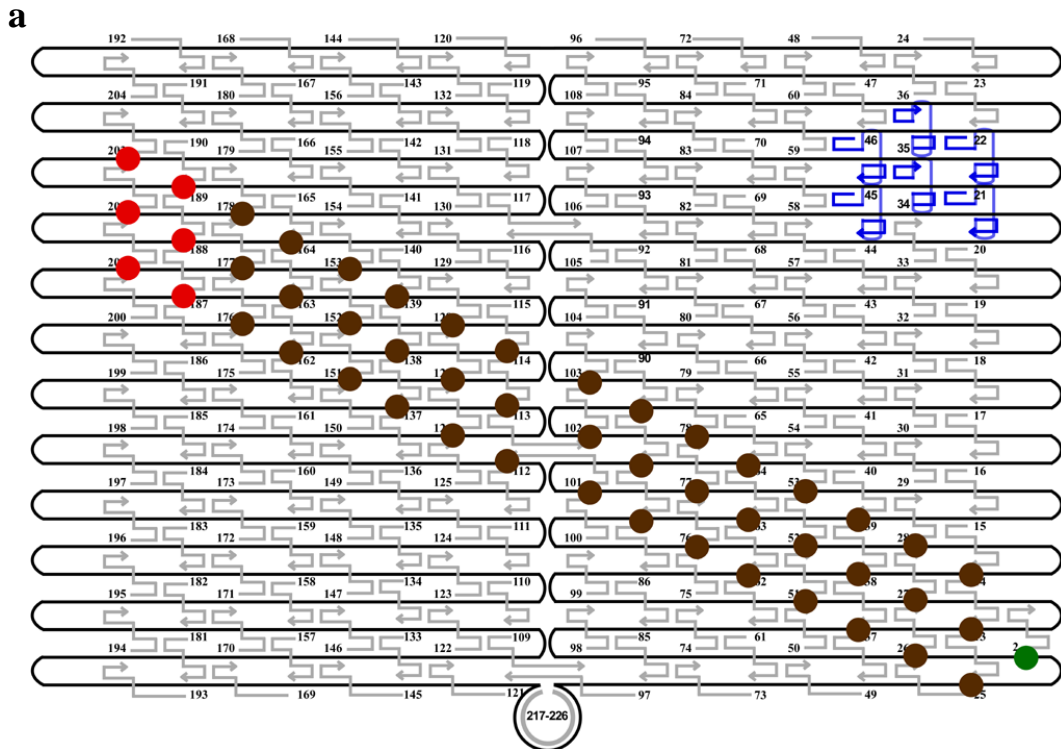
	up	down	#Spiders	START	TRACK	STOP	CONTROL	inscrutable
a	1	0	0	0	0	0	0	0
b	1	0	0	0	0	0	0	0
c	1	0	0	0	0	0	0	0
d	1	0	1	1	0	0	0	0
e	1	0	0	0	0	0	0	0
f	1	0	1	1	0	0	0	0
g								1
h	1	0	0	0	0	0	0	0
i	1	0	0	0	0	0	0	0

Supplementary Figure 16 | Wide Field AFM images and classifications used for statistical analysis of EABC design. AFM images of the spider after release.

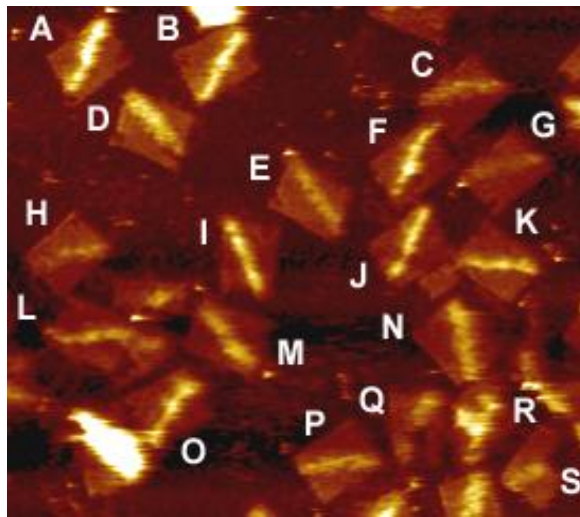


	up	down	#Spiders	START	TRACK	STOP	CONTROL	inscrutable
a	1	0	2	0	2	0	0	0
b	1	0	0	0	0	0	0	0
c	1	0	2	0	1	1	0	0
d	1	0	0	0	0	0	0	0

Supplementary Figure 17 | Schematic of the EAC origami design. Green represents the START position, brown the probes for the substrate, and red the probes for the STOP and CONTROL. **a**, AFM design and **b**, fluorescence microscopy design.

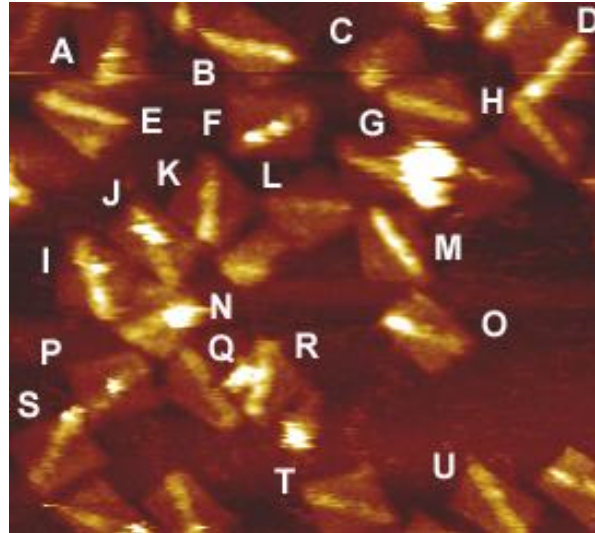


Supplementary Figure 18 | Wide Field AFM images and classifications used for statistical analysis of EAC design. AFM images of the spider before spider is released.



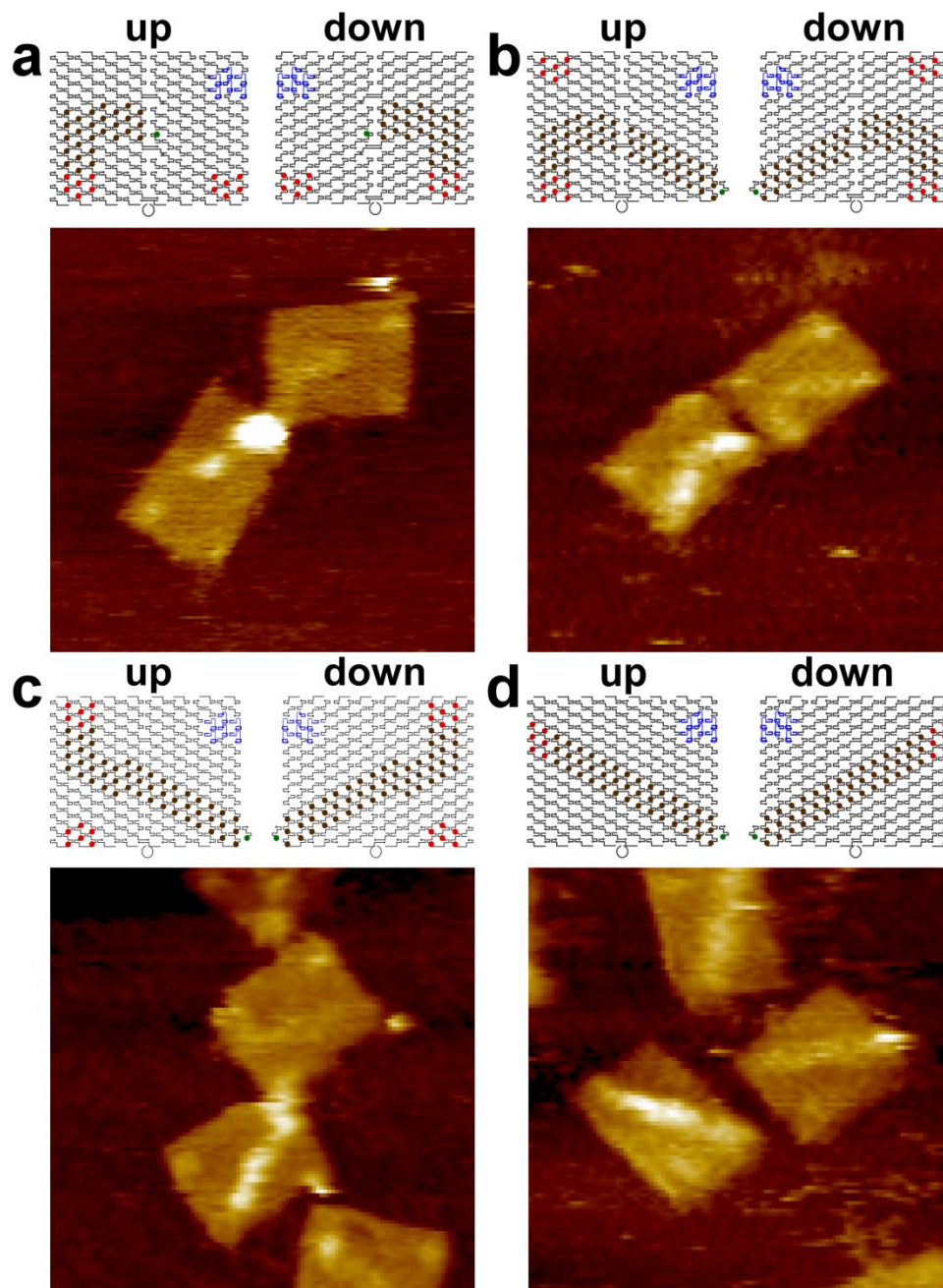
	up	down	# spiders	START	TRACK	STOP	CONTROL	inscrutable
a		1						0
b		1						0
c	1	0	0	0	0	0	0	0
d	1	0	0	0	0	0	0	0
e	1	0	0	0	0	0	0	0
f		1				0	0	0
g	1	0	1	1	0	0	0	0
h	1	0	0	0	0	0	0	0
i		1						0
j		1						0
k		1						0
l		1						0
m								1
n	1	0	0	0	0	0	0	0
o		1						0
p	1	0	0	0	0	0	0	0
q								1
r								1
s								1

Supplementary Figure 19 | Wide Field AFM images and classifications used for statistical analysis of EAC design. AFM images of the spider after release.

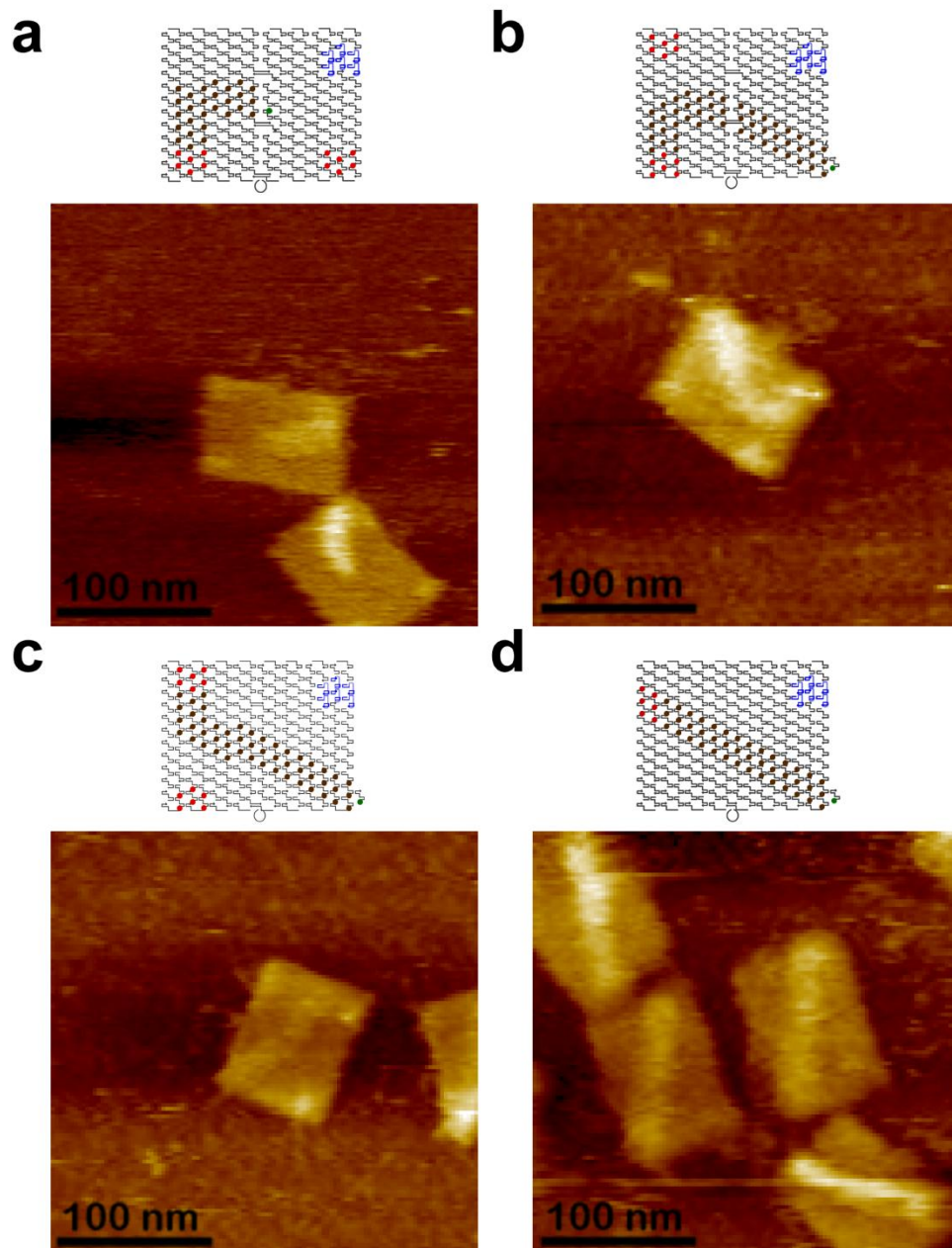


	up	down	# spiders	START	TRACK	STOP	CONTROL	inscrutable
a								1
b								1
c								1
d		1						0
e		1						0
f		1						0
g	1		0	0	0	0	0	0
h	1		0	0	0	0	0	0
i								1
j	1		1		1			0
k		1						0
l	1	0	0	0	0	0	0	0
m		1						0
n								1
o		1						0
p		1						0
q	1	0	0	0	0	0	0	0
r								1
s		1						0
t	1	0	0	0	0	0	0	0
u	1	0	0	0	0	0	0	0

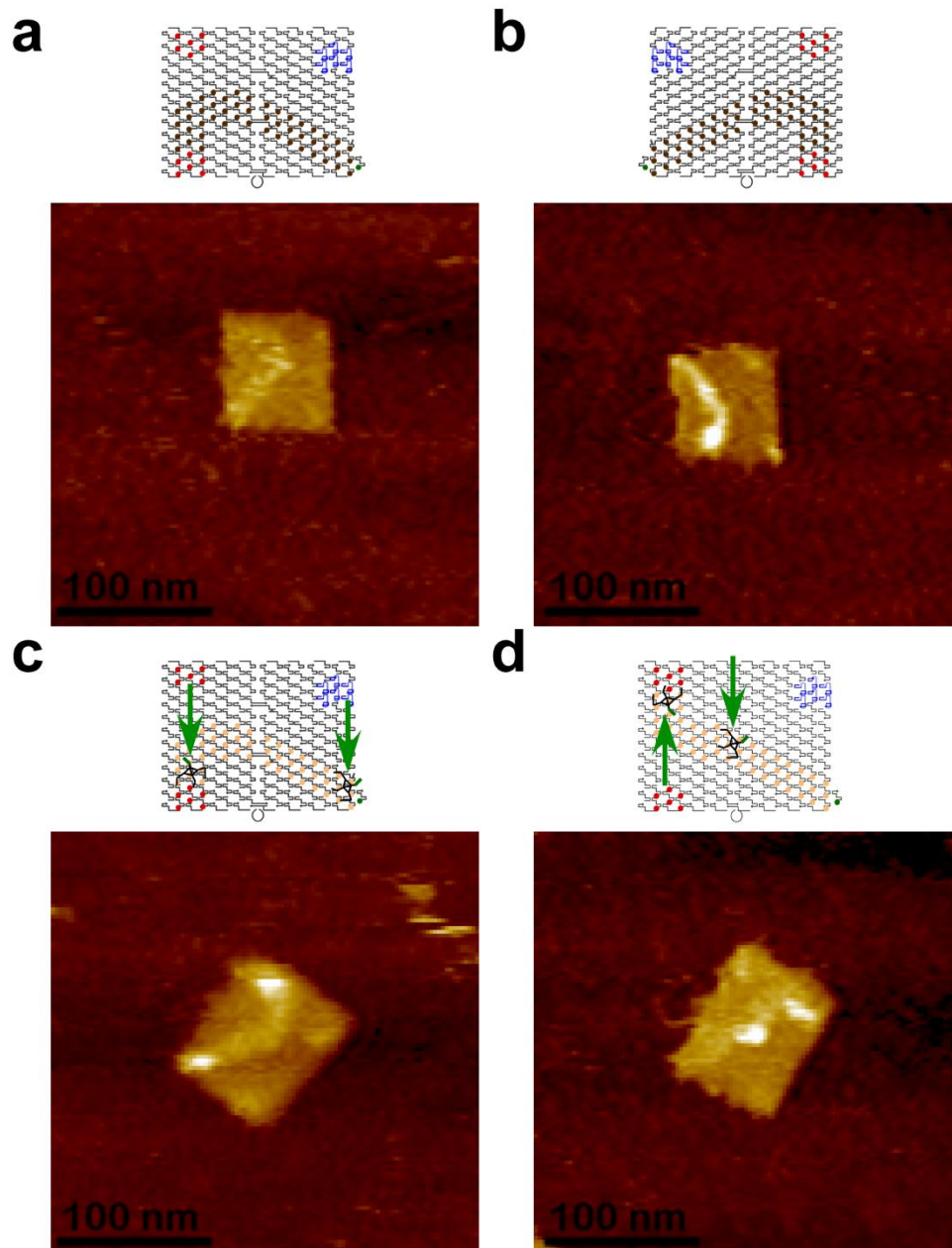
Supplementary Figure 20 | Schematic and AFM images of “face-up” vs. “face-down” arrays. a, ABD, b, EABD c, EABC d, EAC. Images are 300 x 300 nm.



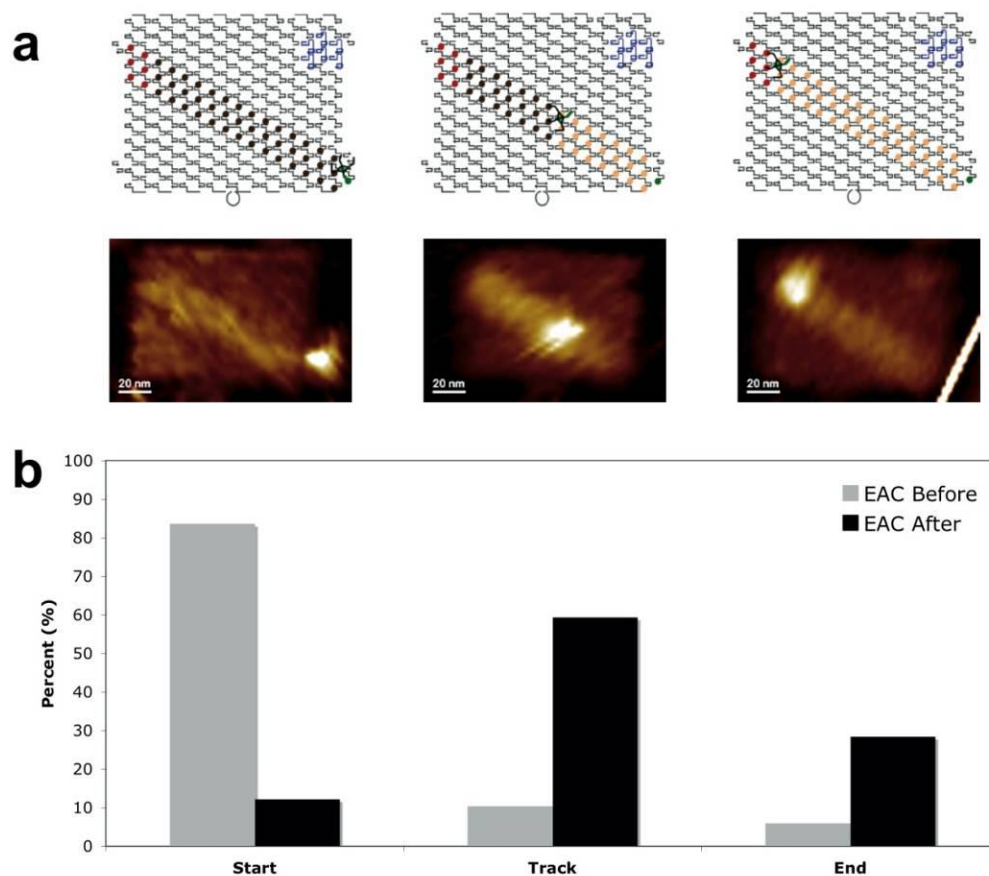
Supplementary Figure 21 | Schematic and AFM images of “face-up” arrays with no spiders. a, ABD b, EABD c, EABC d, EAC. Images are 300 x 300 nm.



Supplementary Figure 22 | Schematic and AFM images of false positive (no spider) and multiples. **a**, Image of “face-up” EABD origami without any spider and **b**, a “face down” EABD from same sample that appears to have a spider near the STOP (even though there was no spider in this sample) **c**, **d**, EABD (**c**) and EAC (**d**) image of two spiders on the array. Images are 300 x 300 nm.



Supplementary Figure 23 | Schematics, AFM images and Graph of EAC before vs. after. a, Schematics and AFM images of the EAC walk before addition of TRIGGER and 30 min after addition of TRIGGER. **b,** Statistical graph of EAC before vs. after.

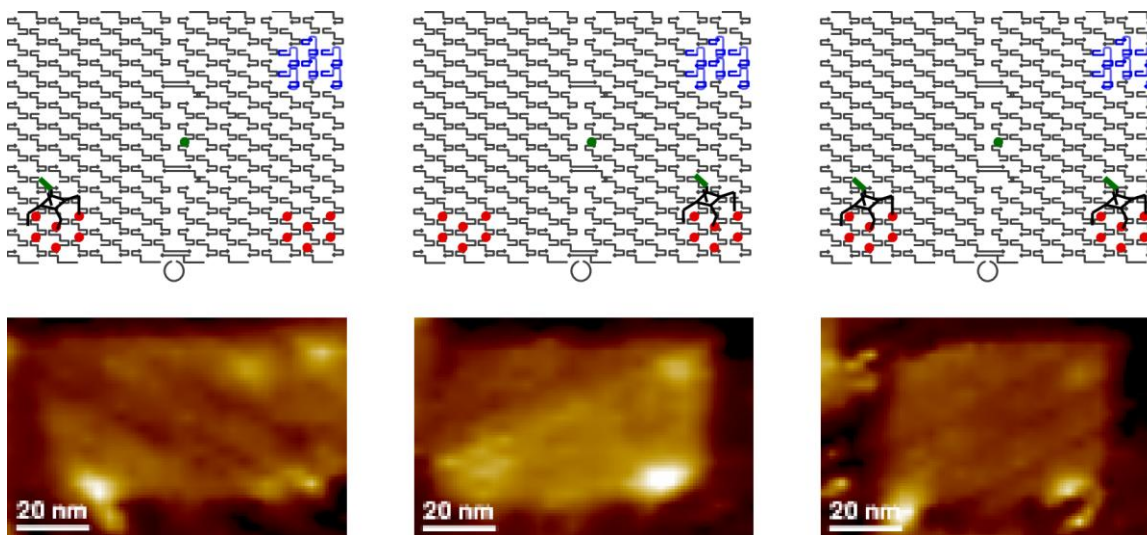


Supplementary Table 1. Data and statistics of “face-up” origami arrays. The number of spiders is the total number of spiders found at START, TRACK, STOP and CONTROL sites on singly-occupied origami. Since the ‘before’ state is the same for the EABD 15 min, 30 min, and 60 min samples, only one set of ‘before’ statistics was collected. We assume that the ‘before’ state for the EABD product 60 min sample was also similar.

Track	Before							After						
	Total spiders	START (% of total)	TRACK (% of total)	STOP (% of total)	CONTROL (% of total)	Multiples	None	Total spiders	START (% of total)	TRACK (% of total)	STOP (% of total)	CONTROL (% of total)	Multiples	None
ABD 30 min	31	28 (90.3%)	1 (3.2%)	2 (6.5%)	0 (0%)	0	67	22	1 (4.5%)	4 (18.2%)	16 (72.7%)	1 (4.5%)	0	42
EABD 15 min								106	19 (17.9%)	68 (64.2%)	15 (14.1%)	4 (3.8%)	15	165
EABD 30 min	113	98 (86.7%)	8 (7.1%)	4 (3.5%)	3 (2.7%)	18	159	76	11 (14.5%)	33 (43.4%)	29 (38.2%)	3 (3.9%)	13	135
EABD 60 min								97	11 (11.3%)	23 (23.7%)	60 (61.9%)	3 (3.1%)	10	179
EABD product 60 min								26	4 (15.4%)	9 (34.6%)	12 (46.2%)	1 (3.9%)	2	37
EABC 30 min	98	78 (79.6%)	8 (8.2%)	12 (12.4%)	0 (0%)	14	149	42	2 (4.8%)	20 (47.6%)	20 (47.6%)	0 (0%)	8	70
EAC 30 min	67	56 (83.6%)	7 (10.4%)	4 (6%)	N/A N/A	7	233	74	9 (12.2%)	44 (59.4%)	21 (28.4%)	N/A N/A	8	197

Supplementary Figure 24 | Schematics and AFM images of spider release control.

The spider was released without the TRACK present and allowed to traverse the array for 30 minutes in solution. The images below show the spider at the STOP and CONTROL of this array and an instance where two spiders were seen occupying both positions on one array.



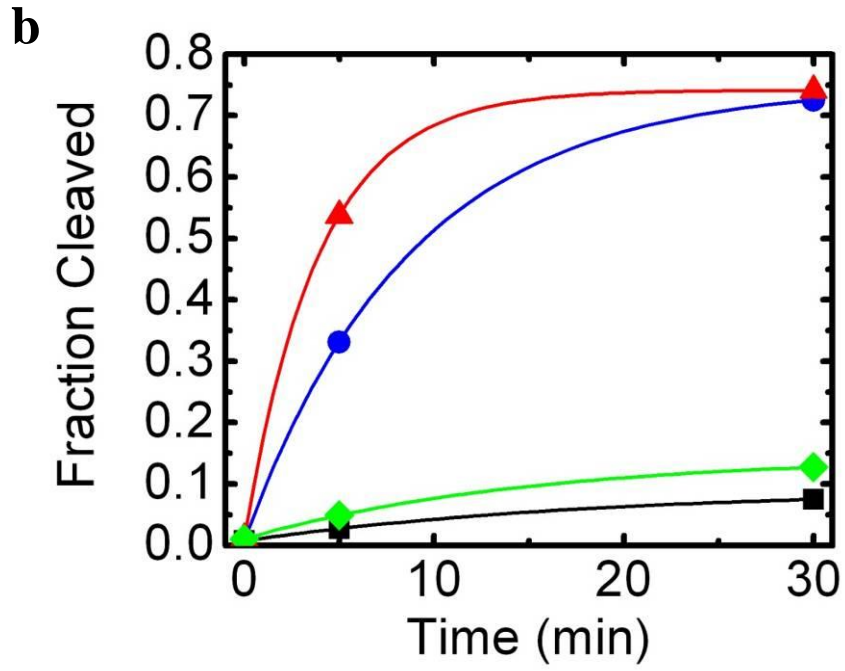
Supplementary Table 2. Data of Spider release without the TRACK

Track	START	STOP	CONTROL
ABD	7	48	45

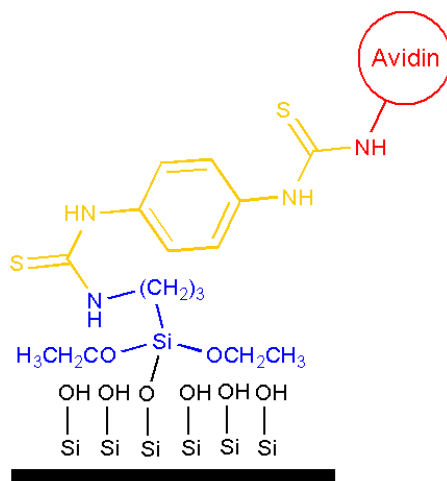
Supplementary Figure 25 | PAGE Characterization of Spider Activity in Solution. **a**, Fluorescence scan of Cy3 and Cy5 in polyacrylamide gel (24% acrylamide). Lane 1 contains an alkali hydrolysis RNA ladder (sequence: 5'-pUGCGUUAGUAGGUUGUAUAGUU-Cy3). Lane 2 contains Cy5-substrate incubated at pH 12 for 5 min at 70°C. Lanes 3-12 contain the products of reactions between spider and Cy5-substrate (S) to form product (P) under the conditions shown in the respective lanes. No cleavage was detected after 30 minutes in absence of either ZnSO_4 (lane 4) or spider (lane 9). **b**, Fraction of substrate cleaved versus incubation time in TA-Mg + 1 mM Zn^{2+} (red triangles), SSC + 10 mM Zn^{2+} (blue circles), SSC + 2 mM Zn^{2+} (green diamonds) or SSC + 1 mM Zn^{2+} (black squares). The cleavage assay in SSC + 2 mM Zn^{2+} is not shown in (a) but was performed in an identical manner to the other assays in a separate experiment. Each curve is fit to a single exponential decay function.

a

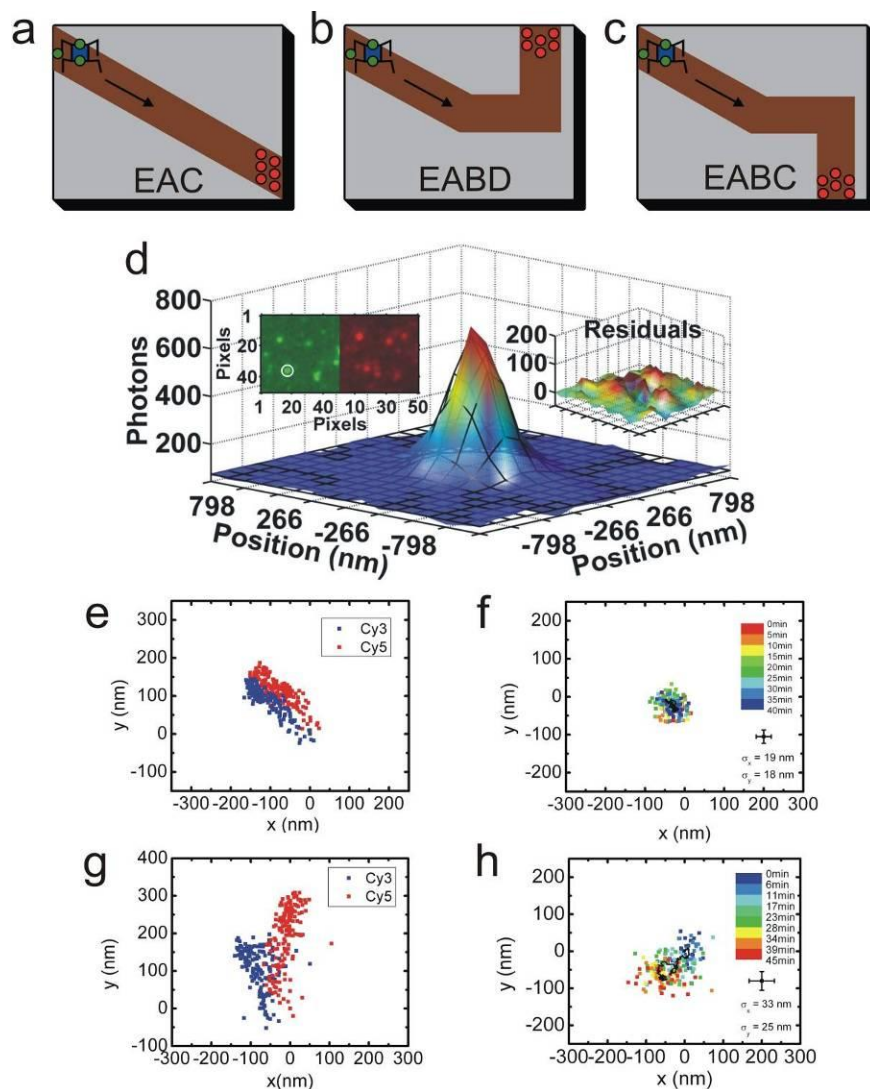




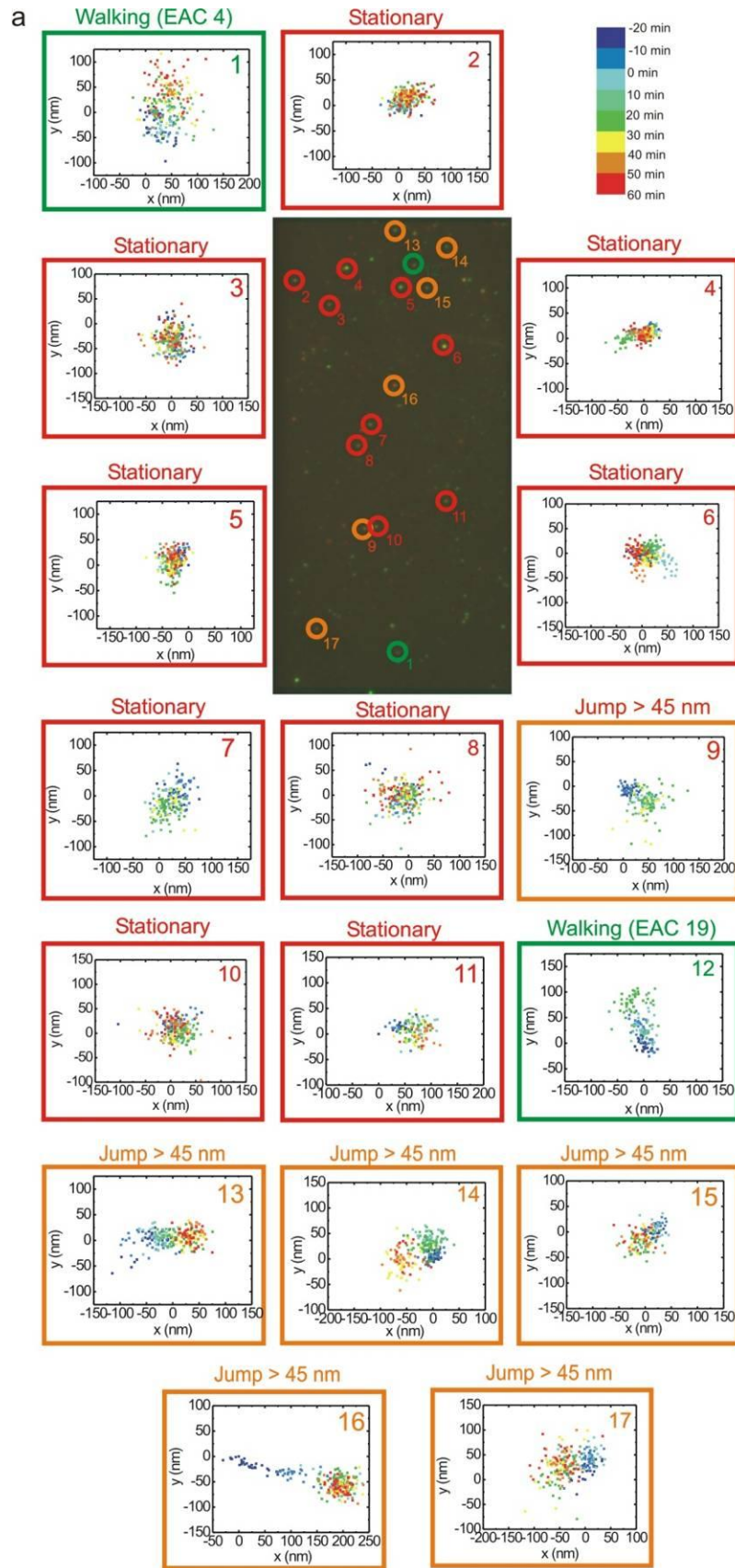
Supplementary Figure 26 | Preparation of microscope slides. Surface coating of the microscope slide, showing the aminosilane (blue), PDITC (yellow), and covalently bound avidin layers (red).

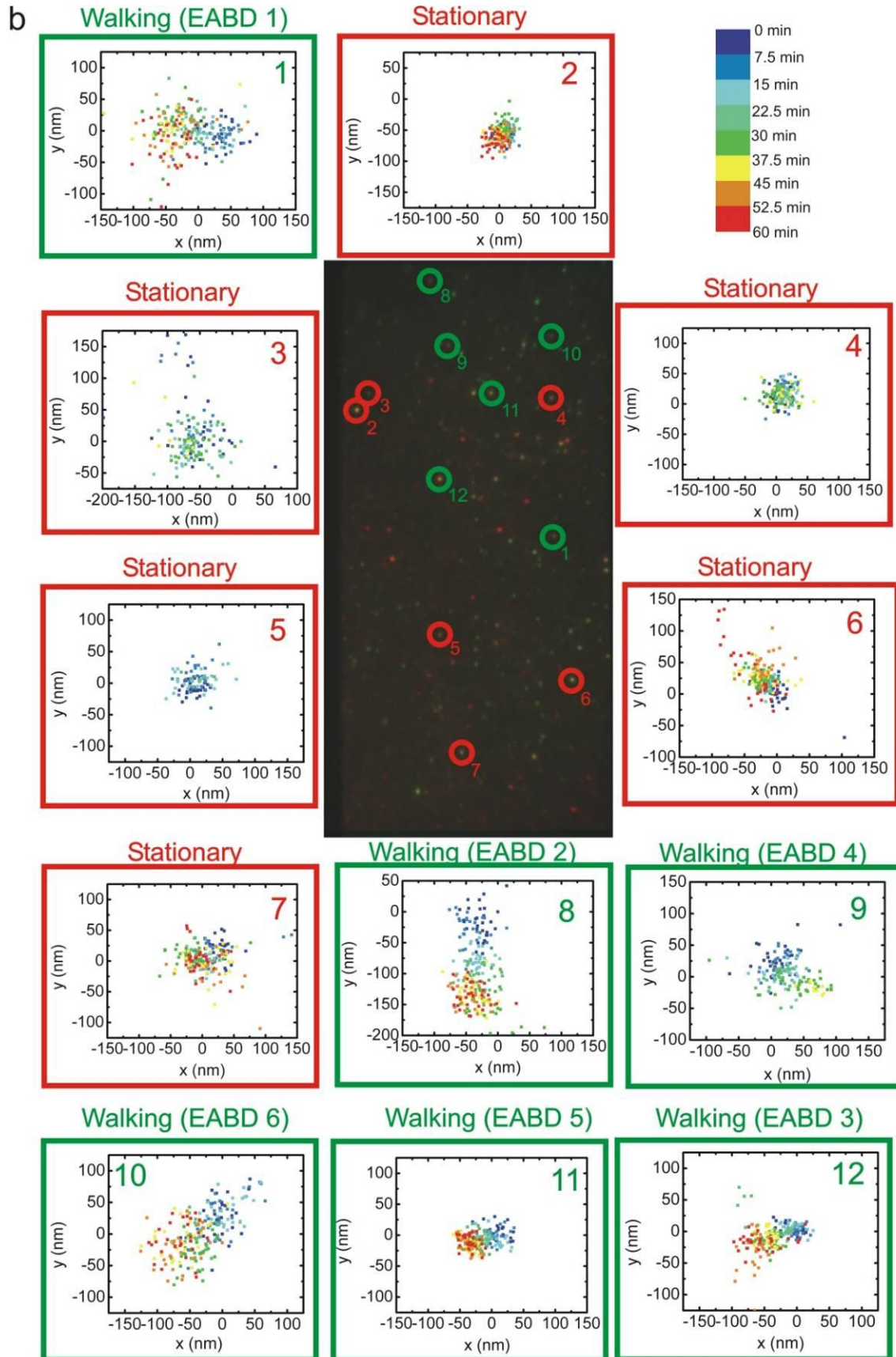


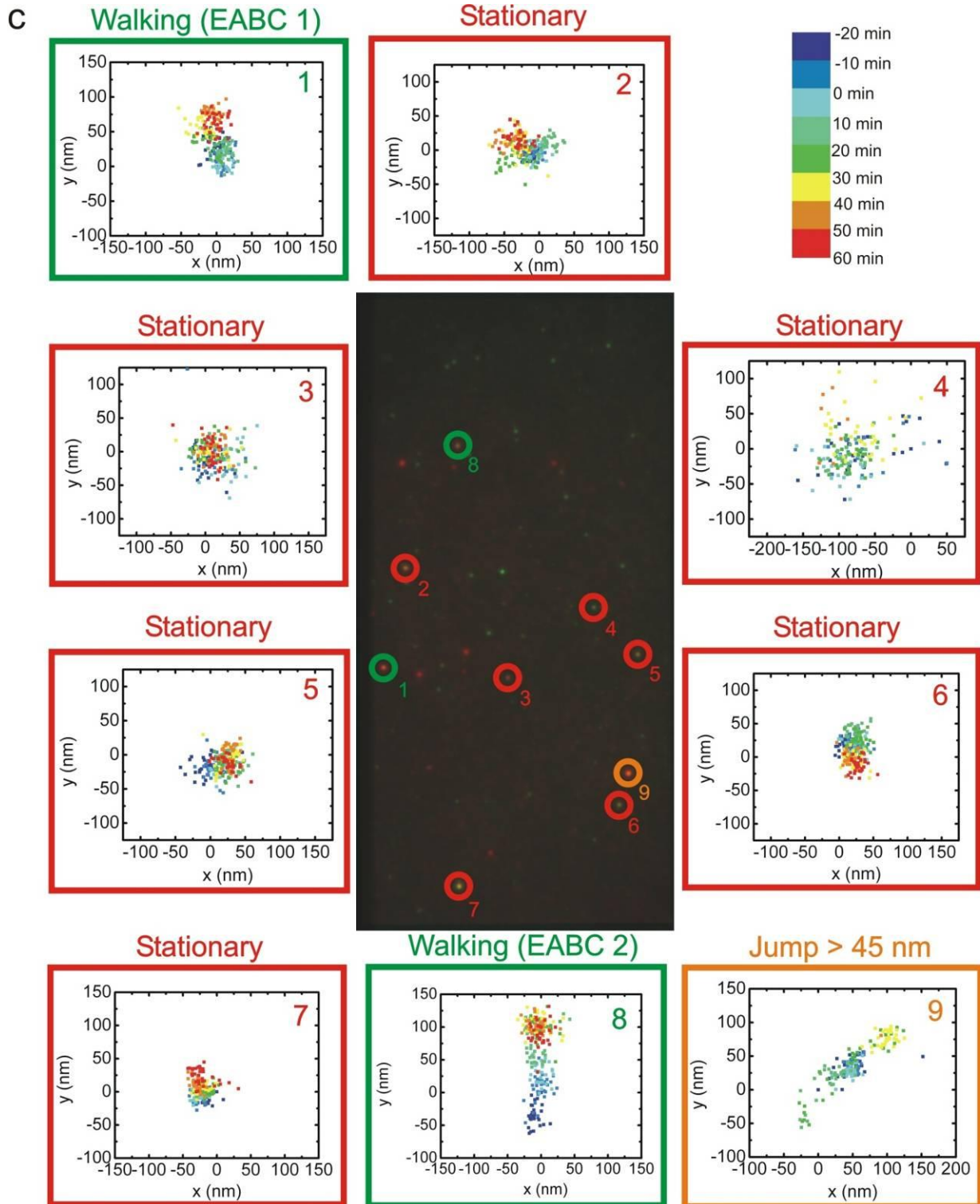
Supplementary Figure 27 | a, b, c, d, e, f, g, h, Schematic representation of the EAC (a), EABD (b), and EABC (c) constructs for fluorescence microscopy. The spider is labeled with 2-3 Cy3 molecules (green) and the STOP with up to 6 Cy5 molecules (red). PSFs from spider-origami pairs are imaged over time and fit, frame-by-frame, to a 2-D Gaussian function; the fit has low residuals (d). The coordinates of each PSF exhibit significant drift through time (e, g) which is corrected by subtracting the coordinates of Cy5 from its proximal Cy3. The resulting coordinate plots (f, h) track the motion of each spider relative to its STOP position. In absence of Zn^{2+} but in presence of TRIGGER in SSC buffer, primarily stationary spiders are observed (e, f); the standard deviations σ_x and σ_y give an estimate of precision in position measurements. In contrast, a spider incubated with TRIGGER and zinc in SSC (g, h) shows a distinctly biased pattern of motion when subtracted (h). The trajectory in (e, f) corresponds to trajectory 4 in Supplementary Fig. 28d, and the trajectory in (g, h) corresponds to EAC 2 (Supplementary Fig. 29).

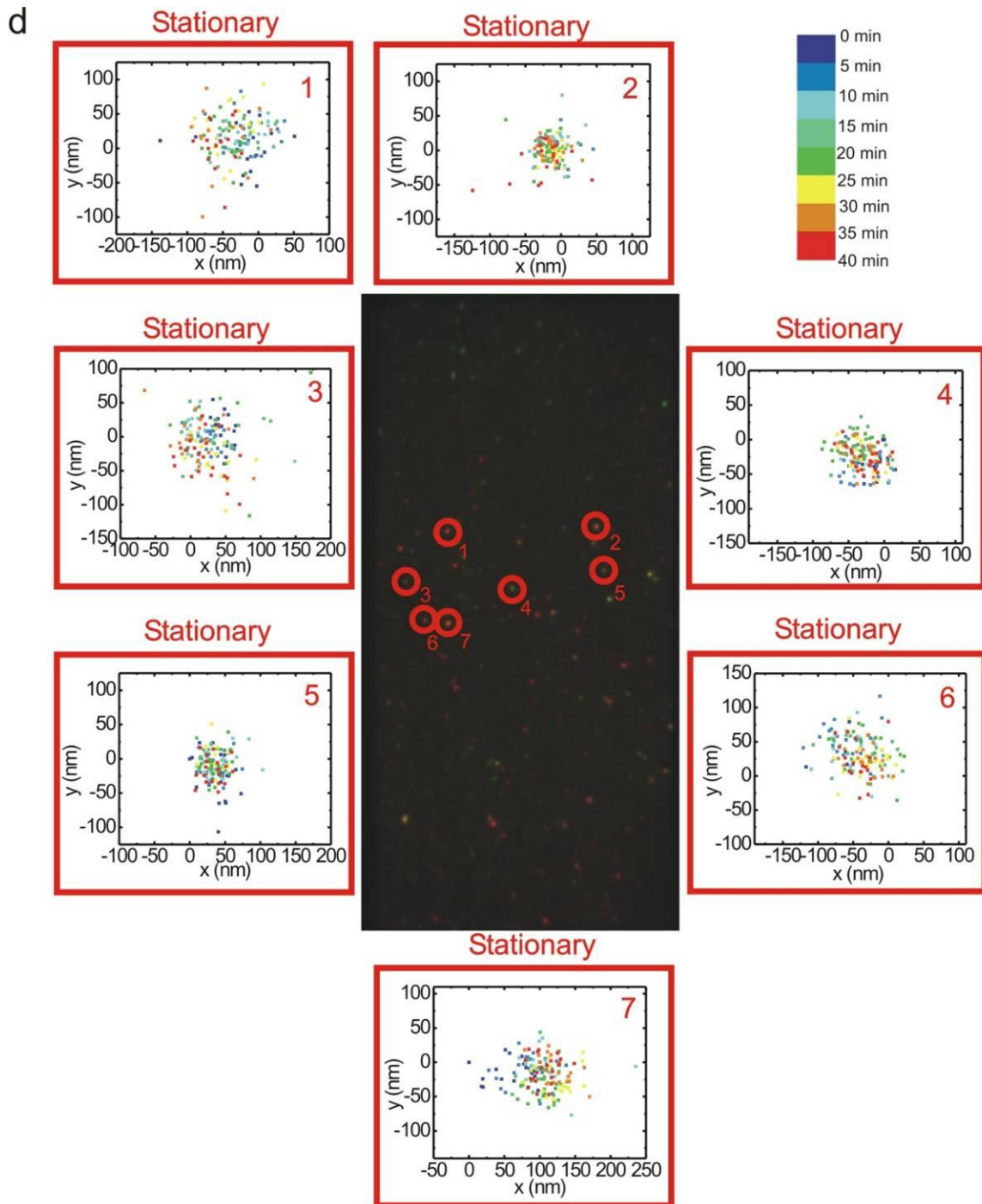


Supplementary Figure 28 | a, b, c, d, example CCD camera images from one of each type of experiment: EAC (**a**), EABD (**b**), EABC (**c**), and EAC in the absence of zinc (**d**). Both EAC experiments are performed in SSC buffer, and the EABC and EABD experiments in TA-Mg buffer as described in the text. The numbered circles mark the coordinates of the PSFs whose positions over time were determined using the Gaussian fitting technique described in Supplementary Fig. 27 as displayed in their corresponding numbered trajectory graphs. The trajectory graphs include spiders that walked continuously with a net displacement > 45 nm (green) as determined from the criteria in the text; PSFs that exhibited discontinuous displacement(s) > 45 nm and were thus determined to not be analyzable spiders (orange); and spiders or PSFs that remained stationary or displayed movement ≤ 45 nm (or 2-3 standard deviations, red). The lack of movement in the (-) zinc control (**d**) is consistent with the fact that cleavage activity is dependent on zinc, and supports the notion that movements seen in the experiments with zinc addition are not optical artifacts. Additionally, the presence of many apparently stationary spiders in the (+) zinc experiments (**a-c**) strongly suggests that the motion of adjacent spiders does not result from systematic instrument drift.







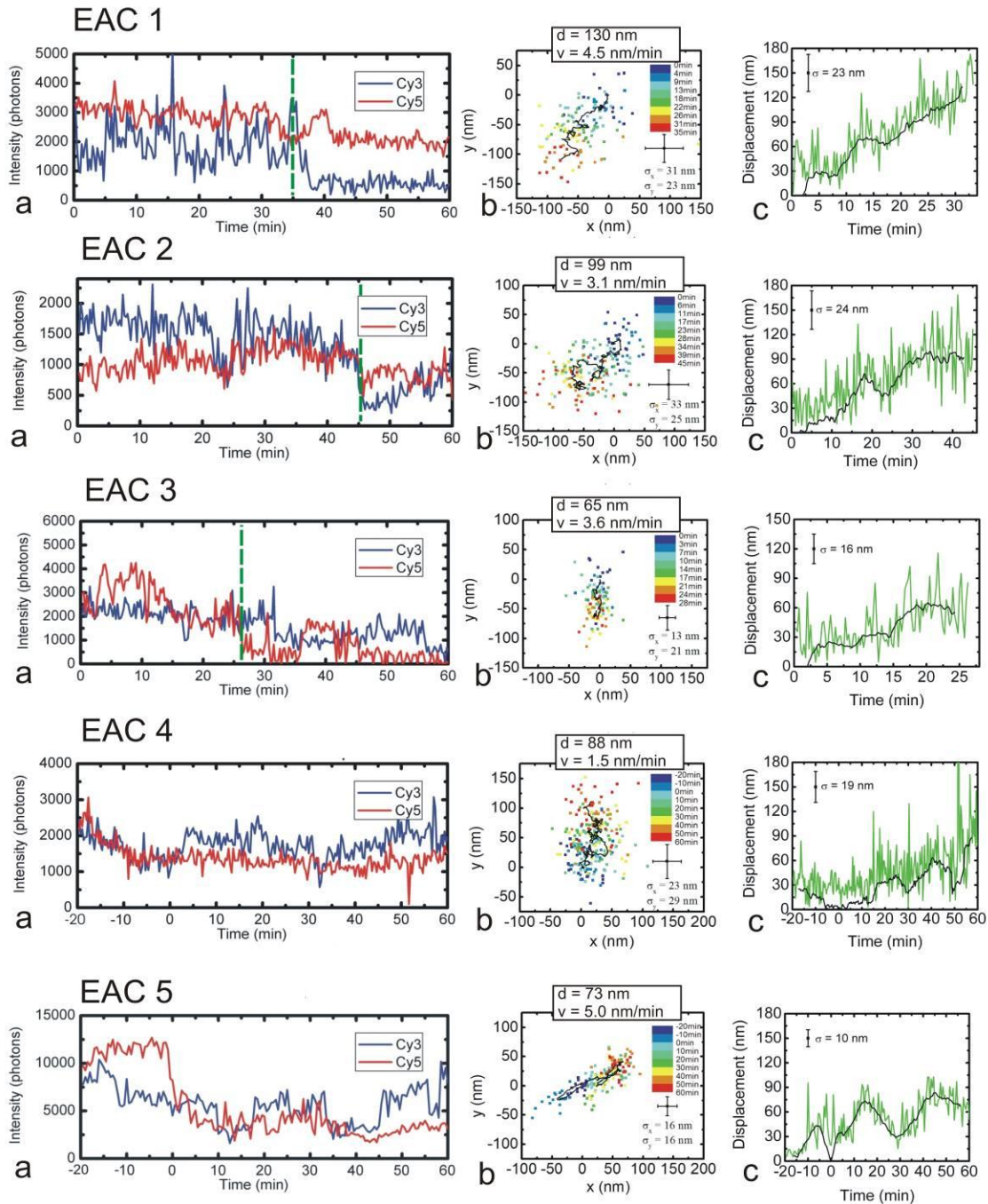


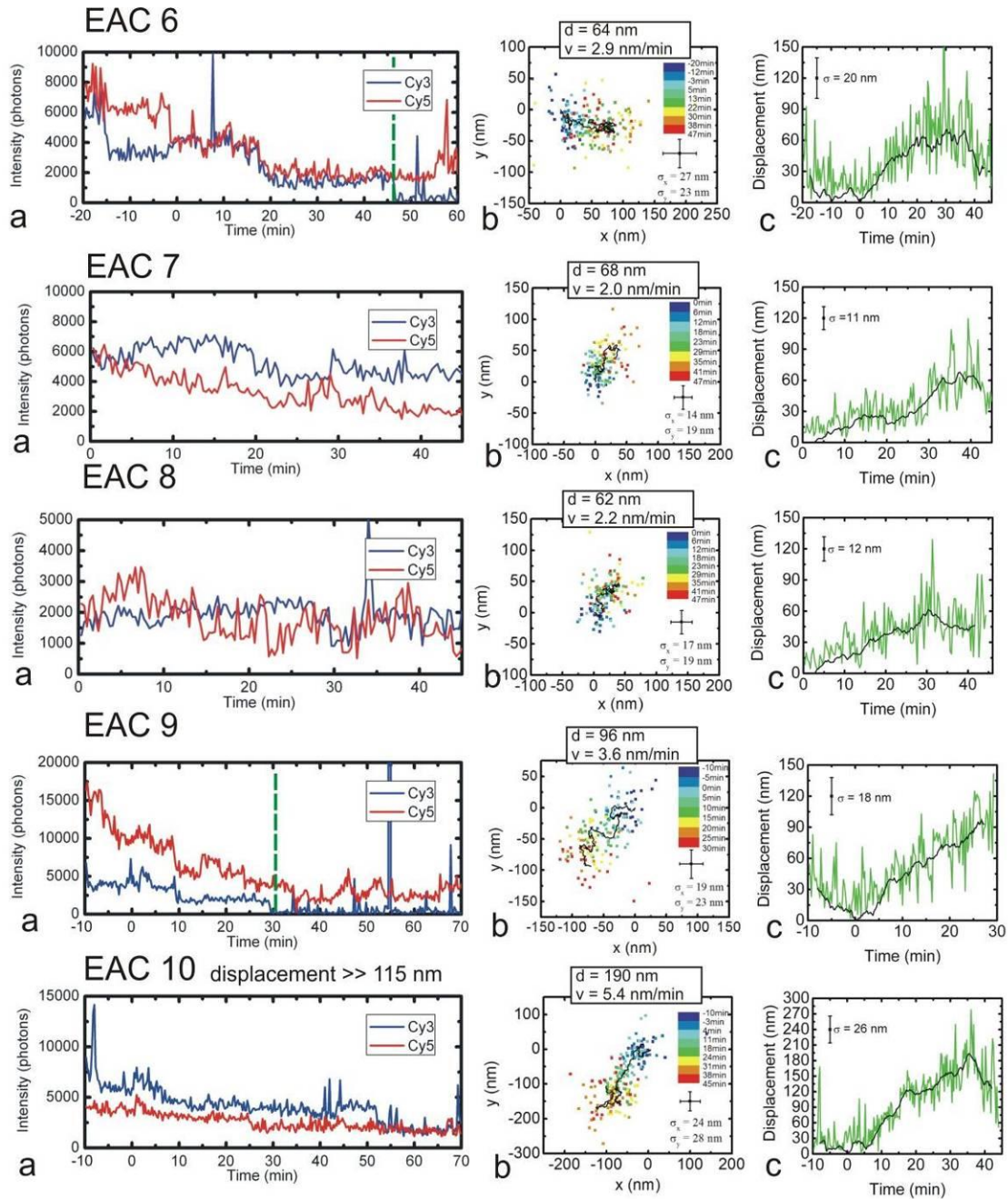
Supplementary Table 3 | Trajectory filtering statistics for spiders imaged by fluorescence microscopy on substrate tracks. These statistics reflect the filtering of raw fluorescence microscopy data to yield the spider trajectories shown in Supplementary Figs 29 and 30. Total PSF pair candidates (column 1) include PSFs identified as possible signal by an automated image analysis routine. Most of these contain detectible signal from only Cy3, only Cy5, or neither. This is highly variable from experiment to experiment and may depend on how free a particular slide is of fluorescent contaminants. PSF pairs were fit to Gaussians (column 2) if both Cy3 and Cy5 were present for at least 25 minutes with at least 1,000 photon counts per movie frame. PSF pairs with satisfactory fitting (column 3) lacked excessive blinking or interference from other nearby PSFs. Finally, putative moving spiders (column 4) satisfy the selection criteria listed in the supplement text and are also shown in Supplementary Figs 29 and 30.

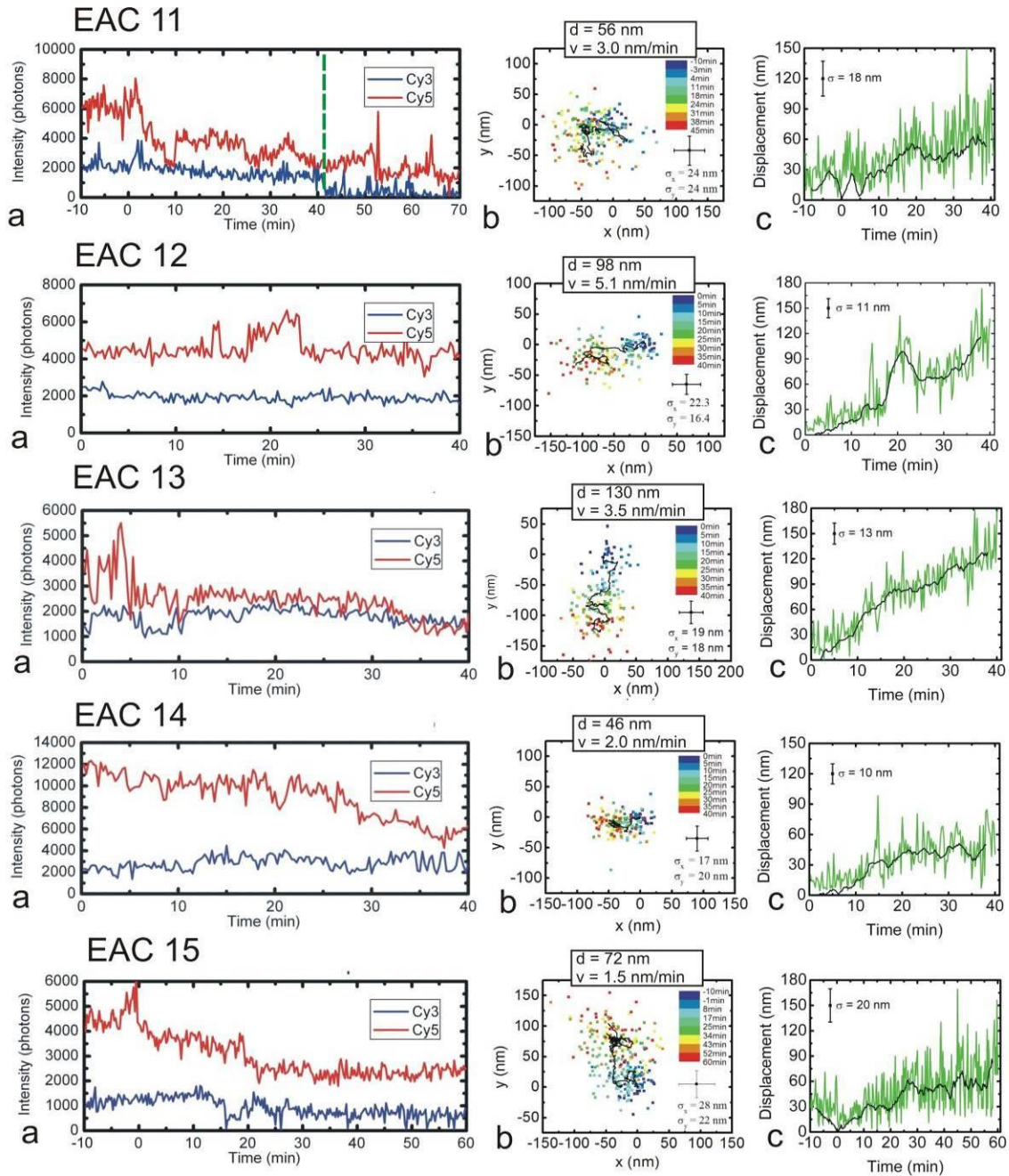
	Total PSF Pair Candidates	PSF Pairs Fit to Gaussians	PSF Pairs with Satisfactory Fitting	Putative Moving Spiders
EAC SSC + Zn²⁺	3,821	139	83	21
EAC SSC - Zn²⁺	303	15	7	0
EAC HBS + Zn²⁺	384	22	15	11
EAC HBS - Zn²⁺	127	22	21	3
EABD TA-Mg + Zn²⁺	477	28	11	6
EABC TA-Mg + Zn²⁺	227	9	7	2

Supplementary Figure 29 | a, b, c, Fluorophore emission intensity over time (**a**) and (non-averaged) 2-dimensional trajectories of the motion of individual spiders relative to the Cy5 PSF (**b**) for the EAC (EAC 1-19), EABD (EABD 1-6), and EABC (EABC 1-2) substrate tracks as viewed by fluorescence microscopy. The EAC traces in this figure were imaged in SSC buffer, and the EABD and EABC traces in TA-Mg buffer as described in the text. EAC traces are divided into “Tier 1” (EAC 1-15) and “Tier 2” (EAC 16-19), traces in the latter group having a lower probability of representing single walking spiders than the former due to reasons state above each trace and discussed in the text. In (**a**), the dashed green line represents the point after which the trace is no longer analyzed due to photobleaching. The black line in (**b**) represents the smoothed trajectory obtained by applying a 16-frame rolling average as described in the text. The position of the origin is arbitrarily chosen as the start of the trajectory. Plots of displacement versus time for the raw trajectory (**c**, green line) and smoothed trajectory (**c**, black line) are also shown for each trace. The addition of 1 mM ZnSO₄ (1-10 mM ZnSO₄ for EAC traces) occurred at $t = 0$ min. The intensity traces show the number of photons collected from each Cy3 or Cy5 point spread function over time, with sharp drops in photon count upon photobleaching of individual fluorophores. Only those time intervals with adequate tracking precision for both fluorophores – generally with more than 1,000 photon counts per frame – are shown in the 2-D trajectories (**b**), and it is these intervals which were analyzed to produce Fig. 4. In the 2-D trajectories, the axes represent spatial dimensions in the fluorescence microscopy image after drift correction. Also shown in panel b are values of net displacement (d) and mean velocity (v) for the EAC track, and mean velocity for the long leg (prior to the 90-degree turn) of the EABC and EABD tracks.

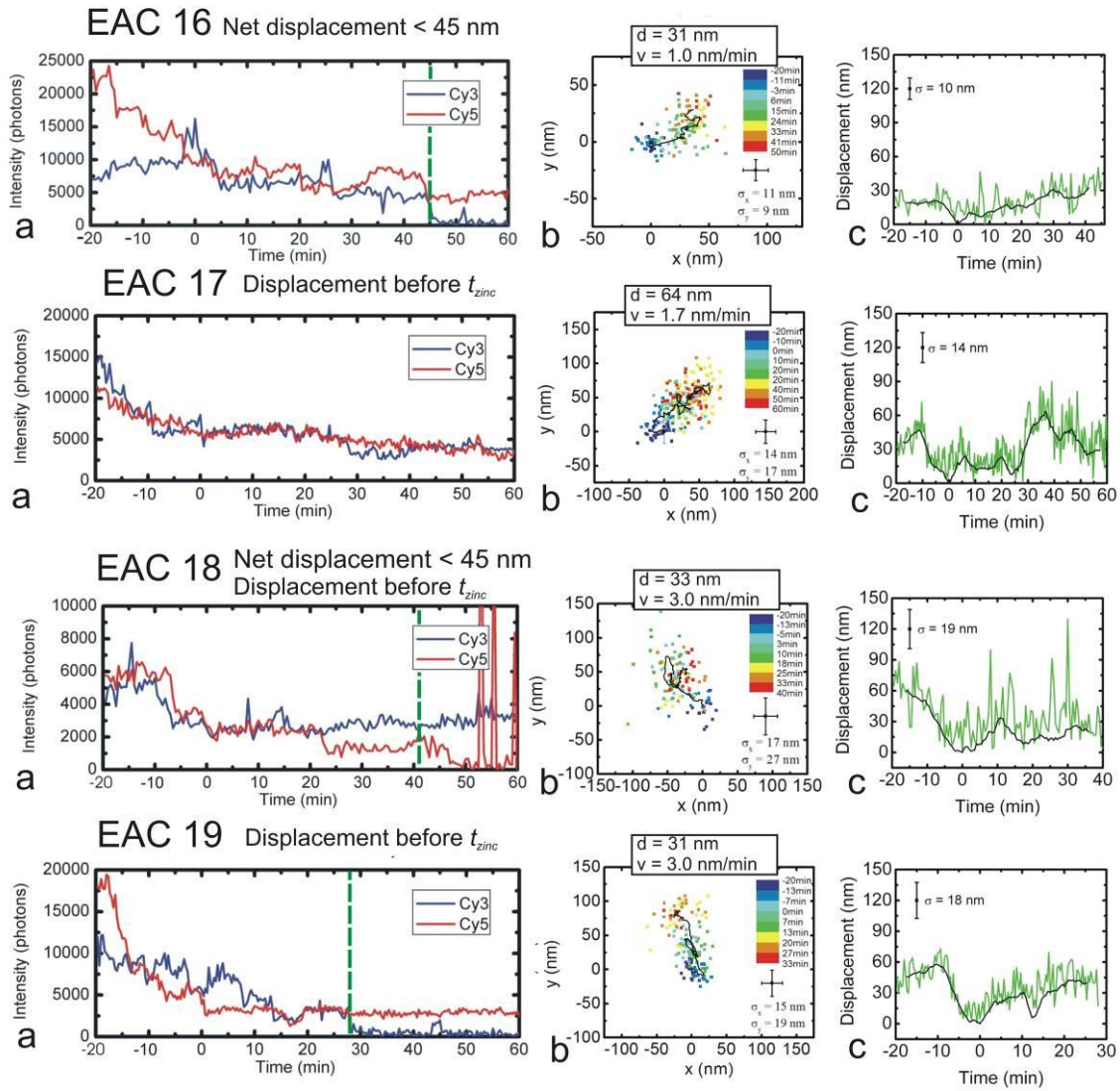
EAC Tier 1



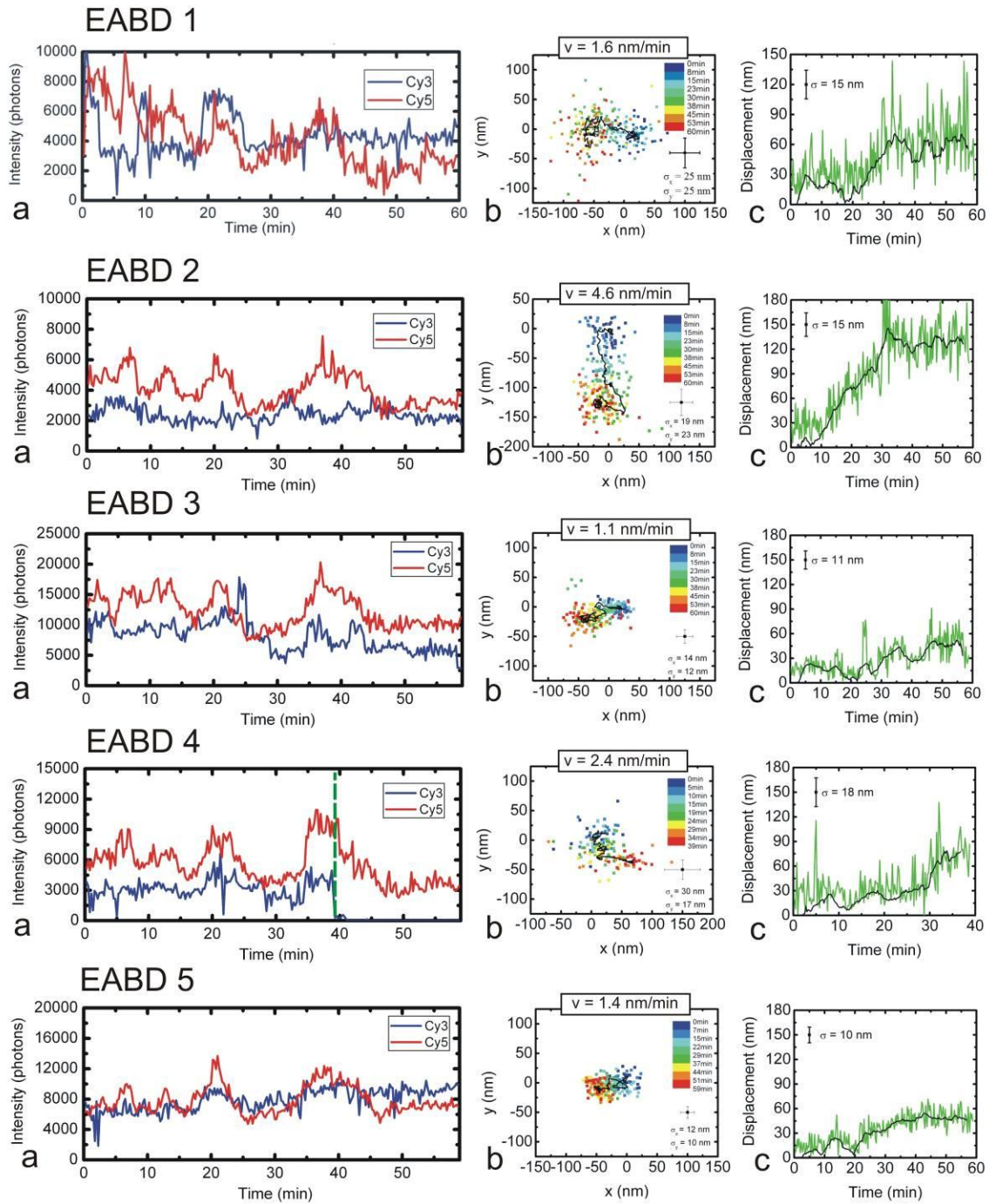


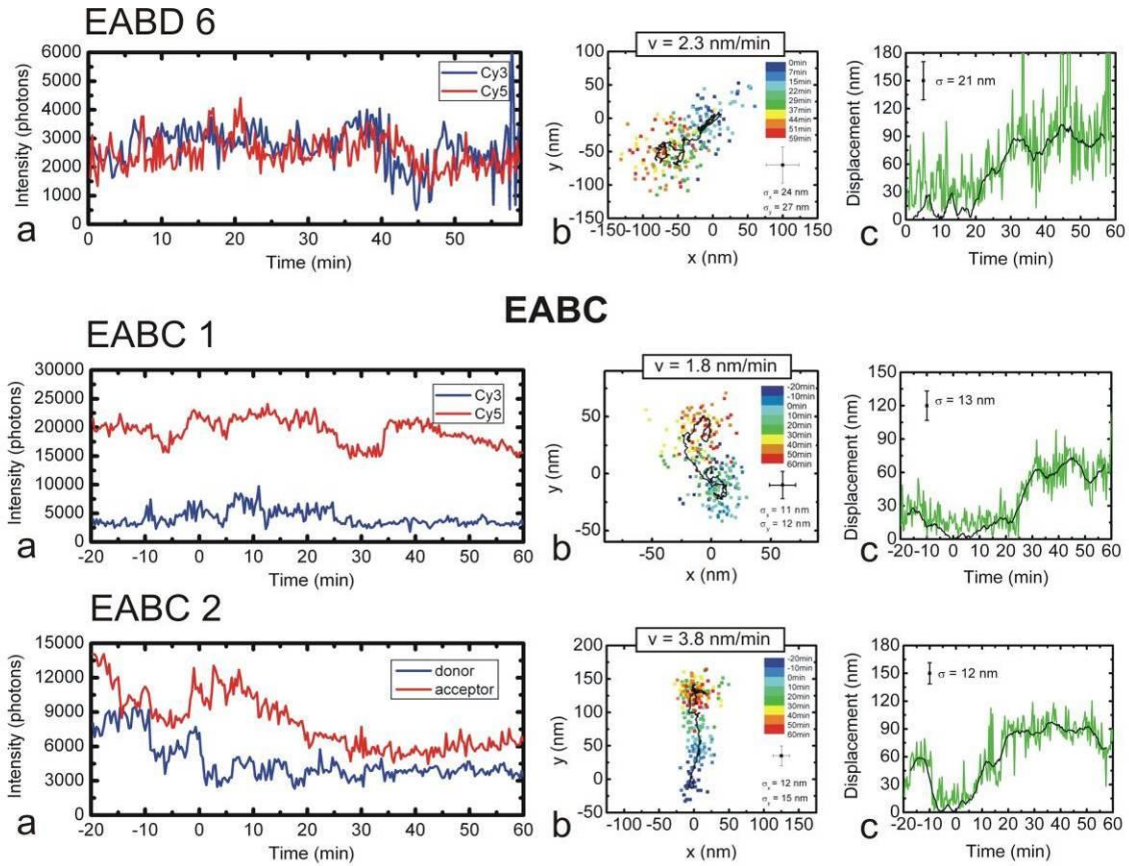


EAC Tier 2



EABD

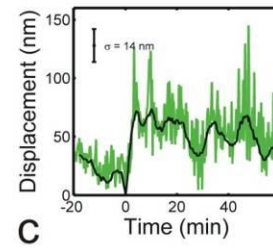
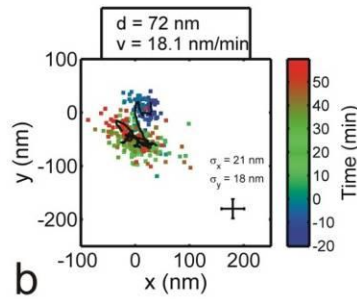
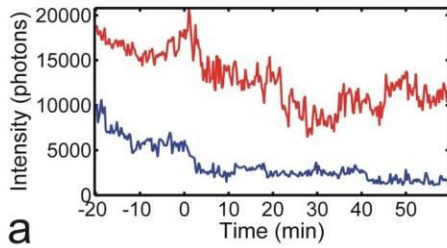




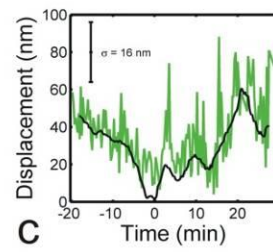
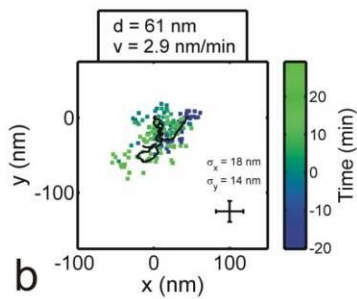
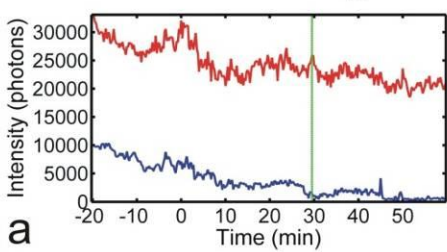
Supplementary Figure 30 | a, b, c, Fluorophore emission intensity over time (**a**), (non-averaged) 2-dimensional trajectories of the motion of individual spiders relative to the Cy5 PSF (**b**), and displacement versus time plots of individual spiders (**c**) on the EAC substrate track as imaged by fluorescence microscopy in 1× HBS buffer with 1× HBS buffer containing 5 mM (EAC HZ 1-16) or 0 mM ZnSO_4 (EAC H 1-21) added after 20 minutes of imaging. In (**a**), the vertical green line represents the point after which the trace is no longer analyzed due to photobleaching. The black line in (**b**) represents the smoothed trajectory obtained by applying a 16-frame rolling average as described in the text. The origin is chosen to coincide with each spider's coordinates at the time of adding 1× HBS buffer containing 0 or 5 mM ZnSO_4 . Plots of displacement versus time for the raw trajectory (**c**, green line) and smoothed trajectory (**c**, black line) are also shown for each trace. The addition of 5 mM ZnSO_4 occurred at $t = 0$ min. Also shown in panel b are values of net displacement (**d**) and mean velocity (**v**) calculated as described in the fluorescence microscopy analysis section. For comparison between experiments performed in 0 and 5 mM ZnSO_4 , all stationary spiders (those with net displacements less than or equal to 45 nm after zinc addition) observed under each set of conditions are also shown. In the presence of 5 mM ZnSO_4 , 12 of 16 trajectories move > 45 nm, while only 3 of 21 trajectories collected in absence of Zn^{2+} ions appear to move > 45 nm.

HBS, 5 mM Zn²⁺ (EAC HZ)

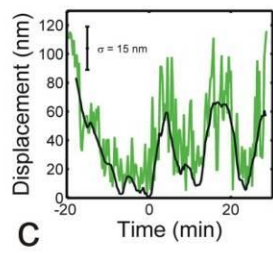
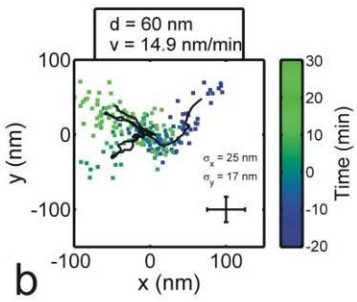
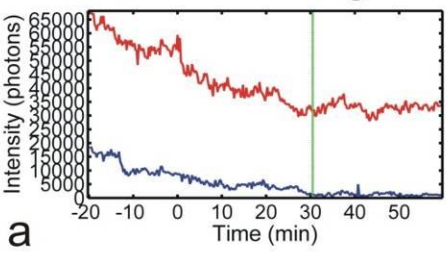
EAC 1HZ: Moving



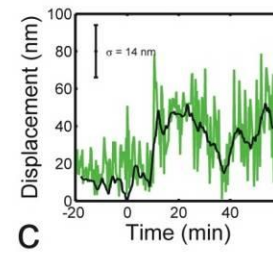
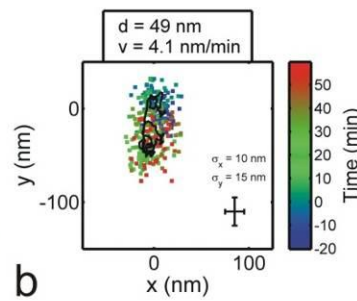
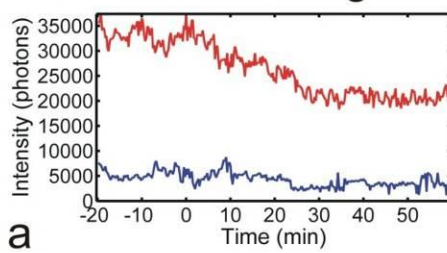
EAC 2HZ: Moving



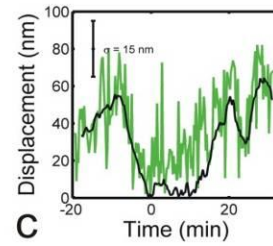
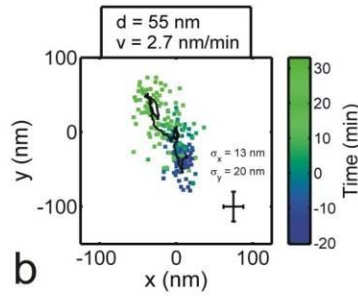
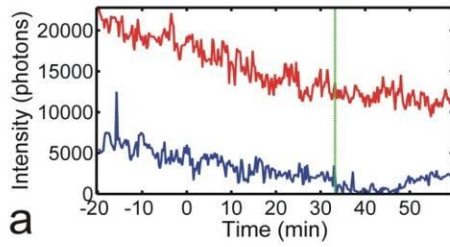
EAC 3HZ: Moving



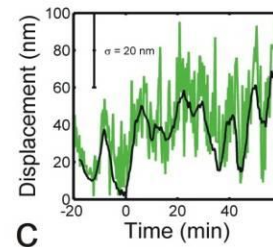
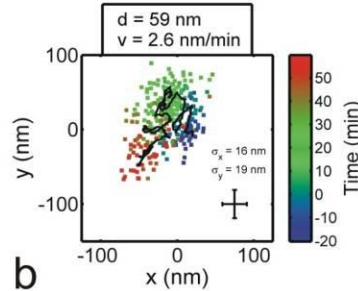
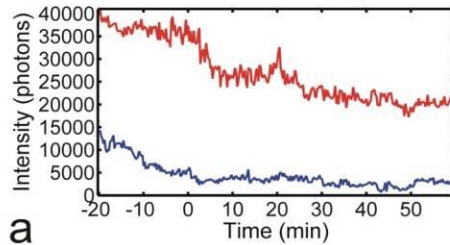
EAC 4HZ: Moving



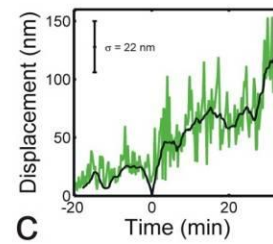
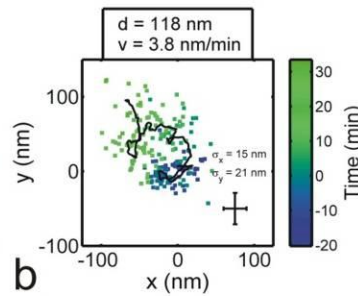
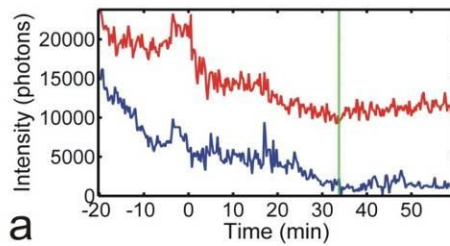
EAC 5HZ: Moving



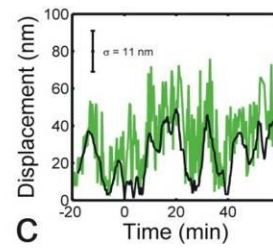
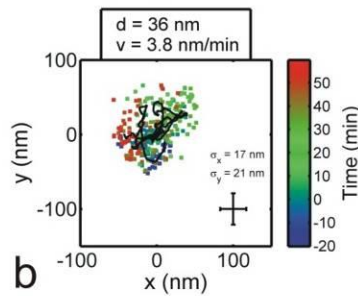
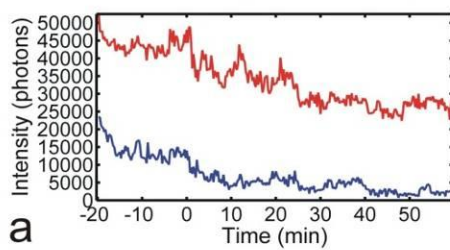
EAC 6HZ: Moving



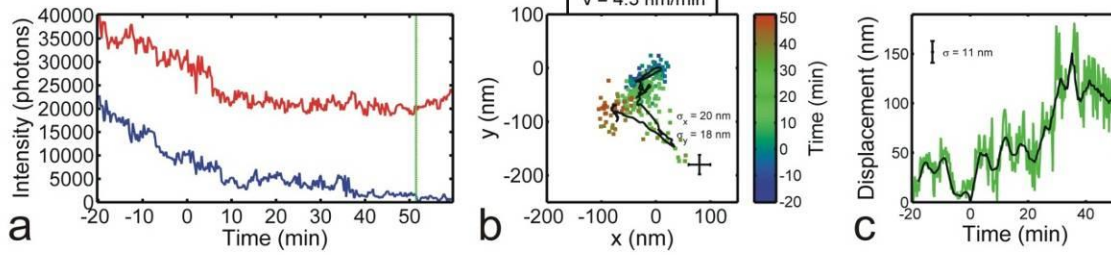
EAC 7HZ: Moving



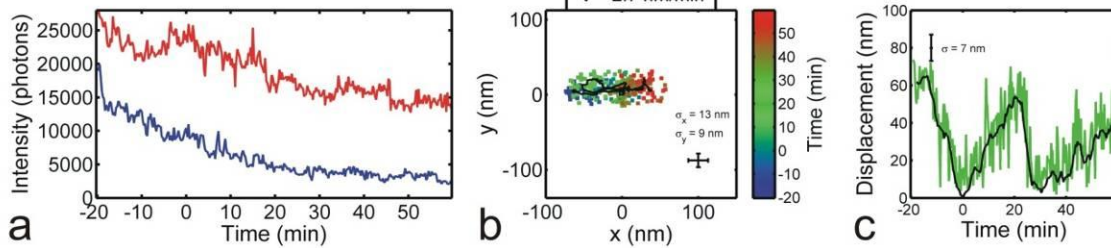
EAC 8HZ: Stationary



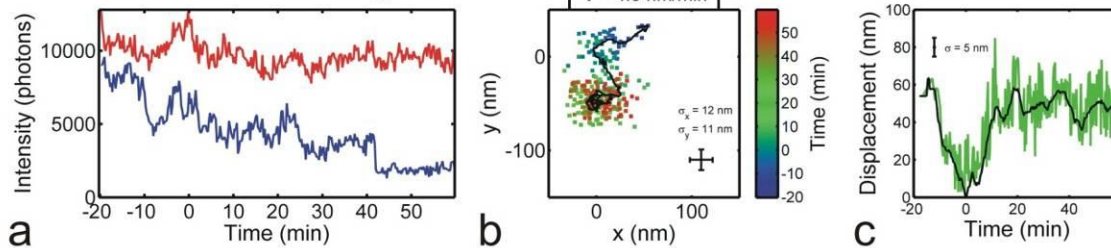
EAC 9HZ: Moving



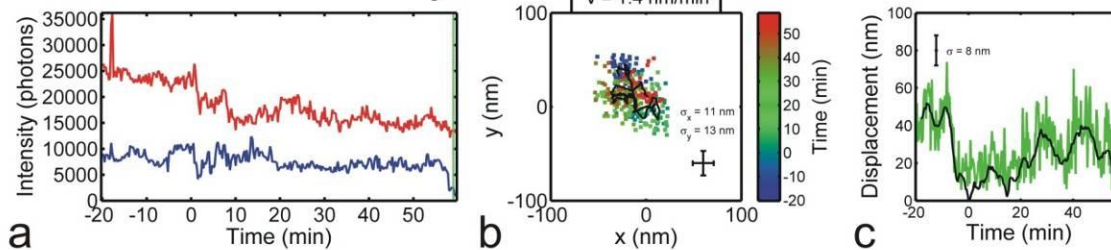
EAC 10HZ: Moving



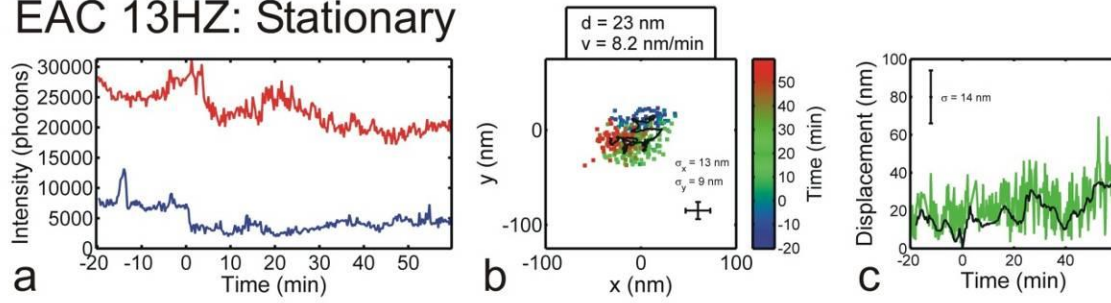
EAC 11HZ: Moving



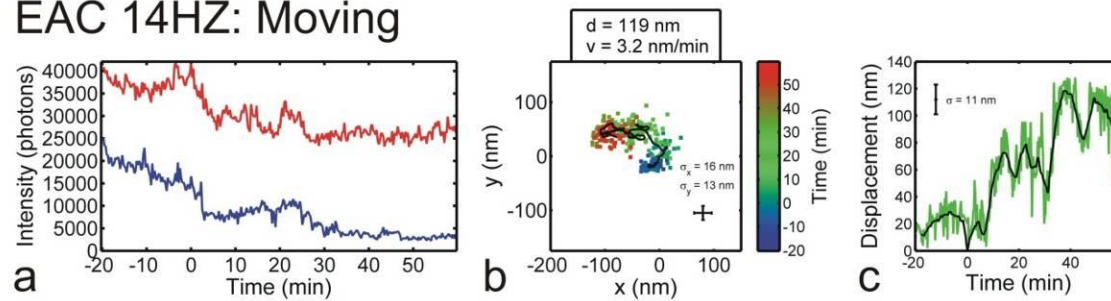
EAC 12HZ: Stationary



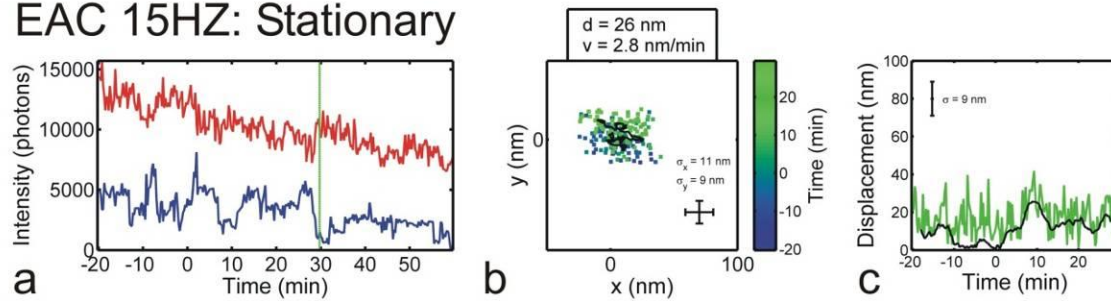
EAC 13HZ: Stationary



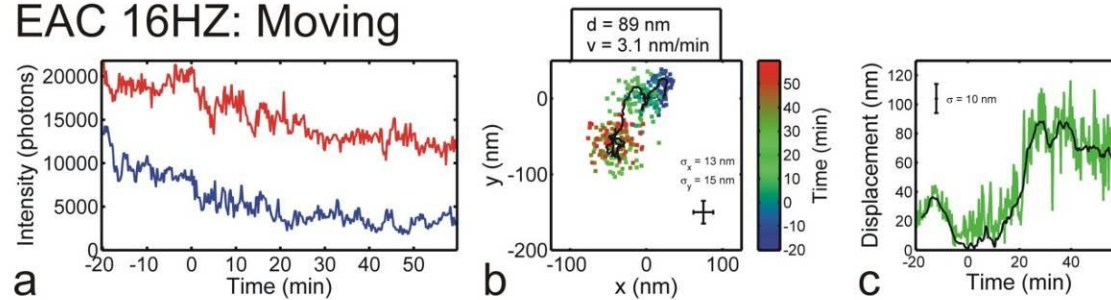
EAC 14HZ: Moving



EAC 15HZ: Stationary

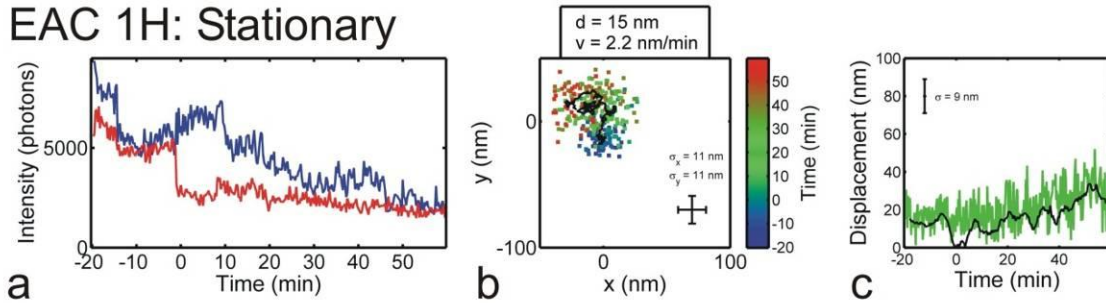


EAC 16HZ: Moving

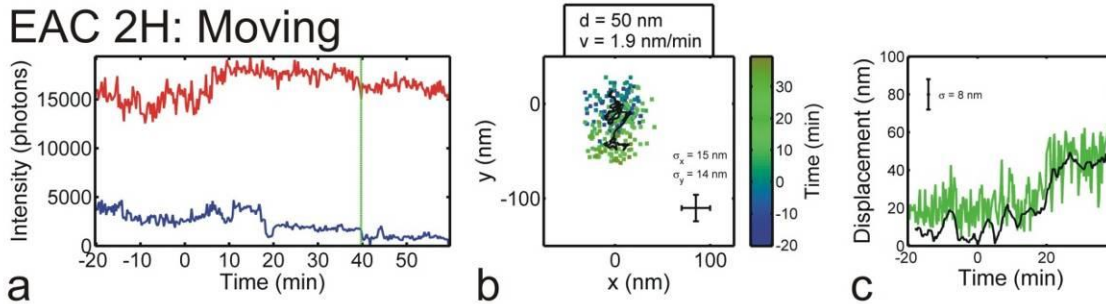


HBS, 0 mM Zn²⁺ Control (EAC H)

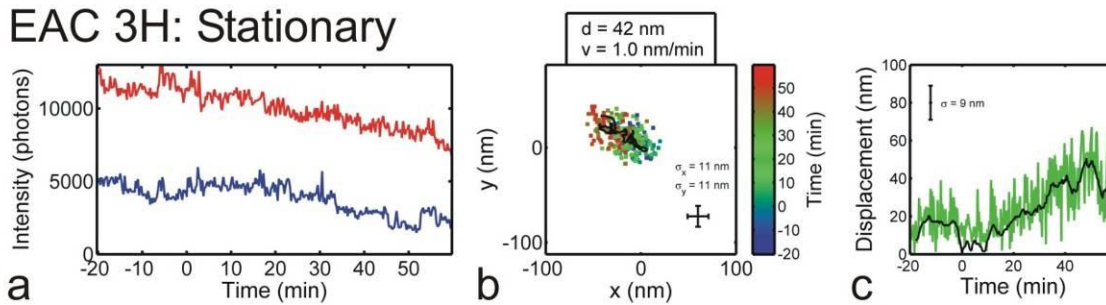
EAC 1H: Stationary



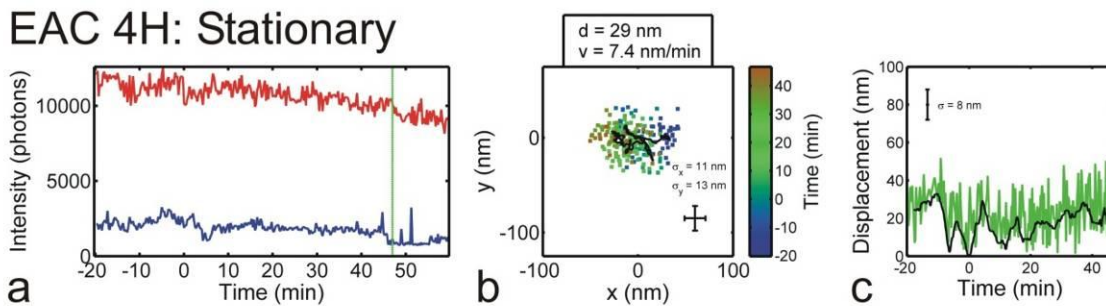
EAC 2H: Moving



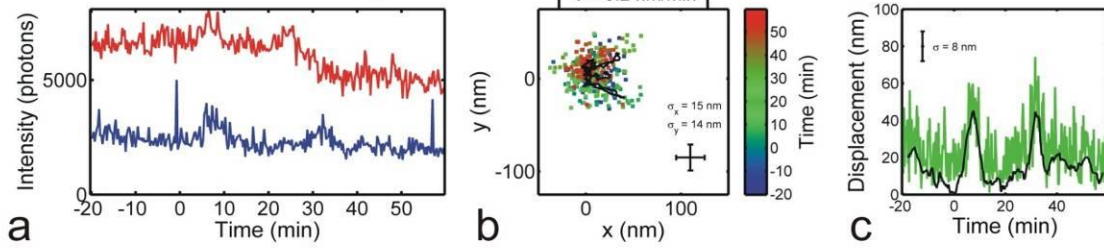
EAC 3H: Stationary



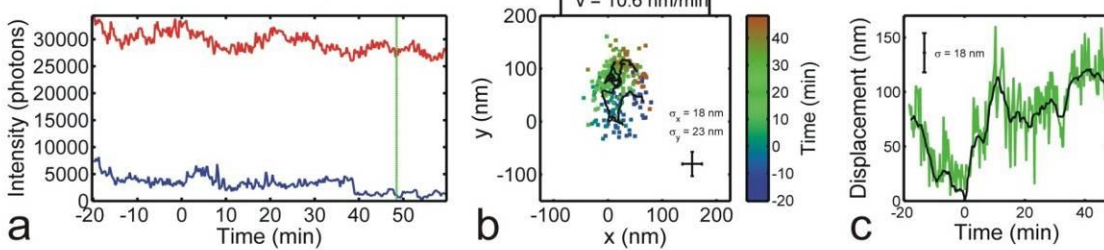
EAC 4H: Stationary



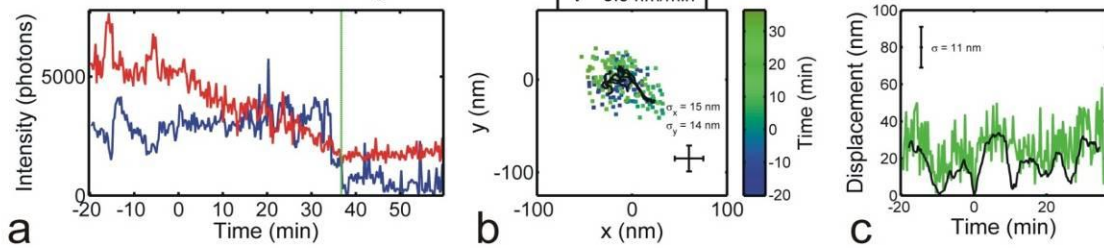
EAC 5H: Stationary



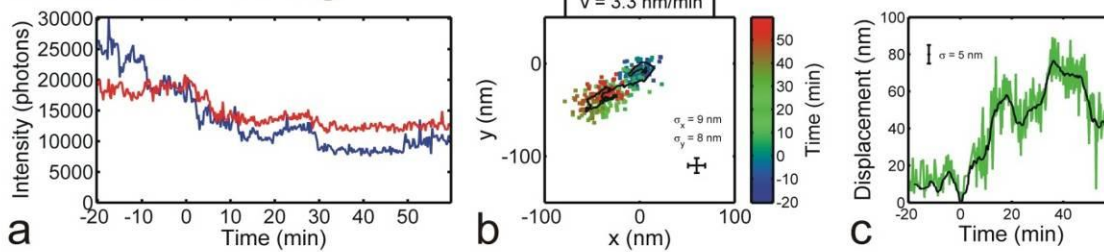
EAC 6H: Moving



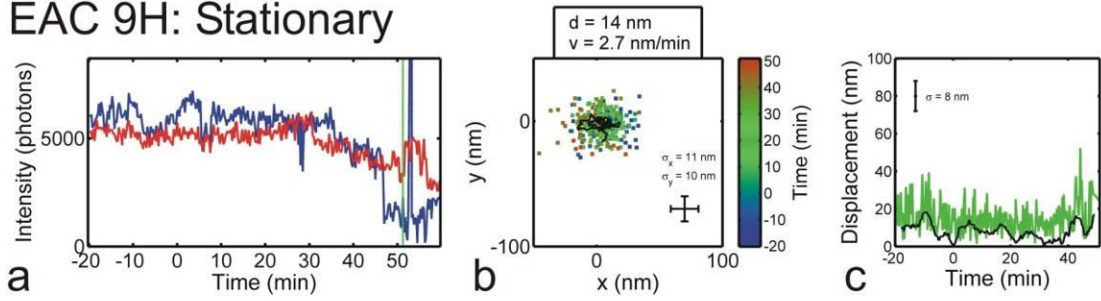
EAC 7H: Stationary



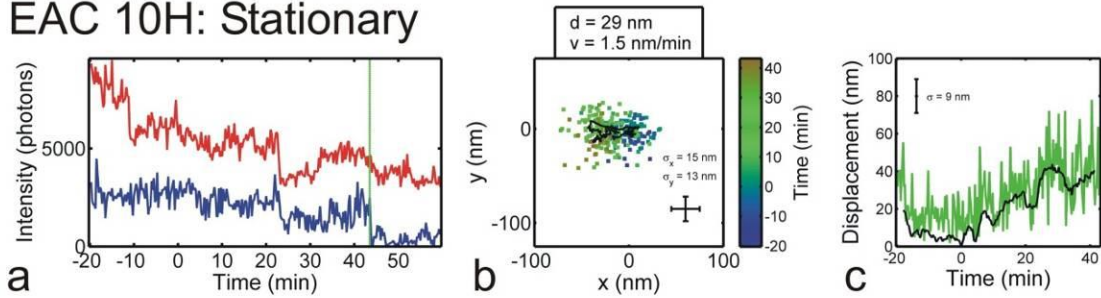
EAC 8H: Moving



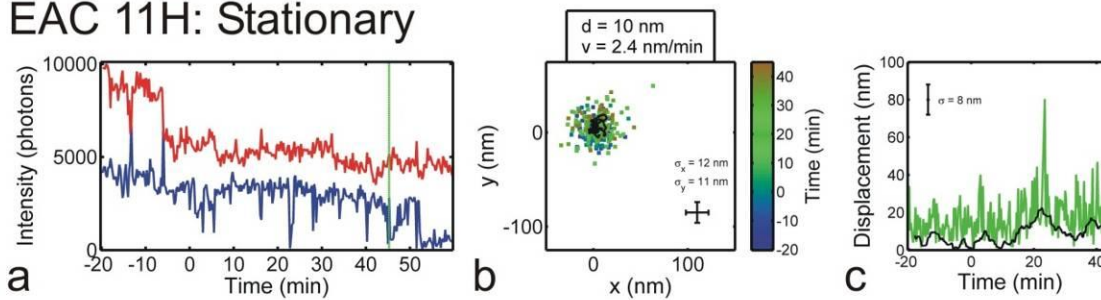
EAC 9H: Stationary



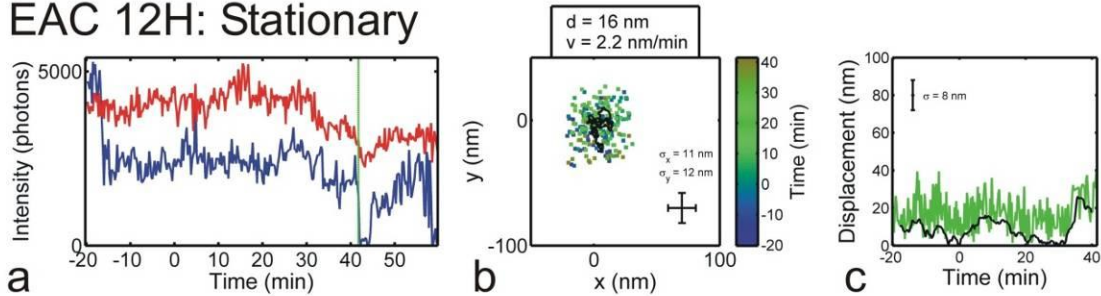
EAC 10H: Stationary



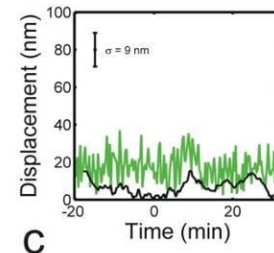
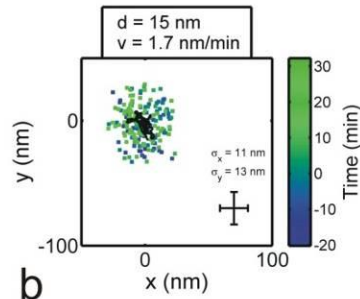
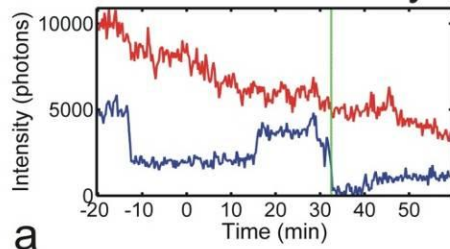
EAC 11H: Stationary



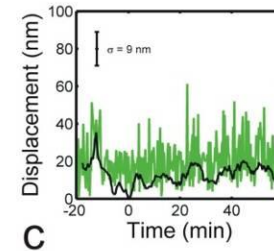
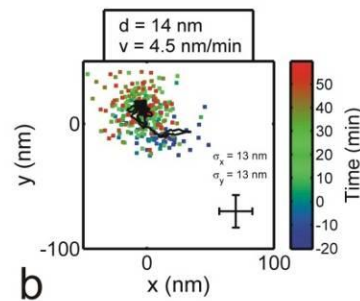
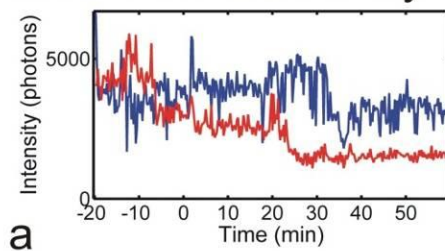
EAC 12H: Stationary



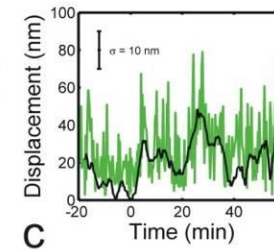
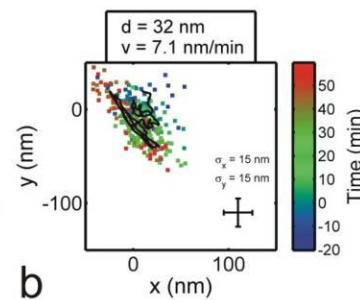
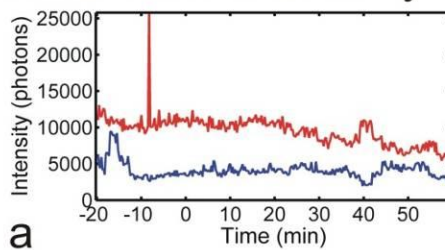
EAC 13H: Stationary



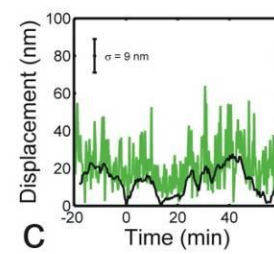
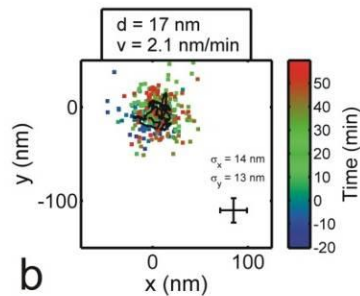
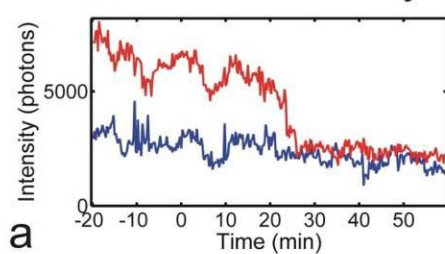
EAC 14H: Stationary



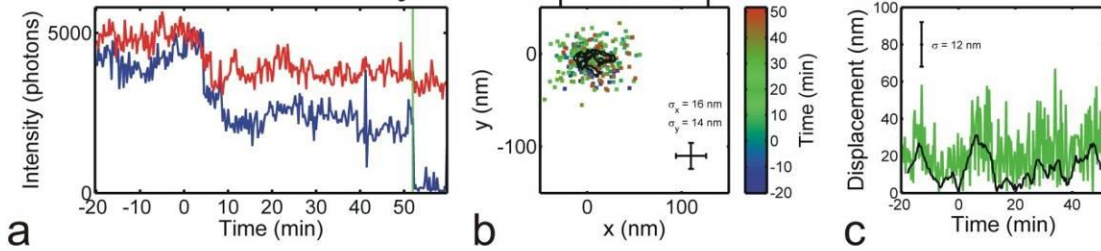
EAC 15H: Stationary



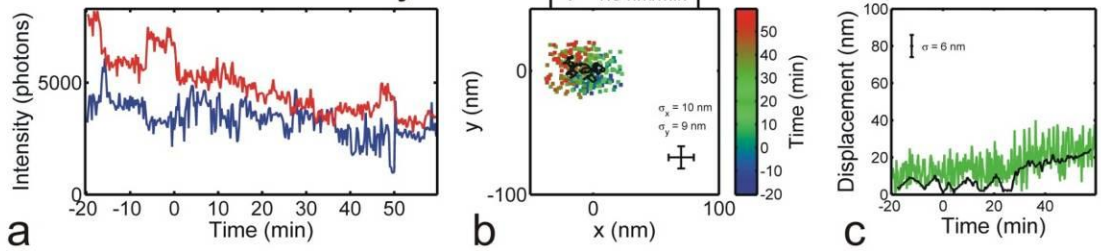
EAC 16H: Stationary



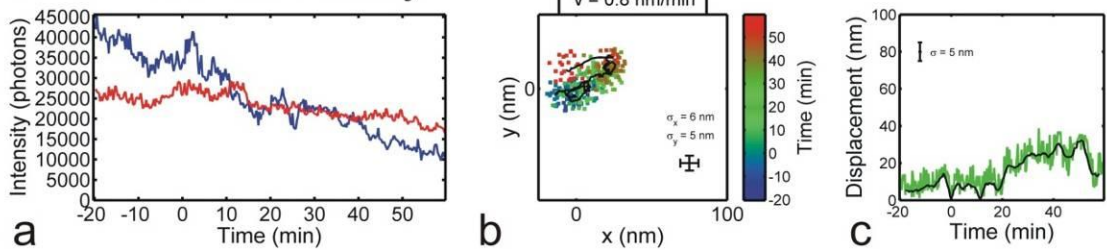
EAC 17H: Stationary



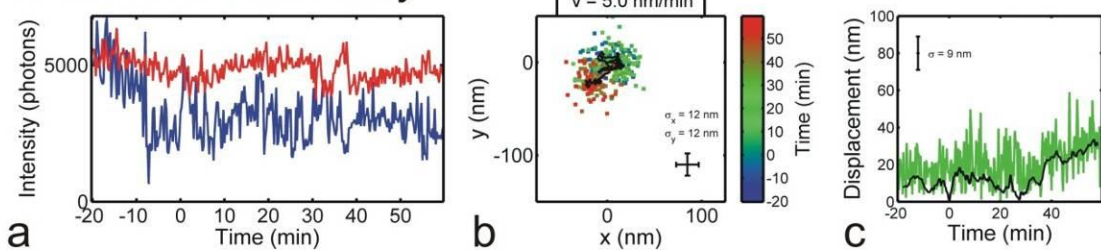
EAC 18H: Stationary



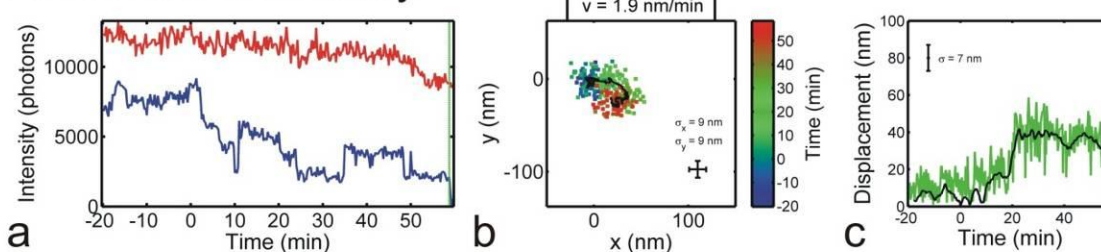
EAC 19H: Stationary



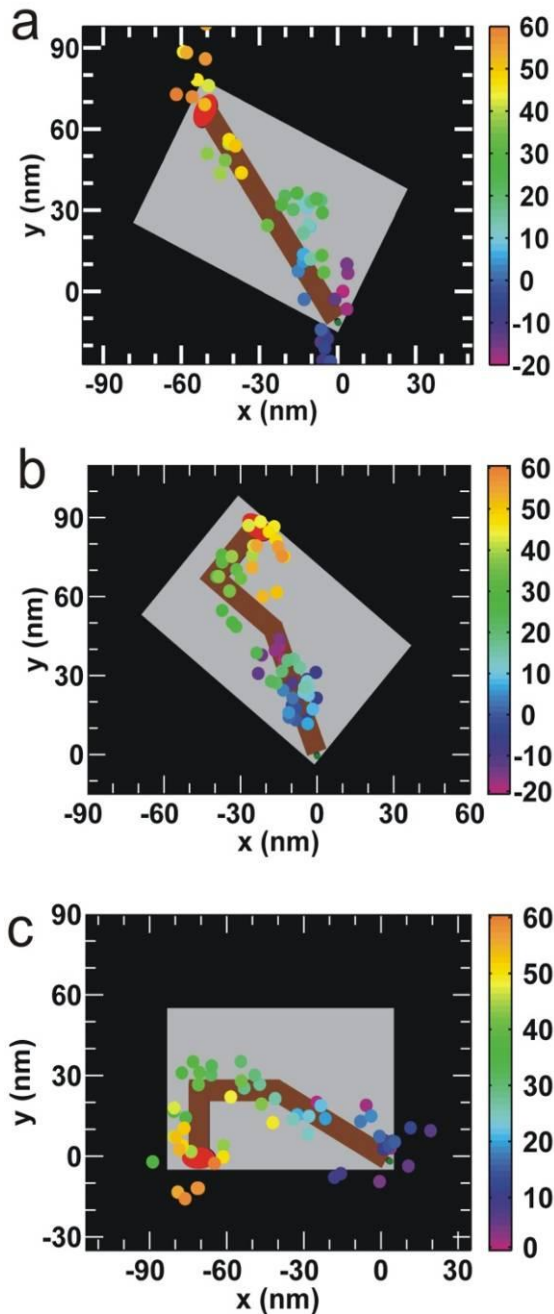
EAC 20H: Stationary



EAC 21H: Stationary



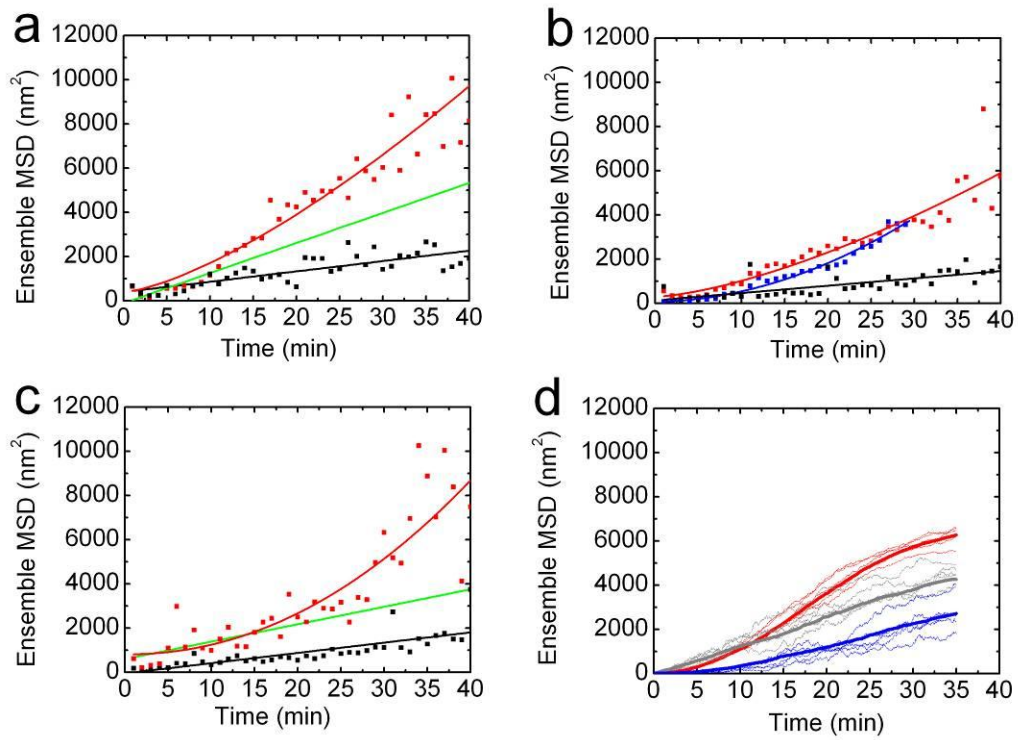
Supplementary Figure 31 | a, b, c, Particularly clean trajectory plots for individual spiders on the EAC (a), EABC (b), and EABD (c) tracks. The EAC trace was collected in $1\times$ HBS + 5 mM ZnSO_4 and corresponds to spider EAC 5H (Supplementary Fig. 30), while the EABC and EABD traces were collected in $1\times$ TA-Mg + 1 mM ZnSO_4 and correspond to spiders EABC 1 and EABD 1 (Supplementary Fig. 29). The color bars on the left indicate the time in minutes. Zinc was added at time 0. Among the x-y plots for EABC and EABD traces, some were consistent with the prescribed turn (as shown here); however, our resolution was not sufficient to extract features of these landscapes such as turn angles with satisfactory confidence.



Supplementary Table 4 | Trajectory filtering statistics for spiders imaged by fluorescence microscopy on the EAC track. These statistics reflect the filtering performed to produce the MSD plot in Supplementary Fig. 32b. The only criterion these spider-origami pairs needed to satisfy is to have detectable Cy3 and Cy5 for at least 1/3 of the experiment's duration (20-30 min). All are imaged in 1× SSC buffer in the presence of Zn²⁺. The EAC substrate track was in all cases incubated with TRIGGER for 30-60 min prior to imaging, while TRIGGER was added to the EAC product track either 30-60 min (row 2) or 10-15 min (row 3) prior to imaging by fluorescence microscopy.

	Total PSF Pair Candidates	Spiders Included in S34b
EAC substrate track	3,821	85
EAC product track, Long TRIGGER pre-incubation	276	29
EAC product track, Short TRIGGER pre-incubation	74	18

Supplementary Figure 32 | a, Ensemble mean square displacement (MSD) versus time calculated from 15 individual Tier 1 spiders on the EAC substrate track (red squares; EAC 1-15 in Supplementary Fig. 29) in 1× SSC. A power law function (red curve) is fit to the MSD from 1-30 min, and a linear function (green curve) is fit to the first 12 min. For further comparison, an MSD plot is shown that is derived from 7 spiders (black circles; traces found in Supplementary Fig. 28d) from a no-Zn²⁺ control experiment in which spiders are not expected to walk. In both types of experiments, the origami-spider complexes were incubated with TRIGGER for 30-60 min prior to imaging. **b**, Ensemble MSD versus time plots comparing behavior on the substrate-covered (red) and product-covered EAC tracks with TRIGGER added either 30-60 min (long incubation, black) or 10-15 min before (short incubation, blue) imaging by fluorescence microscopy in 1× SSC in the presence of zinc. The MSD values were calculated from 85 individual spiders on the substrate-covered EAC track, 29 spiders on the product-covered EAC track incubated for 30-60 min with TRIGGER, and 18 spiders on the product-covered EAC track incubated for 10-15 min with TRIGGER selected according to intensity, ellipticity, and outlier cutoff criteria stated in the supplement text. All three are fit to power law functions (solid curves). The MSD plot for the substrate track is assembled from the same datasets as the red plot in panel (a), but the more relaxed selection criteria result in the inclusion of more stationary or slowly moving spiders, resulting in a shallower curve. **c**, Ensemble MSD versus time plots of spider movement on the EAC substrate track observed in 1× HBS with 1× HBS buffer containing either 0 mM (black curve) or 5 mM (red curve) ZnSO₄ added at time $t = 0$ min. In both types of experiments, the sample was incubated with TRIGGER for 30-60 min prior to the beginning of the experiment. A power law function (red curve) is fit to the MSD with 5 mM zinc from 1-30 min, and a straight line (green curve) is fit to the first 15 min of the MSD with 5 mM zinc. A straight line (black) is also fit to the MSD in 0 mM zinc. **d**, Simulated MSD versus time plots calculated as described in the supplement text from 1,000 spiders (thick lines) or separate trials of fewer spiders (thin lines) for the substrate-covered EAC track (red), and for the product-covered EAC track without (gray) or with a delayed release (blue) from the START region ($t_{1/2\text{release}} = 0$ or 10 min). For the smaller trials, 80 spiders per trial were used for the substrate-covered track, while 20 spiders per trial were used for the product track with and without delayed release (to approximate the numbers of experimental spiders observed in each case).



Supplementary References:

1. Braitenberg, V. *Vehicles: Experiments in Synthetic Psychology*. (MIT Press, 1984).
2. Brooks, R. A. Intelligence without representation. *Artif. Intell.* **47**, 139–159 (1991).
3. Simon, H. A. *The Sciences of the Artificial*, 3rd ed. (MIT Press, Cambridge, Mass., 1996).
4. Siegwart, R. & Nourbakhsh, I. R. *Introduction to Autonomous Mobile Robots*. (MIT Press, 2004).
5. Stojanovic, M. N., Mitchell, T. E. & Stefanovic, D. Deoxyribozyme-based logic gates. *J. Am. Chem. Soc.* **124**, 3555–3561 (2002).
6. Kube, C. R. & Zhang, H. Collective robotics: from social insects to robots. *Adapt. Behav.* **2**, 189–219 (1993).
7. Rus, D., Butler, Z., Kotay, K. & Vona, M. Self-reconfiguring robots. *Commun. ACM* **45**, 39–45 (2002).
8. Dorigo, M. & Stützle, T. *Ant colony optimization*. (MIT Press, Cambridge, Mass., 2004).
9. Turing, A. M. On computable numbers, with an application to the Entscheidungsproblem. *Proc. Lond. Math. Soc. Ser. 2*, 230–265 (1936).
10. Von Neumann, J. & Burks, A. W. *Theory of Self-Reproducing Automata*. (University of Illinois Press, Urbana., 1966).
11. Bennett, C. H. The thermodynamics of computation—a review. *Int. J. Theor. Phys.* **21**, 905–940 (1982).
12. Gajardo, A., Moreira, A. & Goles, E. Complexity of Langton's ant. *Discrete Appl. Math.* **117**, 41–50 (2002).
13. Bath, J. & Turberfield, A. J. DNA nanomachines. *Nat. Nanotechnol.* **2**, 275–284 (2007).
14. Sherman, W. B. & Seeman, N. C. A precisely controlled DNA biped walking device. *Nano Lett.* **4**, 1203–1208 (2004).
15. Shin, J. S. & Pierce, N. A. A synthetic DNA walker for molecular transport. *J. Am. Chem. Soc.* **126**, 10834–10835 (2004).
16. Bath, J., Green, S. J. & Turberfield, A. J. A free-running DNA motor powered by a nicking enzyme. *Angew. Chem. Int. Ed.* **44**, 4358–4361 (2005).
17. Tian, Y., He, Y., Chen, Y., Yin, P. & Mao, C. D. A DNzyme that walks processively and autonomously along a one-dimensional track. *Angew. Chem. Int. Ed.* **44**, 4355–4358 (2005).
18. Yin, P., Choi, H. M. T., Calvert, C. R. & Pierce, N. A. Programming biomolecular self-assembly pathways. *Nature* **451**, 318–U314 (2008).
19. Omabegho, T., Sha, R. & Seeman, N. C. A bipedal DNA brownian motor with coordinated legs. *Science* **324**, 67–71 (2009).
20. Pei, R. *et al.* Behavior of polycatalytic assemblies in a substrate-displaying matrix. *J. Am. Chem. Soc.* **128**, 12693–12699 (2006).
21. Green, S. J., Bath, J. & Turberfield, A. J. Coordinated chemomechanical cycles: a mechanism for autonomous molecular motion. *Phys. Rev. Lett.* **101**, 238101 (2008).

22. Yin, P., Turberfield, A. J., Sahu, S. & Reif, J. H. Design of an autonomous DNA nanomechanical device capable of universal computation and universal translational motion. *Lect. Notes Comput. Sc.* **3384**, 426-444 (2005).
23. Reif, J. H. & Sahu, S. Autonomous programmable DNA nanorobotic devices using DNazymes. *Theoretical Computer Science* **410**, 1428-1439 (2009).
24. Chang, T., Rozkiewicz, D. I., Ravoo, B. J., Meijer, E. W. & Reinhoudt, D. N. Directional movement of dendritic macromolecules on gradient surfaces. *Nano Lett.* **7**, 978-980 (2007).
25. Wang, J. & Manesh, K. M. Motion control at the nanoscale. *Small* **6**, 338-345 (2010).
26. Vives, G. & Tour, J. M. Synthesis of single-molecule nanocars. *Acc. Chem. Res.* **42**, 473-487 (2009).
27. Adleman, L. M. Molecular computation of solutions to combinatorial problems. *Science* **266**, 1021-1024 (1994).
28. Stojanovic, M. N. & Stefanovic, D. A deoxyribozyme-based molecular automaton. *Nat. Biotechnol.* **21**, 1069-1074 (2003).
29. Seelig, G., Soloveichik, D., Zhang, D. Y. & Winfree, E. Enzyme-free nucleic acid logic circuits. *Science* **314**, 1585-1588 (2006).
30. Yan, H., Park, S. H., Finkelstein, G., Reif, J. H. & LaBean, T. H. DNA-templated self-assembly of protein arrays and highly conductive nanowires. *Science* **301**, 1882-1884 (2003).
31. Rothemund, P. W. K., Papadakis, N. & Winfree, E. Algorithmic self-assembly of DNA Sierpinski triangles. *PLoS Biol.* **2**, 2041-2053 (2004).
32. Seeman, N. C. DNA enables nanoscale control of the structure of matter. *Q. Rev. Biophys.* **38**, 363-371 (2005).
33. Rothemund, P. W. K. Folding DNA to create nanoscale shapes and patterns. *Nature* **440**, 298-302 (2006).
34. Aldaye, F. A., Palmer, A. L. & Sleiman, H. F. Assembling materials with DNA as the guide. *Science* **321**, 1795-1799 (2008).
35. He, Y. *et al.* Hierarchical self-assembly of DNA into symmetric supramolecular polyhedra. *Nature* **452**, 198-201 (2008).
36. Jungmann, R., Liedl, T., Sobey, T. L., Shih, W. & Simmel, F. C. Isothermal assembly of DNA origami structures using denaturing agents. *J. Am. Chem. Soc.* **130**, 10062-10063 (2008).
37. Ding, B. & Seeman, N. C. Operation of a DNA robot arm inserted into a 2D DNA crystalline substrate. *Science* **314**, 1583-1585 (2006).
38. Santoro, S. W. & Joyce, G. F. A general purpose RNA-cleaving DNA enzyme. *Proc. Natl. Acad. Sci. USA* **94**, 4262-4266 (1997).
39. Antal, T. & Krapivsky, P. L. Molecular spiders with memory *Phys. Rev. E* **76**, 021121 (2007).
40. Saffarian, S., Collier, I. E., Marmer, B. L., Elson, E. L. & Goldberg, G. Interstitial collagenase is a Brownian ratchet driven by proteolysis of collagen. *Science* **306**, 108-111 (2004).
41. Aitken, C. E., Marshall, R. A. & Pulglisi, J. D. An oxygen scavenging system for improvement of dye stability in single-molecule fluorescence experiments. *Biophys. J.* **94**, 1826-1835 (2008).

42. Walter, N. G., Huang, C.-Y., Manzo, A. J. & Sobhy, M. A. Do-it-yourself guide: How to use the modern single-molecule toolkit. *Nat. Methods* **5**, 475-489 (2008).
43. Churchman, L. S., Okten, Z., Rock, R. S., Dawson, J. F. & Spudich, J. A. Single molecule high-resolution colocalization of Cy3 and Cy5 attached to macromolecules measures intramolecular distances through time. *Proc. Natl. Acad. Sci. USA* **102**, 1419–1423 (2005).
44. Yildiz, A. & Selvin, P. R. Fluorescence imaging with one nanometer accuracy: application to molecular motors. *Acc. Chem. Res.* **38**, 574-582 (2005).
45. Li, J., Zheng, W., Kwon, A. H. & Lu, Y. In vitro selection and characterization of a highly efficient Zn (II)-dependent RNA-cleaving deoxyribozyme. *Nucleic Acids Res.* **28**, 481-488 (2000).
46. Schutz, G. J., Trabesinger, W. & Schmidt, T. Direct observation of ligand colocalization on individual receptor molecules. *Biophys. J.* **74**, 2223-2226 (1998).
47. Schellart, N. Automatic counting of round particles in microscopic images by pattern recognition in *Image Analysis: Methods and Applications, 2nd ed.*, edited by Donat-P, H. (CRC Press, Boca Raton, FL, USA, 2001), pp. 359-361.
48. Toprak, E. *et al.* Defocused orientation and position imaging (DOPI) of myosin V. *Proc. Natl. Acad. Sci. USA* **103**, 6495-6499 (2006).
49. Wetmur, J. G. DNA probes: applications of the principles of nucleic-acid hybridization. *Critical Reviews in Biochemistry and Molecular Biology* **26**, 227-259 (1991).